

**THE EXTRACTION AND ANALYSIS OF DISSOLVED
TRACE METALS FROM SEAWATER USING ON-LINE
FLOW INJECTION INDUCTIVELY COUPLED
MASS SPECTROMETRY**

by

HELEN NICOLIDAKIS

B.Sc. (Hons), The University of British Columbia, 1989.

**A THESIS SUBMITTED IN PARTIAL FULFILLMENT OF THE
REQUIREMENTS FOR THE DEGREE OF
DOCTOR OF PHILOSOPHY**

in

**THE FACULTY OF GRADUATE STUDIES
(DEPARTMENT OF CHEMISTRY)**

We accept this thesis as conforming
to the required standard

THE UNIVERSITY OF BRITISH COLUMBIA

MAY 1995

© Helen Nicolidakis, 1995

In presenting this thesis in partial fulfilment of the requirements for an advanced degree at the University of British Columbia, I agree that the Library shall make it freely available for reference and study. I further agree that permission for extensive copying of this thesis for scholarly purposes may be granted by the head of my department or by his or her representatives. It is understood that copying or publication of this thesis for financial gain shall not be allowed without my written permission.

(Signature)

Department of CHEMISTRY

The University of British Columbia
Vancouver, Canada

Date 95-08-11

Abstract

A method utilizing flow injection (FI) for on-line preconcentration with inductively coupled plasma mass spectrometry (ICP-MS) detection has been developed for analyzing dissolved zinc, cadmium, nickel, copper, lead, manganese, gallium and niobium in seawater. This method was used to investigate the distributions of these trace metals in the western, central and sub-Arctic North Pacific Ocean.

Using on-line FI methods to replace conventional preconcentration/separation techniques results in significant decreases in sample and reagent volumes and sample work up and analysis time. This method used a column filled with 8-hydroxyquinoline on silica resin to preconcentrate up to 18 millilitres of seawater for a minimum sample throughput of six per hour. Concentrations of these elements ranged between 0.01 and 12 nmol/kg, with analytical precision being better than 12 % for all elements except Cu, and detection limits in the low picomolar range (1 - 90 pmol/kg). The accuracy of the technique was verified by analysis of standard reference material from the National Research Council of Canada for Zn, Cd, Ni, Cu, Pb and Mn.

This FI method was also incorporated into the design of a prototype sampler with multi-sampling capabilities which was developed to preconcentrate trace metals from seawater remotely. The sampler was submerged in-house for a period of one week, and operated successfully. Before collecting contaminant-free seawater samples, a second generation sampler is required.

The results obtained for Zn, Cd, Ni, Cu, Pb and Mn using the on-line FI-ICP-MS method developed here showed the expected distributions, agreeing well with profiles previously determined using the same samples and with profiles measured by other labs in the same region of the North Pacific.

The first set of dissolved Ga data from the western North Pacific are presented here. When coupled with published data from the sub-Arctic North Pacific Current and from the central gyre, the new information yields a better understanding of the controls of dissolved Ga behaviour in the North Pacific. At all stations, Ga shows high surface concentrations, a minimum at ~ 1000 m and increases at greater depth. Sub-surface maxima at ~ 500 m are observed in the central gyre and in the sub-arctic North Pacific Current, but not in the western North Pacific. Dissolved Ga in surface waters is highest in the central gyre (14 to 19 pmol/kg), an area with low dust input from the Asian continent and low productivity. In the western Pacific, where dust input and productivity are both high, surface water Ga values are lower (9 to 12 pmol/kg). This indicates that the high levels of Ga in the central gyre and the presence of the sub-surface maximum in this region are not due to advection from the western North Pacific. The lowest surface concentrations (4 to 10 pmol/kg) are found in the sub-Arctic North Pacific Current, an area with low dust input and high productivity.

The first full depth profiles of niobium in the ocean are reported in this dissertation. The Nb distributions in the North Pacific show low surface concentrations and sub-surface and mid-depth maxima coincidental with the boundaries of the O₂ minimum. Nb concentrations range between 10 and 80 pmol/kg in surface waters, 40 and 100 pmol/kg in the upper boundary of the O₂ minimum zone, 40 and 200 pmol/kg in the lower boundary of the O₂ minimum zone and 10 and 100 pmol/kg in deep waters. The concentrations decrease with distance from the Asian continent, and increase in the North Equatorial Current, suggesting horizontal advection of high Nb waters from both the western and eastern Pacific boundaries. The distribution of Nb may also be affected by Mn and nutrient cycling and pH changes in the O₂ minimum zone, though the extent of these cannot be ascertained at present.

Table of Contents

Abstract	ii
Table of Contents.....	iv
List of Tables	ix
List of Figures	x
Glossary	xiv
Acknowledgments	xvii
CHAPTER 1. INTRODUCTION	1
1.1 Background.....	1
1.2 Distributions of Trace Metals of Interest in Seawater	3
1.2.1 General Overview.....	3
1.2.2 Zinc, Cadmium and Nickel.....	8
1.2.2.1 Zinc.....	9
1.2.2.2 Cadmium	9
1.2.2.3 Nickel.....	10
1.2.3 Copper.....	10
1.2.4 Lead	11
1.2.5 Manganese.....	11
1.2.6 Gallium	12
1.2.7 Niobium	13
1.3 Flow Injection Analysis.....	13
1.3.1 Introduction and History	15
1.3.2 Channel Geometry in FIA.....	16
1.3.3 On-Line Matrix Separation and Preconcentration	18
1.3.4 FIA and Seawater.....	19

1.4 Inductively Coupled Plasma Mass Spectrometry	20
1.4.1 History of the ICP-MS.....	20
1.4.2 Instrumentation Overview.....	21
1.4.3 Advantages and Limitations of the ICP-MS.....	23
1.4.4 Sample Introduction Methods.....	24
1.4.4.1 FI-ICP-MS.....	25
1.4.4.2 On-Line Preconcentration and Matrix Separation with FI-ICP-MS	26
1.5 Ship board and <i>In Situ</i> analysis.....	26
1.5.1 Ship board Determinations.....	26
1.5.2 <i>In Situ</i> Measurements and Sampling.....	27
CHAPTER 2. DEVELOPING AN <i>IN SITU</i> SAMPLER.....	30
2.1 Designing the Prototype sampler.....	30
2.2 Components of the Prototype sampler.....	31
2.2.1 Computer Board	33
2.2.2 Interface Circuitry	35
2.2.3 Pump Head and Motor	36
2.2.3.1 Pump Shaft.....	37
2.2.4 Flow Meter Design	38
2.2.5 Valves and Column Design	39
2.2.6 Battery Pack.....	41
2.2.7 Casing	42
2.2.8 Electronics Hardware	43
2.2.9 Filter	44
2.3 Operation of the Prototype Sampler.....	44
2.2.1 General operation	44

2.3.2 Pump Control.....	44
2.3.3 Valve Control.....	45
2.3.4 Flow Meter Control.....	45
2.4 Flow Meter Calibration.....	46
2.5 Prototype Sampler Testing.....	49
2.5.1 Preliminary Testing at Sea.....	49
2.5.2 Submersion Testing.....	50
2.5.3 Contamination Control.....	51
2.6 Conclusions.....	52
CHAPTER 3. EXPERIMENTAL AND TECHNIQUE DEVELOPMENT.....	53
3.1 Materials and Reagents.....	53
3.1.1 Reagents.....	53
3.1.2 Bottles.....	54
3.1.3 Seawater Standards.....	54
3.1.4 Resins.....	54
3.2 Sample Collection.....	55
3.2.1 Seawater Samples.....	55
3.3 On-Line FI-ICP-MS Instrumentation.....	56
3.3.1 Apparatus for Flow Injection Manifold.....	56
3.3.1.1 Valves.....	56
3.3.1.2 Peristaltic Pump.....	57
3.3.1.3 Design of the Extraction Column and FI Fittings.....	57
3.3.2 On-Line FI-ICP-MS Manifold used for Preconcentration.....	58
3.3.3 Automation of the FI manifold and Data Collection.....	60
3.3.3.1 Pump Calibration.....	60
3.3.3.2 Automation and Manifold Control.....	61

3.3.3.3 Data Collection	61
3.3.4 ICP-MS	61
3.3.4.1 Operating Conditions.....	62
3.3.4.2 PlasmaQuad Control and Software	64
3.4 Method Development	66
3.4.1 Chelating Resins Studied.....	66
3.4.1.1 Chelex-100	67
3.4.1.2 8-HQ on TSK.....	67
3.4.1.3 8-HQ on XE-305	68
3.4.1.4 8-HQ on silica	68
3.4.1.5 Comparing 8-HQ on XE-305 and Silica Backbones	68
3.4.2 Silica based 8-HQ pH Studies and Recovery Tests.....	70
3.4.2.1 On-Line Studies.....	70
3.4.3 Flow Rate	73
3.4.4 Interelement Interferences	76
3.4.5 System Blanks and Detection Limits	77
3.4.6 Precision and Accuracy.....	78
3.5 Sample Preparation	81
CHAPTER 4. OCEANOGRAPHIC RESULTS AND DISCUSSION	83
4.1 Characteristics of the Ocean Stations Sampled.....	83
4.2 Dissolved Zn, Cd, Ni, Pb, Cu, Mn, Co and Cr in the North Pacific Ocean ...	85
4.2.1 Nutrient-type Elements (Zn, Cd and Ni)	85
4.2.1.1 Dissolved Zn in the North Pacific.....	85
4.2.1.2 Dissolved Cd in the North Pacific	90
4.2.1.3 Dissolved Ni in the North Pacific	94
4.2.2 Nutrient Type with Scavenging Element (Cu).....	98

4.2.3 Scavenged Type Element with an External Source (Pb).....	102
4.2.4 Oxidative Scavenging Type Elements (Mn)	106
4.3 Dissolved Ga in the North Pacific Ocean.....	112
4.3.1 Ga Distribution in Surface and Intermediate Waters.....	115
4.3.2 Ga Distribution in Intermediate Waters	117
4.3.3 Dissolved Ga Distribution in Deep Waters.....	121
4.3.4 Vertical-Advection Diffusion Model	122
4.3.4.1 Application of this model to Ga.....	123
4.3.5 Comparison with Al.....	128
4.3.6 Conclusions.....	131
4.4 Dissolved Nb in Seawater	133
4.4.1 Depth Profiles.....	133
4.4.1.1 Dissolved Nb in the Surface Waters.....	136
4.4.1.2 Dissolved Nb in the Intermediate and Deep Waters.....	137
4.4.2 Comparison with Dissolved O ₂ and Mn.....	138
4.4.3 North Pacific Intermediate Waters	143
4.4.4 Comparison with V	145
4.4.5 Comparisons with Zr and Mo.....	146
4.4.6 Conclusions	148
CHAPTER 5. CONCLUSIONS	149
CHAPTER 6. FUTURE WORKS	152
BIBLIOGRAPHY	153
APPENDIX A THE INFILTREX II SAMPLER	166
APPENDIX B SOFTWARE ROUTINES	170
APPENDIX C CIRCUIT SCHEMATICS	173
APPENDIX D SIM MODE SCAN OF ELEMENTS	176
APPENDIX E OCEANOGRAPHICAL DATA	178

LIST OF TABLES

Table 2.1	Physical components of the prototype sampler.	33
Table 2.2	The average flow meter response at different flow rates at the 95% confidence limit.....	48
Table 3.1	ICP-MS Operation Conditions.	63
Table 3.2	Recovery of the 6 metals from 6 mls of a 0.5 ppb spiked seawater sample adjusted to pH 8.....	69
Table 3.3	Concentration of metals in the mixed standard solution used for standard additions.	72
Table 3.4	Results of the on-line pH studies.....	73
Table 3.5	Time needed for each preconcentration cycle using 6 mls of seawater and 2 mls of DDI before and after sample loading using the on-line system.....	74
Table 3.6	Potential interferences of the 12 isotopes. From reference [111]....	77
Table 3.7	The average of five system blanks and detection limits (3σ) for 6 mls of seawater in nmol/kg.	78
Table 3.8	The determination of dissolved Mn, Ni, Cu, Zn, Cd, Pb, Ga and Nb in NASS-3 seawater reference material.	80
Table 4.1	Results obtained from the vertical-advection diffusion model for dissolved Ga in the deep waters of the North Pacific.	126
Table 4.2	Enrichment factors of Ga with respect to Al [20, 112] from stations 10, 15 and 16.	130

LIST OF FIGURES

Figure 1.1	The three major distribution types: (A) Conservative. (B) Nutrient Type. (C) Scavenged.....	5
Figure 1.2	Types of FIA manifolds: A. Single line. B. Two line with single confluence point. C. Solvent extraction. D. As (B.) with a packed reactor.....	15
Figure 1.3	Schematics of the most commonly used microreactor geometries found in FIA applications	17
Figure 1.4	A schematic of the VG PlasmaQuad ICP-MS.....	22
Figure 2.1	A schematic of the prototype sampler (a) Front view. (b) Rear view..	32
Figure 2.2	A representation of the Ziatech computer board and connections to the sampler component controllers on the electronic circuit board	36
Figure 2.3	Cross section of top endplate to show a schematic of pump head to pump motor connection..	37
Figure 2.4	Interior of the flow meter hardware.....	39
Figure 2.5	A schematic of the flow manifold used to preconcentrate metals from seawater using the new sampler.....	41
Figure 2.6	Schematic of the battery pack: (A) view from the side (B) view from the top and bottom of battery pack.	42
Figure 2.7	Plots of the 50 data point sets of the flow meter response over a range of flow rates between 0.8 to 8.0 ml/min.	47
Figure 2.8	Flow meter response vs. Flow rate.....	49

Figure 3.1	On-line FI-ICP-MS preconcentration manifold used for: (A) Loading (B) Elution	59
Figure 3.2	A two minute SIM mode scan of ^{114}Cd	65
Figure 3.3	Plots of pH vs. % response for 8 elements studied on-line.	71
Figure 3.4	Metal response vs. flow rate for the 8 elements.	75
Figure 3.5	Dissolved Ga at station P26. A. Data from reference [53]. B. Results from this work.	81
Figure 4.1	North Pacific study area.	84
Figure 4.2	Dissolved Zn in the western North Pacific.	87
Figure 4.3	Dissolved Zn in the central North Pacific.....	88
Figure 4.4	Dissolved Zn in the eastern North Pacific in the sub-Arctic gyre...89	
Figure 4.5	Dissolved Zn vs. the nutrient silicate.	89
Figure 4.6	Dissolved Cd in the western North Pacific.....	91
Figure 4.7	Dissolved Cd in the central North Pacific.	92
Figure 4.8	Dissolved Cd in the eastern North Pacific in the sub-Arctic gyre. 93	
Figure 4.9	Dissolved Cd vs. the nutrient phosphate.	94
Figure 4.10	Dissolved Ni in the western North Pacific.....	95
Figure 4.11	Dissolved Ni in the central North Pacific.	96
Figure 4.12	Dissolved Ni in the eastern North Pacific in the sub-Arctic gyre. ..97	
Figure 4.13	Ni versus phosphate (A, C) and silicate (B, D). A and B: At all depths. C: Upper 800 m. D: Below 800 m.....	98
Figure 4.14	Dissolved Cu in the western North Pacific.....	99
Figure 4.15	Dissolved Cu in the central North Pacific.	100
Figure 4.16	Dissolved Cu in the eastern North Pacific in the sub-Arctic gyre.101	
Figure 4.17	Dissolved Pb in the western North Pacific.....	103
Figure 4.18	Dissolved Pb in the central North Pacific.....	104
Figure 4.19	Dissolved Pb in the eastern North Pacific in the sub-Arctic gyre.105	

Figure 4.20	Dissolved Mn in the western North Pacific.	107
Figure 4.21	Dissolved Mn in the central North Pacific.	108
Figure 4.22	Dissolved Mn in the eastern North Pacific in the sub-Arctic gyre.	109
Figure 4.23	Dissolved Mn and O ₂ versus depth at stations 1, 5, 10, 15, 16 and P26.	110
Figure 4.24	Dissolved Ga in the western North Pacific.	113
Figure 4.25	Dissolved Ga in the central North Pacific.	114
Figure 4.26	Dissolved Ga in the sub-Arctic eastern North Pacific.	115
Figure 4.27	Global fluxes of mineral aerosol to the oceans in mg m ⁻² yr ⁻¹	117
Figure 4.28	Contours generated by combining data from this study with those from previous work [53].	120
Figure 4.29	Element versus salinity plots in deep waters showing net release, conservative mixing and removal by particle scavenging distributions.	122
Figure 4.30	The A) Potential temperature-salinity and B) dissolved Ga-salinity relationships below 700 m at station 10.	124
Figure 4.31	The A) Potential temperature-salinity and B) dissolved Ga-salinity relationships below 700 m at station 16.	124
Figure 4.32	The A) Potential temperature-salinity and B) dissolved Ga-salinity relationships below 750 m at station P 26.	125
Figure 4.33	The A) Potential temperature-salinity and B) dissolved Ga-salinity relationships below 600 m at station 15.	125
Figure 4.34	Potential temperature - salinity relationship below 1000m at station 1.	126
Figure 4.35	Depth profiles of dissolved Al at stations 15 and 16 [112].	128
Figure 4.36	Depth profiles of dissolved Ga/Al ratios at stations 15 and 16. Al data from reference [112].	130

Figure 4.37	Dissolved Nb profiles from the Western North Pacific.....	134
Figure 4.38	Dissolved Nb in the central North Pacific.	135
Figure 4.39	Dissolved Nb in the sub-Arctic eastern North Pacific (P26).	136
Figure 4.40	Dissolved Nb and O ₂ in the North Pacific with respect to depth..	139
Figure 4.41	Dissolved Nb and Mn against depth in the North Pacific.....	141
Figure 4.42	Plots of potential temperature versus salinity to determine the North Pacific Intermediate waters at the six stations.	144
Figure 4.43	Profiles of dissolved V, PO ₄ and O ₂ in the North Pacific.....	146
Figure 4.44	Dissolved Zr and Mo in the North Pacific Ocean [90, 126].	147

GLOSSARY

8-HQ	8-hydroxyquinoline
8-HQ-silica	8-hydroxyquinoline bonded to silica
8-HQ-TSK	8-hydroxyquinoline bonded to a vinyl polymer agglomerate
8-HQ-XE-305	8-hydroxyquinoline bonded to a macroreticular styrene-divinylbenzene
A	amperes
A/D	analog to digital
AV	research vessel "Aleksander Vinogradov"
ASCFA	air segmented continuous flow analysis
CFA	continuous flow analysis
DACA board	data acquisition and control adapter board
dc	direct current
DCP-MS	direct current plasma mass spectrometry
digital I/O	digital input/output lines on a computer used for communications
DPASV	differential pulse anodic stripping voltametry
DPCSV	differential pulse cathodic stripping voltametry
ECD-GC	electron capture detection gas chromatography
FI	flow injection
FI-ICP-MS	flow injection inductively coupled plasma mass spectrometry

GC	gas chromatography
GFAAS	graphite furnace atomic absorption spectrometer
HEPA	high efficiency particle air (filter)
HS	hydrographical station
ICP-AES	inductively coupled plasma atomic emission spectroscopy
ICP-MS	inductively coupled plasma mass spectrometry
kHz	kilo Hertz
mA	milliamperes
mM	millimolar
m/z	mass to charge ratio
NAA	neutron activation analysis
N.C.	normally closed
nM	nanomolar
nmol/kg	nanomole per kilogram
N.O.	normally open
PC	personal computer (386SX)
pM	picomolar
pmol/kg	picomole per kilogram
ppb	part per billion
ppm	part per million

PQ	PlasmaQuad
psi	pounds per square inch
RAM	random access memory
REE	rare earth element
ROM	read only memory
rpm	revolutions per minute
RSD	relative standard deviation
SBSR	single bead string reactor
s	sample standard deviation
salinity	grams of dissolved salts in one kilogram of seawater
SIM	single ion monitoring
V	volts

Acknowledgements

This research could not have come to fruition without the input and assistance of many people. Comments, suggestions and insults from the many group members, both past and present have been very helpful (!), especially those from Dr. Larry Bowman, Dr. Oliver Lee, Dr. Brad McKelvey, Adrian Cook, Robert Mugo, Lucila Lares, Remy Chretien and Lu Chen.

To Dr. Adrian Wade, I appreciate your effort and guidance during this project inspite of your circumstances these last four years. To Dr. Kristin Orians, your enthusiasm, drive and attitude throughout these last six years have been instrumental in keeping me going and helped put things into perspective. A big thanks goes to Dr. Tom Pederson, whose comments during the writing of this dissertation were superb. Much of the technical side of things could not have been started without the work of the Mech. Shop, especially Des Lovrity, Brin Powell and Brian Snapkauskas and Electronics, especially Mike Hatton. Your optimism and solutions to problems, both great and small, were amazing.

I appreciated and miss the many coffee breaks I shared with Dr. Don Yapp and Christopher Alexander during those dark times. I also thank my longtime university comrades from waaaayyyy back: Reka Vasarhelyi, Donnaree Nygard, and Karen Long, all members of Hell's Chemists, and Debra Armitage and her volumes of fun (and in this day and age, safe) farm facts.

Without the moral support of my family, my path in life would have been much different. A simple thank you cannot even begin to convey the gratitude and respect I have for my parents, Tony and Vasso Nicolidakis. Finally, deepest thanks and gratitude to my husband, Kevin Soulsbury, whose knowledge, understanding and patience can never be over-emphasized nor surpassed.

CHAPTER 1. INTRODUCTION

1.1 Background

A trace metal is one whose concentration in seawater is less than a few parts per billion (ppb). Analysis of such elements is very important for understanding environmental systems as these metals are involved in biogeochemical cycles, can be indicators of the effects of human impacts on the natural environment and can act as water mass tracers (*i.e.* follow the movement of bodies of water) in the study of ocean circulation [1].

Few analytical techniques are capable of the precise and accurate measurements needed for determination of these metals in the nanomolar (nM) and picomolar (pM) ranges in the complex seawater media. Atomic spectroscopy techniques are most popular since they generally have the lowest detection limits, typically ranging between sub-part per million (ppm) to low ppb levels [2]. Inductively coupled plasma atomic emission spectroscopy (ICP-AES), which is a multi-element technique, is used moderately for trace metal analysis but suffers from overlapping emission line interferences and from matrix effects. The most commonly used technique in the oceanographic community is graphite furnace atomic absorption spectroscopy (GFAAS). GFAAS has much lower detection limits than ICP-AES for most metals, but GFAAS has a much slower analytical throughput as it is a single element technique and each measurement takes several minutes due to the length of time needed for sample drying and ashing. The recent analytical technique based on mass spectrometry known as inductively coupled plasma mass spectrometry (ICP-MS) is also widely becoming accepted throughout the analytical community, though it is not yet as common as GFAAS. ICP-MS is a multi-element technique which provides rapid sample throughput, detection limits similar to those of GFAAS, a large working

range, and the ability to make isotope measurements [2]. Even with GFAAS or ICP-MS detection, a separation/preconcentration is still needed for seawater samples.

Conventional separation/preconcentration steps for seawater samples involve both a large volume of sample and a long processing time. For example, a method for gallium uses a 4 litre sample of seawater which is processed over a 24 hour period in a class 100 clean room [3]. Methods which minimize either or both sample volumes and processing time are gaining popularity. Of these, flow injection (FI) methods are finding favour for seawater processing. Sample handling, processing time and sample volumes can be greatly minimized by incorporating concepts and principles of FI to seawater analysis.

With FI methods, samples are enclosed in Teflon tubing, minimizing the contact between the sample and the laboratory environment. Minimal contact of the sample with environmental contaminants during processing is vital. Potential sources of contamination in the field and laboratory include bacteria, dust and/or rust present in the air and on clothes of laboratory personnel.

Adapting existing methods to FI involves extensive miniaturization. The sample volume is greatly minimized such that only millilitres are needed. Because the sample is continuously moving, FI methods can be used on-line to separate/preconcentrate trace metals with a variety of detectors.

It would be ideal for trace metal analysis if all processing and detection could take place *in situ* and yield real time multi-elemental results. Samplers exist which measure single elements in real time, but have no facility for preconcentration. Shipboard methods exist which permit preconcentration, but these typically have single elemental detection.

This thesis will detail the development of a prototype *in situ* sampler for multiple sampling of a variety of elements from seawater per sampler

deployment, and the development of an on-line FI-ICP-MS system used to preconcentrate and analyze Mn, Ni, Cu, Zn, Ga, Nb, Cd and Pb in stored seawater samples.

Chapter 1 contains an introduction to trace metal behaviour in seawater and a detailed description of the aforementioned trace metals. This chapter also details the evolution of FI methods for seawater, the use of the ICP-MS, and gives examples of present day on-board trace metal measurements and *in situ* analyzers. Chapter 2 presents a detailed description of the development of a new *in situ* sampler for extracting trace metals from seawater. Chapter 3 describes the development of the on-line FI-ICP-MS system used to analyze the metals which was designed and constructed in-house. The results obtained from the analysis of stored seawater using the FI-ICP-MS system will be discussed in Chapter 4. Finally, conclusions resulting from the whole body of work, and potential future experiments will be detailed in Chapters 5 and 6.

1.2 Distributions of Trace Metals of Interest in Seawater

1.2.1 General Overview

The behaviour of metals in seawater is complex with dissolved salts comprising between 2.8 to 3.8 % by weight of seawater [1]. The oceanic distributions and biogeochemical behaviour of dissolved metals are controlled by the complex interactions between inputs, internal cycling and removal processes, coupled with physical transport and mixing within the oceans.

Elements enter the oceans through a variety of sources at the boundaries. For example, rivers are a major source of Cl, Ba and Ca, but are not a significant source for Fe [4-5]. The sources for some elements can also act as sinks (*i.e.* removal) of other elements. The atmosphere is a source of gases, including CO₂, O₂ and N₂ [6,7]. The atmosphere is also a source of

trace metals (e.g. Al and Pb) as winds carry continental dust to the sea [6-9]. The atmosphere also acts as a sink for Na due to salt spray being transported to land. Hydrothermal vents in the ocean floors are a source of Li, Rb, Mn and Fe but a sink for Mg, F, and S [10, 11]. Sediments and pore waters, which are contained within the sediments, are a sink for many elements. Elements can also undergo biological and physical interactions within the ocean.

Some elements are utilized by phytoplankton and grazing zooplankton [12]. The subsequent sinking and decomposition of dead phytoplankton and the production of fecal pellets by grazing zooplankton are sources of particles, which are also important in controlling the distribution of some trace metals. Particles may also adsorb many trace metals as they sink. Eventually, the particles either redissolve at depth, freeing bound metals back into the ocean or are buried within the sediments, thereby acting as a sink [13-15].

These interactions also control the average length of time an element resides within the oceans before it is removed. Oceanographers estimate this residence time by assuming that the ocean is a uniformly mixed reservoir at steady state [16]. The residence time of an element (τ) is defined as the total amount of that element in the ocean divided by either the rate of its supply to the sea or its rate of removal, *i.e.*,

$$\tau = \frac{A}{\left(\frac{dA}{dt}\right)_{s \text{ or } r}} \quad (\text{eq. 1.1})$$

Where A is the amount of the element dissolved in the ocean and $(dA/dt)_{s \text{ or } r}$ is the amount introduced or removed each year. Elements which are reactive can not be assumed to be fully mixed within the ocean. Therefore residence times

which are calculated to be less than the ocean's mixing time (ca. 1000 years) indicate element reactivity.

To elucidate the interactions of an element and to discern its behaviour in the oceans, it is useful to look at variations in concentration as a function of depth at a given location (*i.e.*, a depth profile). Generally, depth profiles can be described as one of (or in some cases a combination of) three distribution types: conservative, nutrient-type and scavenged (Figure 1.1).

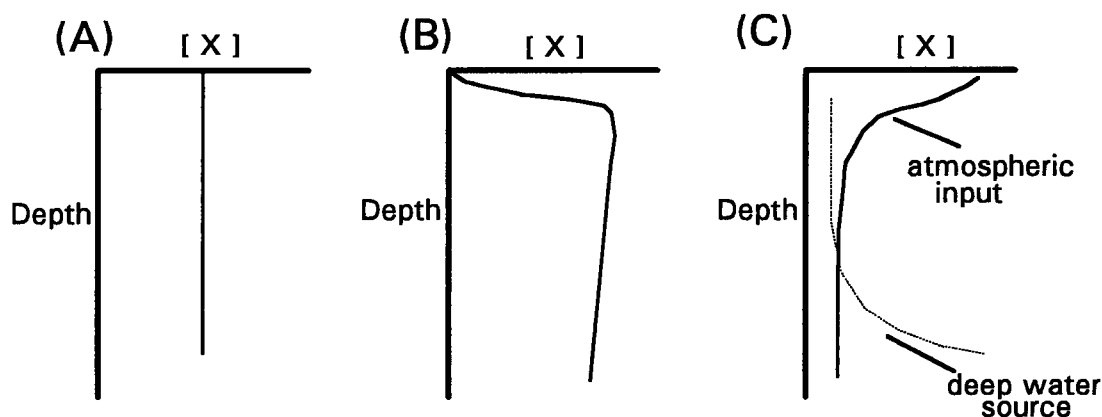


Figure 1.1 The three major distribution types:
(A) Conservative. (B) Nutrient-type. (C) Scavenged.

Conservative elements have concentrations that vary only with salinity. These metals are present in higher concentrations in the oceans relative to their crustal abundance, are removed slowly from the oceans and thus have long residence times. While almost all the major elements which exist in millimolar range (e.g. Na, K, Mg and Cl) behave in this manner, only a few trace elements have conservative distributions, e.g., U and Cs.

Some trace metals, such as Cd, Ni and Zn, exhibit nutrient-type behaviour in that they show a strong correlation with macronutrient distributions (*i.e.*, phosphate, nitrate and silicate). Vertical distributions of these elements show a surface depletion due to biological uptake, and an increase to a mid-depth

maximum which may then decrease slightly with depth. The maximum is due to the decomposition of sinking organic matter and fecal pellets which release nutrients and associated metals at depth. There are two general types of nutrient distribution based on whether an element correlates with either hard or soft part macronutrients (shell formation or metabolism, respectively).

Scavenged elements, such as Al and Pb, are rapidly removed from the water column, primarily by adsorption onto sinking particles. Metals with this type of distribution strongly reflect their external sources with their concentrations rapidly decreasing with distance from that source. These metals have short oceanic residence times (i.e. less than 1,000 years), differ in concentration in different ocean regions and have low concentrations relative to their crustal abundance. Scavenged metals are valuable as tracers for elucidating the transport and mixing mechanisms in the oceans.

The ability to measure trace metals accurately in seawater, over the last 20 years, is a result of the realization of contamination controls during all seawater handling stages and the advent of analytical instrumentation with sufficient sensitivity and selectivity for measuring these elements. Trace metal analysis requires careful planning for sample collection, storage, preconcentration/matrix separation processes to extract trace constituents from major ions, and determination. Minimizing contamination risks is of utmost importance for reliable trace metal data. Many trace metals are present in terrestrial sources, *i.e.*, dust, and in the ship's environment (*e.g.*, rust) in levels much higher than seawater. Reasonable avoidance of contamination was not fully realized until the late 1970's with the development of a clean method for sampling lead by Schaule and Patterson [9]. By 1979, Bruland *et al.* [17] developed clean seawater sampling utilizing Teflon-coated Go-Flo bottles attached to Kevlar line, and clean seawater handling by filtering seawater at sea

in a special clean area on board ship. Further processing is then carried out in shore based laboratories in Class 100 clean rooms requiring acid cleaned bottles, specially designed equipment and ultra pure reagents.

The most common analytical methods used in trace metal analysis involve preconcentration and matrix separation steps, such as ion-exchange or chelating resins, solvent extraction or co-precipitation, with detection by GFAAS or ICP-AES [1,18-30] or more recently, ICP-MS (which is discussed in detail in section 1.4). Even with preconcentration, detection of most trace metals can still prove difficult. Other methods used for trace metal preconcentration and detection are differential pulse anodic stripping voltammetry (DPASV) and differential pulse cathodic stripping voltammetry (DPCSV) [31-33].

Bruland [18] used dithiocarbamate extractions and Chelex-100 ion-exchange for determining Cd, Zn, Ni and Cu in the North Pacific using GFAAS detection. Dithiocarbamate extraction with GFAAS detection has also been used to preconcentrate Cd, Cu, Fe, Ni and Zn in samples from the North-east Atlantic and Al, Cd, Co, Cu and Ni from waters collected near the British Isles [19, 20]. Extractions using 8-hydroxyquinoline (8-HQ) have been used for Al and Mn in samples from the Pacific [21, 22]. Chelex-100 has also been used for Pb, Cd, Co, Cu, Mn, Ni, Fe and Zn in different seawater samples [23-25]. Ion-exchange methods using 8-HQ bonded onto different backbones have also been used, including 8-HQ-TSK (a vinyl polymer agglomerate resin gel) to extract Al, Mn, Fe, Co, Cu, Cd and Cd from seawater [26] and 8-HQ bonded to silica (8-HQ-silica) and other polymer supports to preconcentrate Cd, Pb, Zn, Cu, Fe, Mn, Ni and Co [27, 28]. Co-precipitation has also been used for Cu and rare earth elements (REEs) [29, 30]. DPASV has been used to measure Cd, Cu, Pb and Zn in seawater, and DPCSV has been used for Cu and Zn [31-33].

With the difficulty involved in taking replicate samples at each sampling location, an alternative criterion for accepting the validity of trace element measurements is commonly used. This criterion is the concept of oceanographic consistency [34]. Oceanographically consistent data show smooth variations that are related to known physical, chemical and biological processes. Thus, the concept requires that trace metal concentrations change smoothly with depth in the open ocean due to the long mixing time of seawater and the long distances between strong trace element sources at the oceans' margin and interior.

1.2.2 Zinc, Cadmium and Nickel

Cadmium, nickel and zinc are discussed together as they all exhibit nutrient-type distributions in seawater and their concentrations in seawater are controlled by internal cycling. Though some of these elements do play active roles in biological systems, their distribution in the oceans may be controlled primarily by other indirect mechanisms. Zn is a biologically important trace metal, and next to iron perhaps the second most important essential trace element. It is present in many enzymes involved in carbohydrate, lipid and protein metabolism [12,35]. Directly below Zn in the periodic table is Cd. While Cd has a similar distribution type as Zn, it is not known to be biologically essential [18, 36]. Nickel, a first row transition element, is biologically essential and is found in some proteins [12].

While these three metals have similar distribution types in seawater, they have different ocean chemistries. In general, the vertical profiles of these three metals show a surface depletion, increasing concentrations with depth, reaching a maximum coherent with the nutrient maxima. Below this maximum, the concentrations of these dissolved metals decrease slightly in the deep sea, due

to deep ocean circulation patterns and the intensity of respiration. A more detailed background will now be given on each of these elements.

1.2.2.1 Zinc

Zinc is a first row transition metal which exists as a divalent ion in seawater, primarily as a mixture of its free ion, hydroxy-, carbonato- and chloro-complexes. Its concentration ranges from ca. 0.05 to 9 nmol/kg (0.003 - 0.6 ppb). The first contamination free and oceanographically consistent data for Zn were reported in 1978 by Bruland *et al.* [35] using two different concentration techniques - a dithiocarbamate organic solvent extraction technique and a Chelex-100 resin ion-exchange resin, and analyzed using GFAAS. The distribution of Zn is highly correlated with that of silicate, a major nutrient in the oceans [35, 37, 38]. Silicate is found in opal, which is used by some organisms to construct protective hard shells. Silicate and Zn are involved in a deep regeneration cycle (e.g., have concentration maxima deeper in the water column than "soft part" nutrients, such as phosphate and nitrate), as it takes a longer time for the shells to dissolve as they sink towards the ocean floor. This is a little surprising since Zn is important in soft part processes. Clearly Zn involvement in hard part cycles is the dominant control.

1.2.2.2 Cadmium

Cadmium is a second row transition metal, directly below Zn in the periodic table. It is divalent in seawater and primarily exists as chloro-complexes in the oceans and is a non-essential element, though it exhibits a nutrient-type distribution. One explanation is that Cd may be taken up by phytoplankton in their quest for Zn in low Zn regimes [39, 40]. The oceanic concentrations of Cd range between 1 pmol/kg and 1 nmol/kg (0.0001 - 0.1 ppb). Its oceanic distribution is dominated by its involvement in a shallow regeneration

cycle similar to the soft part nutrients, PO_4^{-3} and NO_3^- , thus its maximum concentration is correlated to that of these nutrients. The distribution of Cd in the Pacific was first determined in 1976 [41] using a method based on the co-precipitation of Cd with dithiocarbamate followed by GFAAS determination.

1.2.2.3 Nickel

Nickel is a first row transition metal and is divalent in the oceans, existing primarily as the free hydrated ion and chloro- and carbonato- complexes. The concentration of Ni in seawater ranges between 2 and 12 nmol/kg (0.1 - 0.7 ppb). The first oceanographically consistent profiles for Ni were obtained in 1976 [42] using a co-precipitation method with GFAAS detection. The vertical profile for Ni obtained was found to be similar to those of the micronutrients indicating involvement in the biogeochemical cycle, with Ni being regenerated both at shallow depths, like NO_3^- and PO_4^{-3} , and in the deep waters, like silicate [18,37,38].

1.2.3 Copper

Copper is a first row transition metal and in seawater is a divalent ion primarily existing as the carbonato- and hydroxy- complexes, as the free hydrated ion and in organic complexes. Copper concentrations in seawater range from 0.5 to 6 nmol/kg (0.03 - 0.4 ppb). While it is a required micro-nutrient in seawater, its distribution in seawater is unique, exhibiting nutrient type behaviour in the surface waters, removal in intermediate and deep waters, and a bottom water source [18, 43]. The first consistent results for Cu in seawater were reported in 1977 [44] using co-precipitation and GFAAS detection.

Vertical profiles of dissolved Cu are controlled by internal cycles, showing a surface depletion with a linear increase in concentration towards the bottom. The apparent deviation from a typical nutrient type profile is due to *in situ*

scavenging in the deep waters. With this type of distribution, a simple advection-diffusion model can be used to estimate the (first order) scavenging removal rate in deep waters [29]. The residence time of Cu in the deep waters has been reported to be roughly 1000 years [18, 29, 43].

1.2.4 Lead

Lead is a heavy metal and is a divalent ion in seawater, existing as the chloro- and carbonato- complexes. The concentration of Pb in the open ocean ranges between 5 and 175 pmol/kg (0.001 - 0.04 ppb). It is a non-essential and potentially toxic metal. Its distribution in seawater is driven by scavenging removal processes and external inputs primarily due to anthropogenic sources, specifically atmospheric inputs of alkyl leaded gasoline [9, 45, 46]. The first reliable data for Pb distributions in seawater were obtained in 1976 [9] using isotope dilution mass spectrometry detection.

Once introduced into the ocean, Pb is rapidly removed via scavenging which results in decreased concentrations the deep sea. With the declining use of leaded gasoline over the last 20 years, Pb surface concentrations have been decreasing, resulting in a subsurface maximum in most regions [9]. The extent of anthropogenic perturbation of Pb is unique among trace element distributions known to date, but does have an analogue in the distributions of nuclear bomb-produced radionuclides (^{137}Cs and ^3H).

1.2.5 Manganese

Manganese exists in seawater primarily as the free hydrated Mn^{+2} ion and as its chloro- complexes. The sources of Mn into the ocean are riverine, atmospheric and submarine hydrothermal inputs [22, 47-50]. Dissolved Mn concentrations range from 0.2 to 3 nmol/kg (0.01 - 0.2 ppb) . Manganese participates in a wide range of biogeochemical processes, including being

released from aeolian particles in surface waters [22, 47] and adsorbed onto sinking particles [49]. It is also a required micro-nutrient and involved in internal cycling [47, 49]. The first geochemically consistent study of Mn in seawater was reported in 1977 [50] using neutron activation analysis (NAA) and GFAAS.

Manganese can exist in a variety of oxidation states under different environmental conditions. In sub-oxic or anoxic water (water with O_2 concentrations $\leq 10 \mu\text{mol}$), it exists as dissolved Mn (II). Although Mn (II) is thermodynamically unstable in oxic waters, it is kinetically inert and thus is slowly oxidized to insoluble Mn (III, IV) oxyhydroxides. The oceanic distribution of Mn is dominated by external sources, resulting in maxima in the surface waters and in the deep ocean near hydrothermal regions. Internal cycles which produce an oxygen-minimum zone also results in dissolved Mn maxima [51].

1.2.6 Gallium

Gallium is a multi-isotopic metal, which lies below Al in the periodic table. In seawater it is a trivalent ion which exists as hydroxides, i.e., $\text{Ga}(\text{OH})_3$ and $\text{Ga}(\text{OH})_4^-$. The first set of Ga data, published in 1958, which used a co-precipitation method with spectrophotometric detection, indicated that the element concentration in seawater was *ca.* 0.4 nmol/kg [52]. With the advent of trace metal clean sampling and handling techniques and the availability of advanced instrumentation, recent results using GFAAS and ICP-MS detection after preconcentration using 8-HQ on TSK showed that Ga actually exists in seawater at low picomolar concentrations (10 to 50 pmol/kg) [3, 53, 54].

The primary source of Ga to the open ocean may be atmospheric inputs of crustal dust to the surface water and diffusion out of the sediments and/or a sediment surface remineralization source to the deep water [3, 54]. Vertical distributions of the element in these more recent studies show a sub-surface

maximum, low concentration in the intermediate waters and increasing levels with depth into the deep water. The sub-surface maximum may be caused by either horizontal advection and/or a vertical process involving exchange with sinking particles. These profiles of dissolved Ga suggest complex controls including multiple sources, reversible exchange and scavenging processes all contributing to the distribution of dissolved Ga in the ocean.

1.2.7 Niobium

Niobium sits directly below vanadium in the periodic table. It is thought to exist in seawater in the +5 oxidation state, primarily as $\text{Nb}(\text{OH})_6^-$. The only known data on Nb in seawater are from 1958 where Carlisle and Hummerstone analyzed two filtered samples from the English Channel and found values ≤ 0.5 nmol/kg [55]. Naturally occurring Nb and radioactive ^{95}Nb , an important fission product in fallout, have been found to bioaccumulate in terrestrial plants, marine plants, molluscs and fish [56,57]. In fish, ^{95}Nb was apparently found to be bound organically in viscera [57].

1.3 Flow Injection Analysis

Most manual methods of analysis undertaken in research laboratories involve the handling and processing samples in the form of liquids. Many of these methods involve repeated steps for each sample before an analysis can be made. Some methods involve the use of potentially hazardous chemicals or environmentally sensitive compounds. Over the last 20 years, many manual methods involving repetitious steps and/or the handling of sensitive or hazardous chemicals have been successfully automated with the development of flow injection analysis.

Flow injection analysis (FIA) has been demonstrated as an ideal tool for handling and processing samples prior to their determination [58]. Sample

handling using FIA may be as simple as transporting the analyte to the detector or as complex as a solvent extraction, a reaction and a back extraction of the analyte prior to detection.

Simple FIA consists of pump(s), tubing, an injection valve and a flow through detector. The most common means of propulsion in FIA is the peristaltic pump. Examples of FIA manifolds are shown in Figure 1.2.

FIA is based on a combination of three principles: sample injection, controlled dispersion of the injected sample zone and reproducible timing of its movement from the injection point toward and into the detector. Applying FIA to automated chemical analysis results in a versatile system which yields fast, precise and accurate results. Systems using FIA have improved repeatability, lowered reagent and/or sample consumption and shortened analysis times [58, 59] when compared with batch sample handling.

Using FIA systems, reproducible timing is possible for repeated injections of sample(s), stream switching, reaction and detection operations. Each sample in a FIA system is under identical conditions at identical points in the system. Therefore, the sample can be measured at one point even if the reaction has not gone to completion or if the analyte is unstable. Separation techniques such as liquid-liquid or liquid-solid extractions which may have less than 100% sample recovery can still give highly reproducible and quantitative results.

A FIA system also provides a means of carrying out an analysis in a closed system. This allows the use of materials which are toxic or unstable in air as they are not exposed to the user or the environment. This also enables the analysis of samples such as trace metals in seawater which can be easily contaminated in an open laboratory environment.

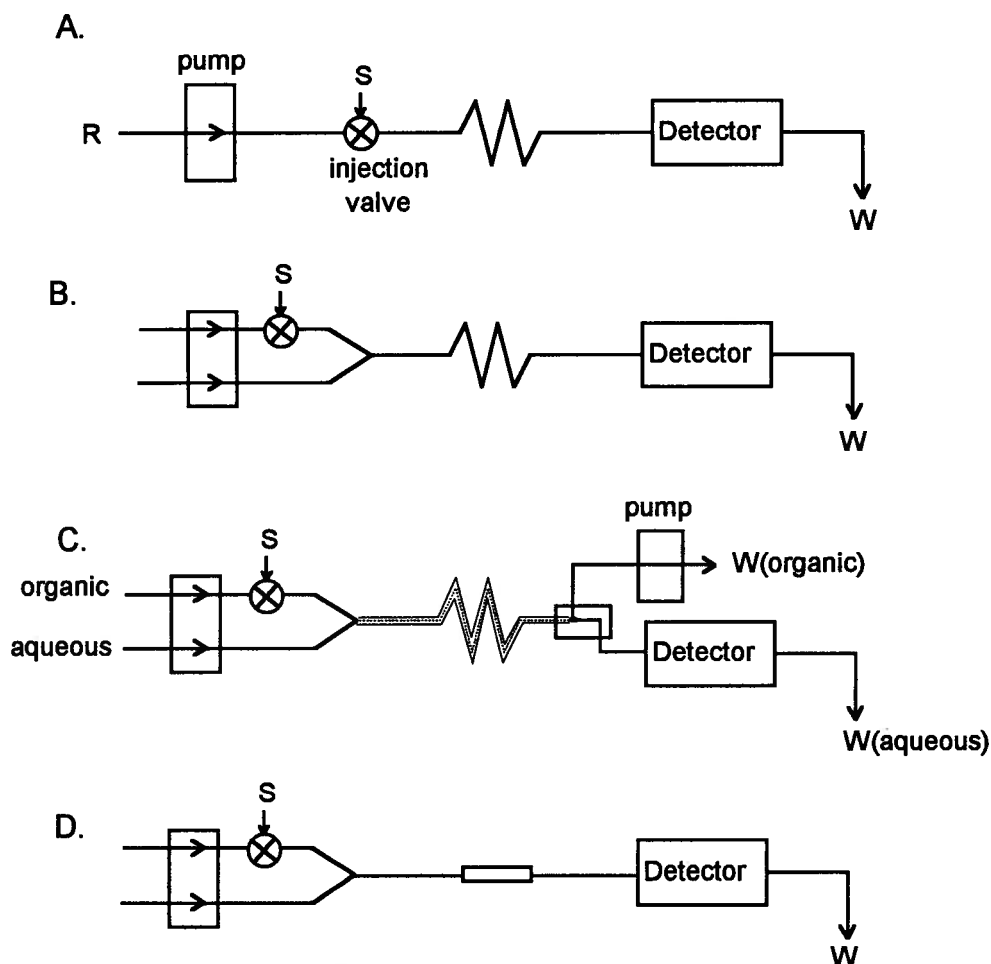


Figure 1.2 Types of FIA manifolds:
 A. Single line. B. Two line with single confluence point.
 C. Solvent extraction. D. As (B.) but incorporating a packed reactor.

1.3.1 Introduction and History

The term *flow injection analysis (FIA)* was first used by Ruzicka and Hansen in 1974 [60]. FIA can be considered a branch of continuous flow analysis (CFA). An older and more established form of CFA is air segmented continuous flow analysis (ASCFA). In ASCFA samples are separated by either air bubbles or inert fluid when first sampled. This breaks the stream into many smaller, nominally identical segments. Appropriate reagents are added and the

product is detected typically by a colorimeter once a “steady state” is reached between the sample and reagents. Since the air bubbles are compressible, highly reflective and electrically non-conductive, they can severely distort the analytical signal. This distortion can be removed by using a cell volume less than the sample volume, removing the bubbles prior to measuring the sample or digitally discriminating the bubbles and sample using either the difference in reflectivity or conductivity and reproducible system timing. While the presence of air bubbles does have drawbacks, positive effects are also found. The presence of air bubbles in the stream limits sample dispersion, promotes mixing of the sample and reagents by generating turbulent flow and also scrubs the inner walls of the analytical conduits.

In FIA, individual samples are injected into a moving, non-segmented continuous stream. Nagy was the first to use sample injection into non-segmented flow streams in electrolyte experiments in 1970 [61]. In 1974, Ruzicka and Hansen [60] and Stewart *et al.* [62] independently demonstrated the advantage of flow-induced sample dispersion as the sample carrier stream is pumped through narrow bore tubing. This affected the controlled mixing of the sample with the stream resulting in a transient response. They proved that CFA without air segmentation is possible and that the “steady state” assumption inherent to ASCFA is unnecessary. Since its inception, over 3000 papers on FIA have now appeared in the literature, the majority concerned with replacing conventional manual procedures with FIA systems.

1.3.2 Channel Geometry in FIA

The analyte signal in FIA is normally in the form of a peak, its height, width or area related to concentration. The FIA peak is a result of two kinetic processes which occur simultaneously when the sample is injected into a

reagent stream. The first is the physical process of zone dispersion which is well reproduced for each individual injection cycle. This results in a concentration gradient of sample within the sample stream. The second is the chemical process(es) which result from reactions between sample and reagent species.

Different geometric forms of the FIA microreactor have been used to increase the intensity of radial mixing. This reduces the parabolic velocity profile in the axial direction and results in the reagent becoming more readily mixed with the sample. The different geometries are straight, coiled, knitted and single bead string reactor. These are illustrated in Figure 1.3.

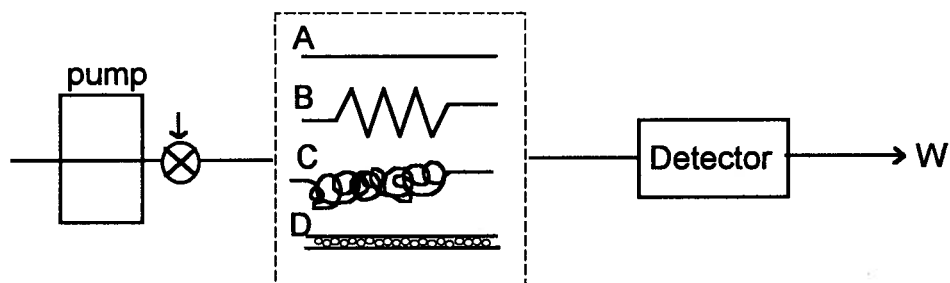


Figure 1.3 Schematics of the most commonly used microreactor geometries found in FIA applications:
 A. Straight open tube. B. Coiled tube. C. Knitted reactor.
 D. Single bead string reactor.

If a straight channel (Figure 1.3 A) is used the laminar flow is undisturbed and the radial diffusion is not sufficient to affect the axial dispersion formed during sample injection. This results in an asymmetrical peak. The coiled geometry (Figure 1.3 B) is the most common and when used causes secondary flow within the coiled tube which promotes mixing in the radial direction and yields a more symmetrical peak [63]. The "knitted" reactor (Figure 1.3 C) is a result of tightly and irregularly knotting an appropriate length of tubing [64]. This tubing configuration causes the carrier stream to move in a chaotic manner

which effectively promotes radial dispersion. All these reactors have the same surface to liquid ratio.

The single bead string reactor (SBSR) (Figure 1.3 D) is the most effective device for promoting radial mixing in a tubular reactor [58]. It was originally used in post column derivatization [65] and was introduced to FIA by Reijn *et al.* [66]. The SBSR consists of packed glass beads in a piece of FIA tubing. It allows symmetrical peaks to be obtained within the time domain and channel length of a typical FIA experiment and prevents peak broadening. Due to the presence of the beads, the surface to liquid ratio is very high. This is beneficial if liquid-surface interaction is desirable, as when using immobilized reagents, enzymes or packed reactors.

1.3.3 On-Line Matrix Separation and Preconcentration

Packed reactors subject an injected sample to appropriate on-line pretreatment in order to facilitate the detection of the analyte [67]. Different materials have been used in these packed reactors or columns. Ion-exchange resins have been used to preconcentrate an analyte or remove any background matrix components which could interfere with the analysis.

In FIA preconcentrations, the dispersion of the injected sample is reduced by first introducing a relatively large volume of sample solution from which the analyte is retained on an incorporated miniaturized packed reactor (e.g., a microcolumn), and then released, normally in a much smaller volume, and passed through a detector. This was originally proposed to enhance the sensitivity of the measurement of trace cationic elements in very dilute aqueous samples in flame atomic absorption spectroscopy (AAS). The system involved a single-line, two valve FIA system with a packed reactor downstream from both valves but before the detector [68].

Many methods have been published using a variety of resins and more complicated manifolds, [e.g. 69-71], including a two directional operation of a microcolumn when loading sample to prevent matrix material from entering the flow through detector [72]. Other refinements include the use of time-based injections for sample, where the sample is loaded onto a microcolumn for a set period of time [69]. Multi-elemental determinations were also made using ICP-AES detection [72].

1.3.4 FIA and Seawater

FIA is suited to the analysis of metals in seawater since the sample is entrained in narrow bore poly fluorocarbon tubing (*i.e.*, Teflon), protecting it from any surrounding contamination sources and minimizing sample volume. Teflon is an inert fluoro-polymer which, once cleaned, is free from contamination. FIA has been used in combination with many detection methods for determining a number of trace elements from seawater. It has been employed for on-line sample processing, particularly sample preconcentration and matrix separation by incorporating an ion-exchange or chelating resin in the manifold.

A number of methods using FIA for on-line preconcentration and matrix separation have been developed with a number of detectors for single element measurements from seawater. Chemiluminescence has been used with FIA to measure Co, Fe and Mn [73-75]. Manganese has also been measured using a spectrophotometric method after on-line preconcentration using FIA [76]. These detectors can also be used for ship board work since they are robust. The use of FIA for on-line preconcentration reduces exposure of the sample to potential contamination from the ship. Together they provide the scientist tools to analyze metals from seawater soon after sample collection.

On-line preconcentration methods using FIA have been coupled with atomic absorption spectrometry (AAS) and ICP-AES detection for the multi-elemental determination of some first row transition and heavy metals. Fang *et al.*, measured Cu, Zn, Pb and Cd using Chelex-100 for preconcentration, resulting in up to a 105 fold concentration and a sampling frequency of 60 samples per hour using a dual column FIA manifold with flame AAS detection [71]. Another method used ICP-AES detection to measure Cu, Co, Cd, Pb and Zn in seawater after on-line preconcentration using 8-HQ immobilized on porous glass [69]. More recently, FIA has been used for on-line preconcentration and matrix separation of trace metals from seawater with ICP-MS detection [77,78]. More details are given in section 1.4.4.2.

1.4 Inductively Coupled Plasma Mass Spectrometry

1.4.1 History of the ICP-MS

The concept of combining a plasma as a source of ions with mass spectrometry detection for trace metal analysis was developed by A.L. Gray in 1970 [79]. Initially, this was developed as a tool for geologists who found that inductively coupled plasma atomic emission spectroscopy (ICP-AES) gave poor results for many elements of geological importance (e.g., the rare earth elements). ICP-AES is plagued by complex spectra and poor detection limits for many elements. Matrix interferences from line-rich elements such as calcium and aluminum and easily ionizable elements such as sodium and potassium are also a problem. Gray demonstrated a direct current plasma-mass spectrometry (DCP-MS) technique for determination of trace metals in solution. While DCP-MS gave low backgrounds and simple spectra, it was evident that the DCP was a far from ideal source. It suffered from poor sample volatilization, dissociation and ionization.

Inductively coupled plasma mass spectrometry (ICP-MS) was first proposed in 1975. In 1977 the Ames Laboratory in the US collaborated with the British Geological Survey to develop the technique. In 1980, Houk *et al.* [80] produced the first spectra of Ar^+ , H^+ and O^+ from the ICP. Later, spectra of analyte ions (i.e., Mg^+ , Cr^+) were produced. The first commercial instrument was introduced by SCIEX at the 1983 Pittcon analytical conference, with VG instruments introducing theirs shortly after.

1.4.2 Instrumentation Overview

An overall schematic of the ICP-MS system is shown in Figure 1.4. The liquid sample is pumped by a peristaltic pump into the nebulizer where an aerosol is formed. The aerosol droplets from the nebulizer are separated according to size in the spray chamber. Small droplets are not condensed or impacted on the double-pass spray chamber walls but are transported to the ICP by the argon carrier gas. The larger droplets are prevented from reaching the plasma since they may not completely desolvate in the plasma and thus contribute to water loading. Typically only ca. 1% of the sample solution actually reaches the ICP for most basic set-ups.

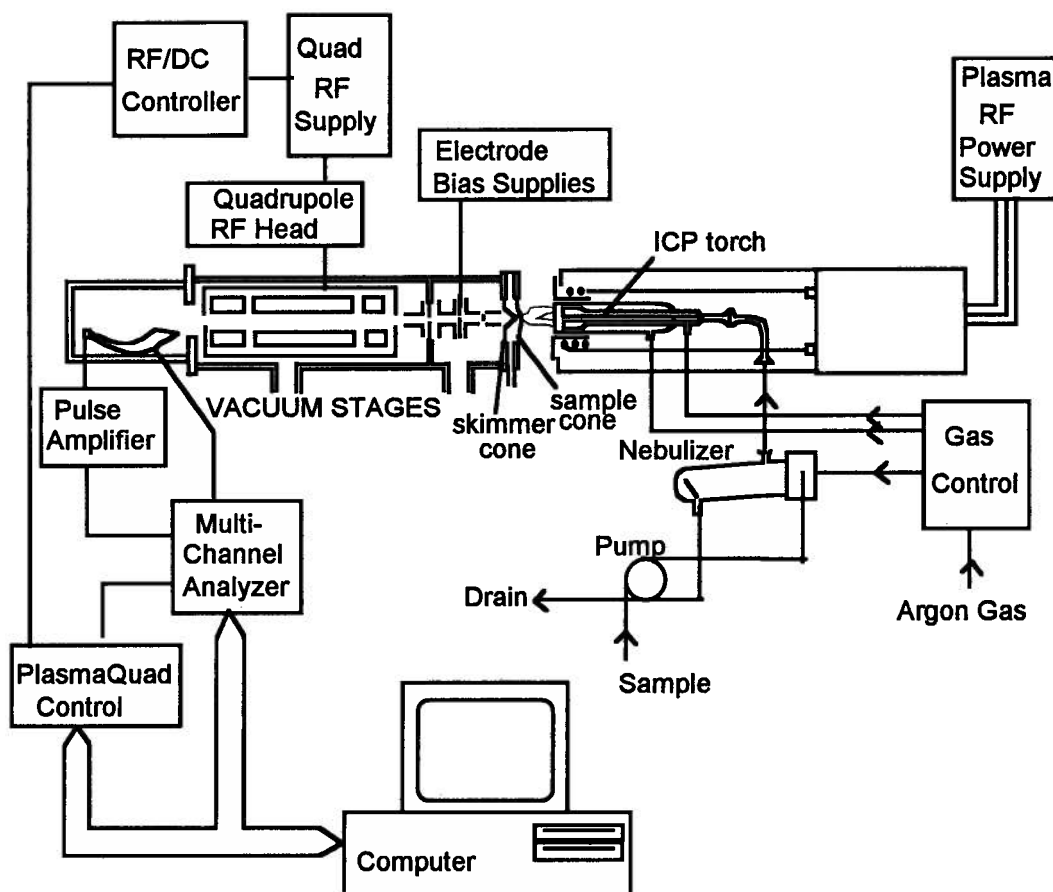


Figure 1.4 A schematic of the VG PlasmaQuad ICP-MS.

In the ICP, the aerosol droplets are desolvated, vapourized, atomized and then ionized, mainly as a result of the high temperatures within the plasma. Some of the ions are then extracted into a high vacuum region in two steps. First the ions from the central channel of the ICP are extracted by the aperture of the sampling cone. Behind the sampling cone, the gas pressures are reduced to about 5 mbar by a rotary pump. The gas expanding into the lower pressure region causes the temperature to drop rapidly preventing further reactions which could change the gas composition. Part of the gas jet formed is extracted into the aperture of the skimmer cone. Beyond this point the gas (containing ionized sample) enters an even lower pressure region ($< 3 \times 10^{-6}$ mbar).

The ions pass through a series of electrodes, or lenses, which focus the ions into the mass spectrometer. The quadrupole mass analyzer operates as a tunable variable bandpass mass filter where ions are resolved (0.5 to 1.0 amu resolution) on a basis of mass-to-charge (m/z) ratio. A full scan of the mass range is accomplished in under a second. Only ions with the selected m/z ratio are transmitted through the quadrupole mass analyzer to subsequent detection by a channel electron multiplier. The channel electron multiplier can operate in either of two modes, pulse counting or analog counting mode. In pulse counting, pulses from individual ions above a set discriminator level are counted. This gives the highest possible sensitivity and is used for samples of sub-ppm concentrations. In analog mode, the electrons are collected by the normal collector electrode and the current is then amplified by a linear amplifier with the applied voltage set at -1500 V. This gives a faster response and is used for samples with ppm or greater concentrations.

The pulses from the detection system are fed to a microprocessor-controlled multichannel scalar data acquisition unit. A second microprocessor looks after the overall instrument operation. The overall system is controlled by a personal computer.

1.4.3 Advantages and Limitations of the ICP-MS

Since the ICP-MS became commercially available, it has been accepted for oceanographic analyses [34]. The advantages of the ICP-MS for trace metal detection over other detection systems are many. It is highly sensitive with detection limits on a par with GFAAS for most elements. It measures multiple elements and isotopes facilitating elemental determinations by isotope dilution. The mass spectra of the analytes are simple with any overlap interferences by other species predictable. It has a working range covering six orders of

magnitude and less than 1 second is required per isotope determination. It also enables one to easily measure refractory elements [34, 81].

Unfortunately, there are also disadvantages to the ICP-MS. It is an expensive instrument to purchase (at present, ca. \$250 k) and expensive to run. Overlap interferences due to plasma and solvent ions can give extremely high backgrounds. These interferences can be from isobaric ions, oxide formation and doubly charged ions. To minimize the formation of oxides and double charged ions, gas flow rate, RF power and ions lens settings have to be optimized. Matrix interferences are also a potential source of high backgrounds or signal suppression. This results in not being able to directly nebulize seawater due to its high salt content (ca. 3%), thus requiring a separation step. While these problems can be severe, generally, the advantages of the ICP-MS outweigh its disadvantages.

1.4.4 Sample Introduction Methods

Sample introduction into the ICP-MS by nebulization has been the weak link in the whole system. Solution nebulization introduces large amounts of O, N, S and Cl from water or acid matrix into the plasma. Tan and Horlick studied the effects of various acid matrices on metals [82]. Nebulizing sampling systems also cannot tolerate high salt matrices which can clog some nebulizers or upon ionization of the matrices within the plasma, cause clogging of the cone orifice [83,84]. While continuous nebulization of concentrated acid (> 5%) into the ICP-MS does not generally affect the nebulizer, it does accelerate cone deterioration [83].

Memory effects can also be a problem if large volumes of samples, or samples with high concentrations of certain analytes are nebulized through the system. Memory effects occur when an element "sticks" to surfaces in the

analyte pathway and slowly comes off over time. This can result in high backgrounds of that analyte until the analyte is completely removed by rinsing the system with concentrated acid for a period of time [85]. Coupling the nebulizer with different sample introduction methods can minimize some of these problems.

1.4.4.1 FI-ICP-MS

The first work using a simple flow injection loop to introduce smaller and discrete samples into the ICP-MS instead of continuous nebulization was carried out by Houk and Thompson in 1983 [86]. Volumes of 50 to 200 μL of a 1% HNO_3 solution with Mg and Ni were injected into the ICP-MS. Detection limits of 2 to 50 mg/L, with a precision of 1 to 3 %, were found. Injection of 100 or 200 μL volumes of a 40 mg/L Mg standard 50 times did not plug the sample orifice. It was also possible to inject urine and serum directly into the ICP-MS with only a five fold dilution.

The use of an FI loop to introduce samples minimizes cone clogging and deterioration and memory effects [83-86]. It is also necessary if only a small volume of sample is present. For example, a method for determining Zr from seawater results in a final analyte volume of less than two mls [87]. The analyte is drawn into a 300 μL FI loop by a pump allowing for a second measurement to be made. Even after injecting this small volume into the ICP-MS, the system needs to be rinsed with 2 N HNO_3 for several minutes to bring the background to acceptable levels and minimize any memory effects before another measurement can be made. Gold was also determined using FI-ICP-MS by incorporating an FI loop after the pump with the sample being drawn into the loop by suction to minimize contamination from the pump tubing [88].

1.4.4.2 On-Line Preconcentration and Matrix Separation with FI-ICP-MS

The use of FIA for on-line preconcentration and seawater matrix separation has also been coupled with ICP-MS detection [77, 78]. Beauchemin and Berman adapted the off-line immobilized 8-HQ-silica method of the National Research Council of Canada (NRC) group [89] for on-line preconcentration by passing up to 10 ml of seawater through a 80 mg resin column to measure Mn, Cu, Co, Mo, Cd, Pb and U. McLaren *et al.* [78], have modified a commercially available chelation concentration system for on-line preconcentration to permit the simultaneous determination of Fe, Mn, Co, Ni, Cu, Zn, Cd and Pb in 5 ml seawater samples in under 10 minutes by ICP-MS. Columns used in this system contained MetPac CC-1 resin, which came with the system, and 8-HQ-silica resin. Accurate determinations for all elements except for Fe and Co were found for both NASS-1 and CASS-3 certified standard seawaters.

1.5 Shipboard and *in situ* analysis

1.5.1 Shipboard Determinations

There are many advantages for performing analyses while at sea. These include checking for sample contamination, providing immediate results which may aid in choosing sampling locations and obtaining data on metal speciation which can change during sample storage [34, 90]. A reliable seagoing method should either physically contain the sample or alter the chemistry of the analyte(s) in the sample to reduce the potential of shipboard contamination. As ship time is expensive [91], minimizing the sample processing and analysis time is desirable. The simplest way to maximize sample throughput is to minimize the volume of seawater needed to preconcentrate the metal(s) for detection. Finally, the seagoing detector must have low detection limits and function well under rough conditions.

Measures and Edmond [92,93] developed a seagoing method based on electron-capture detection gas chromatography (ECD-GC) to analyze Be, Al, As and Se as volatile metal-chelates. This method is also multi-elemental as the GC separates the metal-chelates before they reach the ECD. The same method was adapted by Mugo and Orians to measure Cr (III) and total Cr [90]. Seagoing techniques using DPASV and DPCSV for the speciation of Zn, Cd, Cu, Pb, Co, Ni and Fe have also been developed [31-33, 94].

Flow injection methods using suitable detectors are being accepted as seagoing methods for the same reasons as FI is suited for seawater processing and analysis. Sample and reagent volumes are minimized and the Teflon tubing common to FI manifolds encloses sample and minimizes contact between the sample and the ship environment. Seagoing methods using on-line column preconcentration using flow injection with 8-hydroxyquinoline resin has been used with chemiluminescence detection to measure Co and Mn [73,75] and with spectrophotometry to measure Mn [76].

1.5.2 *In situ* Measurements and Sampling

Long-term monitoring is essential to discern processes which lead to the natural variability in the oceans and to assess the anthropogenic impact on geochemical cycles. Temporal changes in the oceans, including spring blooms, other seasonal activities, etc., require a ship to be present for sampling. The lack of long-term oceanographic studies at most locations severely limits understanding of ocean processes. With the prohibitive costs of operating a modern research vessel [91], and the decreasing availability of ship time, it is becoming necessary to develop remote *in situ* sensing and measurement devices.

In situ measurement systems, which can be moored and operate unattended for long time periods, such as up to one year, are now being developed in order to overcome the lack of long-term monitoring of the ocean. Automated chemical analyzers have met with limited success since they are subject to sensor drift and biofouling, though some progress has been made [95]. Another approach for long-term sensing is the use of chemical sensors [34].

Sensor systems, which use electrodes, fiber-optics or chemical field-effect transistors, are mechanically simple [96]. Currently, the most common chemical sensors use oxygen and pH electrodes [97]. These systems are not used widely for other analytes, because very few chemistries are known which are reversible, have quick response times and have the sensitivity and selectivity to detect analytes at low to sub micromolar concentrations.

Short-term, *in situ* determinations of a series of elements have been done using unsegmented, continuous-flow analyzers, using colourimetric detectors, known as scanners (submersible chemical analyzers) [98]. Nitrate concentrations have been measured *in situ*, to a depth of 2000 m by a scanner tethered to a vessel [99]. Redox species such as sulfide, Mn and Fe have been measured in hydrothermal vents at depths of 2500m by mounting scanners on manned submersibles or towed from a research vessel [100].

Speciation measurements on Zn have also been made *in situ* using thin-film gels. An ion-exchange resin with an ion-permeable gel membrane barrier of known thickness is suspended in natural waters. Quantitative data on concentration and speciation are then obtained over time periods between 1 hour to one week [101].

One limiting factor of these *in situ* analyzers and sensors is that they do not provide simultaneous multi-elemental results. An *in situ* sampler can be

optimized to collect multi-element samples but the collected samples need to be analyzed at a shore based laboratory. Commercially available *in situ* samplers include Axys Instrument Ltd's INFILTREX II [102]. Another sampler (non-commercial) uses a fluidized bed of complexing agent and has been optimized for seven elements (Cd, Cu, Fe, Ni, Mn, Pb and Zn); no results based on this method have been published as yet [103].

Generally, the area of *in situ* samplers for trace metals is a young field. Samplers that do exist are either in prototype stages or are adaptations of existing samplers used for the collection of organics. Rarely do these samplers collect both multi-elemental and multiple samples.

CHAPTER 2: DEVELOPING AN *IN SITU* SAMPLER

This chapter describes the development and evaluation of a new prototype sampler with the capability of multiple sampling for *in situ* preconcentration of trace metals in natural waters. This prototype was modeled on a commercially available apparatus, the INFILTREX II which is manufactured by Axys Environmental Ltd. (Sidney, BC) and was designed in conjunction with Dr. L.E. Bowman of the Chemistry Department, UBC. Initially, the intent was to modify the INFILTREX II for our purposes [104], but it became apparent that a new sampler had to be designed. Detailed descriptions of the INFILTREX II sampler, its operation, limitations and attempted modifications are found in Appendix A.

2.1 Designing the Prototype sampler

The prototype sampler was initially designed to operate at flow rates less than 10 ml/min and have miniature columns for multiple samples, incorporate a buffer or standard solution stream, monitor the flow rate over the course of a sample preconcentration and withstand pressure to seawater depths of 3000 m. The sampler was to be controlled by an on-board computer which could be accessed using another PC, and operate remotely at preprogrammed time intervals.

It was important for the sampler to operate at slow flow rates (e.g. less than 15 ml/min) since in most ion-exchange extractions, including the use of 8-HQ resins, the binding kinetics between the free metal ions in seawater and the chelating resin could result in less than total recoveries at higher flow-rates due to insufficient contact time between the seawater and the resin. Typical flow rates are between 0.5 and 5 mL/min [27, 105 -106]. At faster flow rates,

depending on resin used, the possibility of incomplete metal extraction from seawater may result in artificially low concentration measurements.

The sampler was designed to hold up to six separate columns. This multiple sampling capability would reduce the need to redeploy the sampler when gathering replicate samples, full depth profiles or undertaking temporal variability studies. The columns were miniaturized to decrease the amounts of resin and reagents needed, as well as decrease column blanks.

To preconcentrate trace elements which are not readily extracted at ambient seawater pH, a separate channel was incorporated to allow the addition of a buffer to the seawater stream before it passed through the resin columns. This increases the versatility of the sampler. To determine the volume of seawater through each column without having to physically collect the seawater, the flow rate was monitored during each preconcentration cycle.

2.2 Components of the Prototype sampler

The overall design of the new *in situ* sampler, front and back, is shown in Figure 2.1. Table 2.1 lists the physical components of the prototype sampler, together with a brief description of each component. The circuitry and software necessary for controlling the sampler are described later in this chapter.

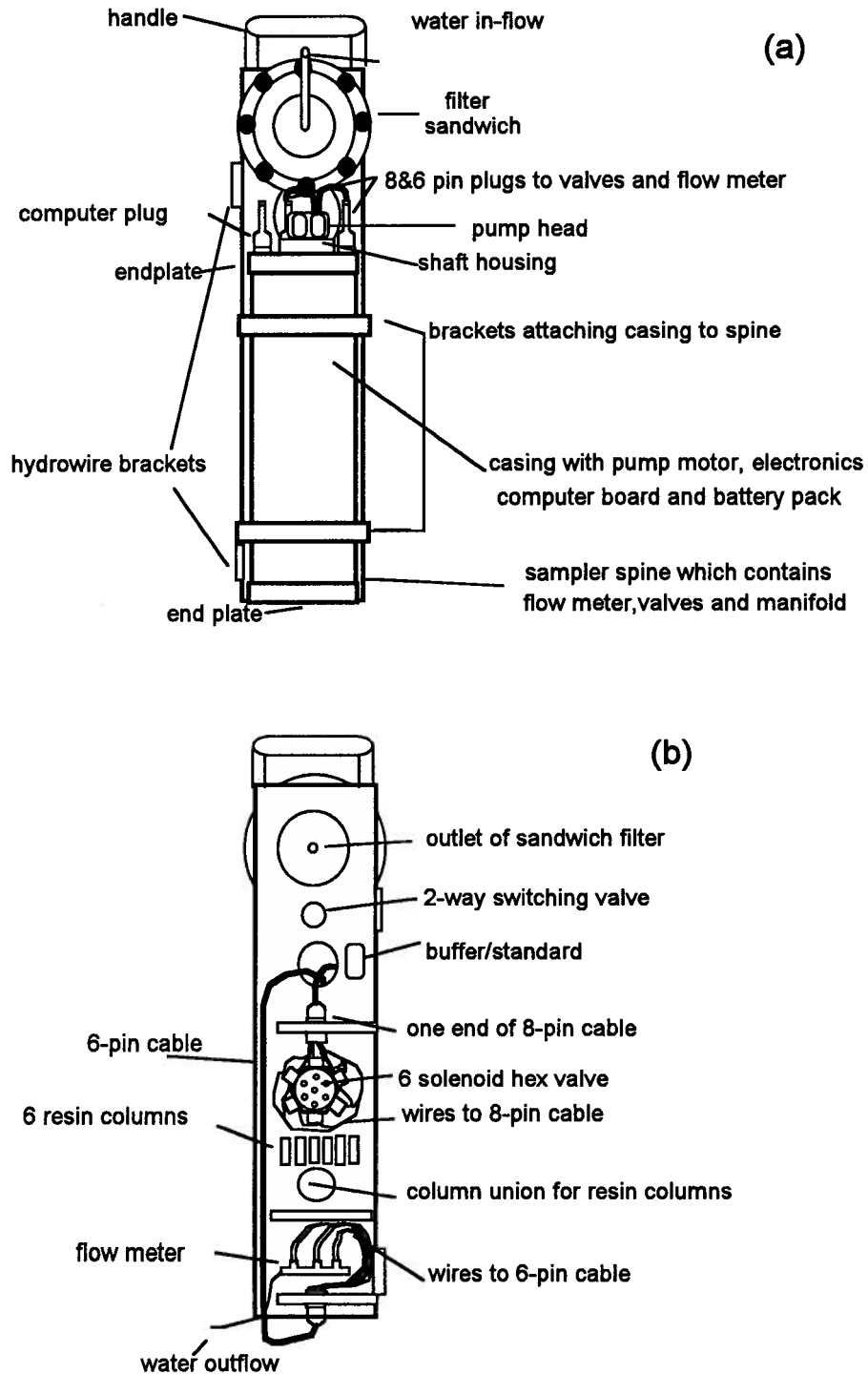


Figure 2.1 A schematic of the prototype sampler
 (a) Front view. (b) Rear view.
 In (b) the Teflon tubing manifold has been removed for clarity.

Component	Description
Computer Board	On-board timer and enough digital I/O to control sampler. Programmed through another PC.
Pump	Peristaltic pump head driven by a gear motor
Valves	(a) One six solenoid normally closed hex-valve (b) One two-way switching valve
Flow meter	Time-of-flight design, using three thermistors
Columns	Mini-columns with resin, also used for on-line work
Casing	Aluminum pressure housing with spine
Pre-filter	142 mm filter sandwich with 0.45 μm filter
Battery pack	45 "D Cells" batteries, 9 sets of 5 in series

Table 2.1 Physical components of the prototype sampler.

2.2.1 Computer Board

A computer board to control the operation of the sampler was sought to use in the prototype sampler. The following criteria were assessed when choosing the computer board:

1. Communication between the computer board and a personal computer must be possible to permit the programming of the computer board prior to deployment. The RS-232 mode of communication was preferred for the prototype system.
2. The computer board must control a number of valves as well as the pump and the flow meter. To accomplish this, the computer board must have at least eight digital input/output lines (digital I/O's).

3. The computer board must contain a timer/counter as this would be required when using the flow meter.
4. The computer board must contain sufficient memory to run the control software and to store any data collected. A minimum of 64 K of random access memory (RAM) was envisaged.

The computer board chosen to control the prototype sampler was a Ziatech ZT88CT01 computer board (Ziatech Corp., San Luis Obispo, CA). Brief details are given below regarding the operation of the computer board. The reader is referred to the manufacturer's instruction manuals for more details [107, 108].

The Ziatech computer board required a power supply of 7 V dc with 0.8 A current. On initialization, the computer board is set with three drives; two (assigned P: and Q:) which are read only memory (ROM) drives and the third (assigned R:) which is a RAM drive and comes with a total of 128 K RAM. The ROM drives contain the operating system. To change any program contained in the operating system (*e.g.*, AUTOEXEC.BAT), that program must be copied to the R: drive and then altered. When the Ziatech board is powered, the R: drive is checked for any altered operating system programs and then any operating system programs not found on the R: drive are run from the ROM drives.

The Ziatech computer board comes with Microsoft DOS 3.3 (Microsoft Inc., Mississauga, ON) in the EPROM, 48 programmable digital I/O lines, a real time clock and a counter/timer. It is accessed by another PC by using an RS-232 serial cable. Once connected to the PC, the Ziatech board installs the C: and A: drives of the PC as remote drives (U: and T: respectively). To test and debug programs using the Ziatech computer board with the PC still connected, an executable version of the program is run from either of the remote drives. If the program is to be tested using the Ziatech computer board only, *i.e.*, the PC is

disconnected, then a different procedure is utilized. Prior to the installation of the program on the Ziatech computer board, a second RAM drive (assigned S:) must be formatted and assigned up to 64 K of the available RAM. The executable version of the program is then copied to this drive. Changes are then made to the operating system programs so that the required program is run on power-up. The interface between the Ziatech computer board and the PC did not function correctly when the operating system installed on the PC was Microsoft DOS version 6 and upwards. Problems were experienced when accessing the remote drive U:, *i.e.*, drive C: on the PC. In any event, the Ziatech board still can read remote drive T: (drive A: on the PC).

All the software written during the development of the prototype sampler, was coded in Microsoft BASIC 7.0 (Microsoft Inc., Mississauga, ON).

2.2.2 Interface Circuitry

Connections between the Ziatech computer board and the electrical components of the prototype sampler are shown in Fig. 2.2. The status of the valves, the pump motor and the length of the heating pulse for the flow meter were controlled via the digital I/O port (connector J7). The signal from the flow meter was monitored using the counter/timer (connector J2). The communications port (connector J6) was used when accessing the computer board by a PC.

The digital I/O lines on the Ziatech computer board defaulted to a HI state (+5 V) on initialization. This was problematic as the valves and pump were powered by this operation. As a result, a program was included in the operating system of the computer board to set the digital I/O's to a LO state prior to operation of the sampler. The source code for this program (HIGHLO.EXE) is

given in Appendix B., together with the source code of the program (SAMPLER.EXE) used to run the sampler.

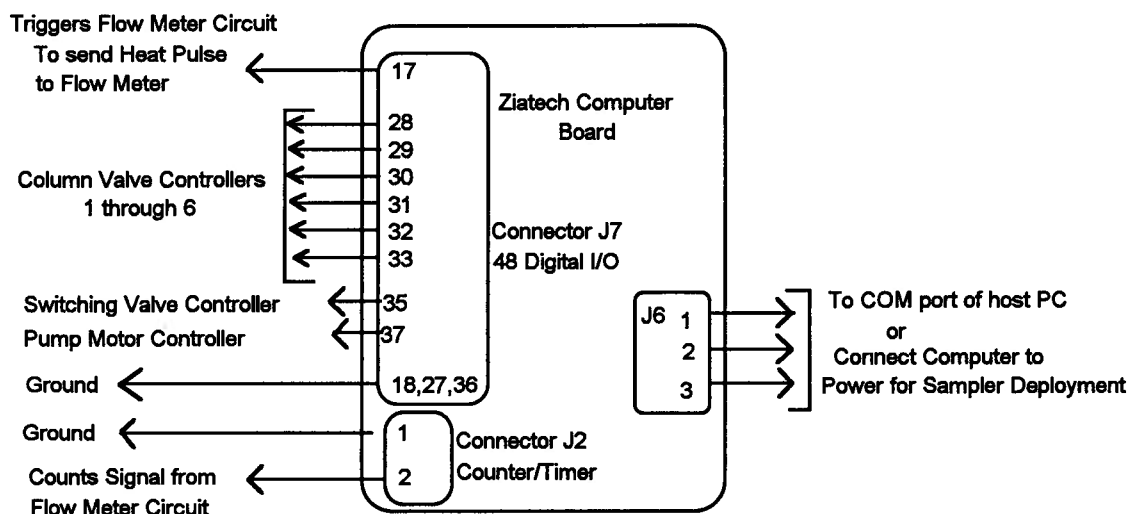


Figure 2.2 A representation of the Ziatech computer board and connections to the sampler component controllers on the electronic circuit board.

2.2.3 Pump Head and Motor

The pump design was based on the *in situ* analyzer, the SCANNER, developed by Johnson *et al.* [98] at Moss Landing, CA. This analyzer has been used to study manganese in hydrothermal vents at depths greater than 2500 m. In the prototype design, a MASTERFLEX[®] size 13 peristaltic pump head (Cole-Parmer Instrument Co., Chicago, IL) was affixed to the outside of the top endplate. The pump head sat on a pump shaft which protruded through the endplate. The pump shaft was rotated by a 24 V brushless gear motor (Pittman, Harleysville, PA), with a 19.7:1 gear reduction, situated inside the pressure housing. A schematic of the pump interface shown in Figure 2.3. This arrangement ensured that the flow manifold was kept at ambient seawater pressure during deployment of the sampler. In this way, the seawater is

preconcentrated at its own pressure and flow problems due to pressure differences in the flow manifold are removed.

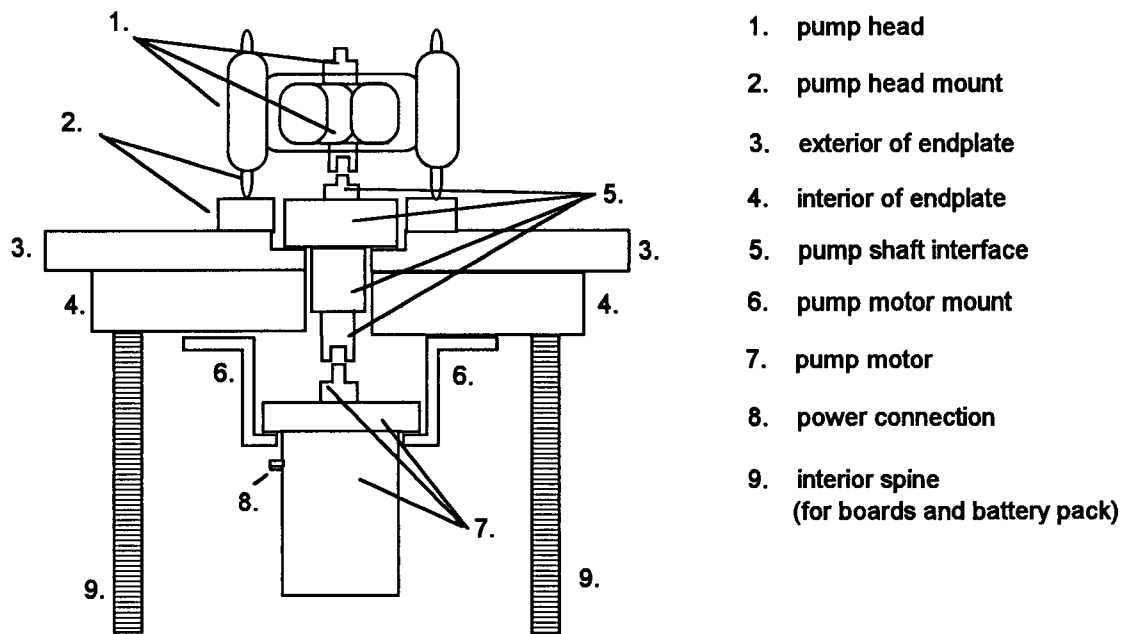


Figure 2.3 Cross section of top endplate to show a schematic of pump head to pump motor connection. Parts not associated with the pump interface have been omitted for the sake of clarity.

2.2.3.1 Pump Shaft

The pump shaft was designed and constructed after much consultation with members of the UBC Dept. of Chemistry mechanical shop. The pump shaft linked the pump head, in seawater, to the pump motor inside the pressure housing. In the oceans, the pressure increases from atmospheric at the surface to atmospheric plus one atmosphere for every 10 m of depth. The pressure inside the pressure housing was at atmospheric. Due to the potential pressure differential between seawater and the inside of the housing, it was necessary to design a special housing for the pump shaft which kept seawater from leaking into the pressure housing, while allowing the pump shaft to turn easily.

Several pump shafts were built using special bearings. These were all tested for several days by placing the water-filled housing under a pressure of 2700 psi, using compressed N₂. The special bearings seal when they are under pressure. Before the pump shaft was used, the bearings were sealed by tightening a series of screws on the top plate of the pump shaft assembly, wherein the bearings are contained. This ensured that the seal was sufficient to prevent the leakage of seawater at shallow depths when the seawater pressure is close to atmospheric. To check the seal, the pump shaft was connected to the motor which was powered by a 15 V power supply. The bearings provided some resistance to shaft rotation, which was quantified by monitoring the current drawn from the 15 V power supply. Experience showed that a proper seal was formed when the current drawn by the motor was between 300 and 400 mA.

2.2.4 Flow Meter Design

The flow meter incorporated into the prototype sampler was based on a thermal-pulsed time-of-flight liquid flow meter developed at Dow Chemical Ltd. for use in liquid chromatography [109]. The flow meter (Fig. 2.4) is essentially three glass-tipped thermistors (Fenwal Electronics, Milford, MA), placed in series. The flow meter was placed downstream of the extraction columns to prevent any contamination of sample due to the glass coating. The heating thermistor (model #121-402EAJ-Q01) was pulsed with 100 mW of power for 400 milliseconds. The sensing thermistor (model #123-802EAJ-P01), placed downstream, sensed the heat pulse. An identical thermistor was added to the flow meter upstream of the other two to monitor the ambient seawater temperature.

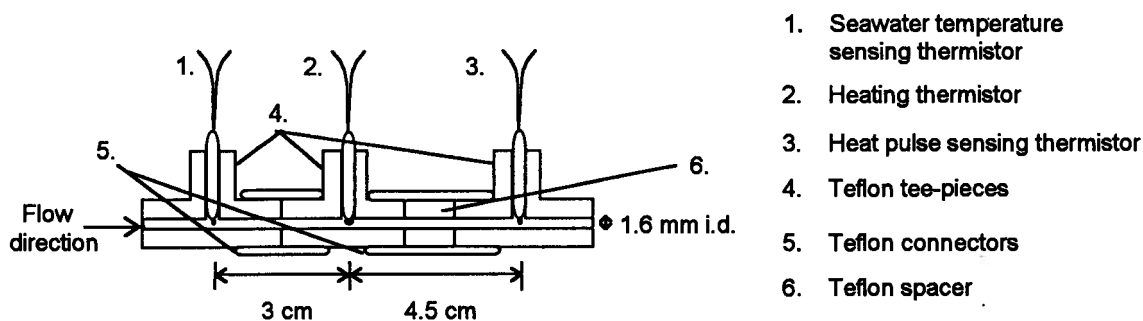


Figure 2.4 Interior of the flow meter hardware.

Each of the three thermistors was imbedded in commercially available Teflon® tee-pieces (i.d. 0.8 mm, Omnifit, Rodchester, NY) using clear marine silicone sealant. Before sealing, the thermistors were placed so their tips were in the centre of the tee-piece junction. Teflon® connectors were constructed to connect the tee pieces in series. The reference and heating thermistors were separated by 3 cm, *i.e.*, the lengths of the arms of the tee pieces. The distance between the heating and the sensing thermistor was 4.5 cm.

The wires from each thermistor were connected to one end of the 6-pin underwater pluggable cable ensemble. The other end connected the thermistors to the flow meter circuitry situated inside the pressure housing. As the flow meter was in contact with seawater and the wires of each thermistor were fragile, it was necessary to minimize corrosion and breakage by covering all exposed wiring with thin plastic and a silicone sealant.

2.2.5 Valves and Column Design

The choice of switching valves was very critical when designing the prototype sampler. The valves needed to function underwater and under pressure. In addition, the valves had to be compact and self-contained due to space considerations. This precluded the use of pneumatic valves and led to the appropriate solenoid valves being sought. Finally, to prevent contamination,

all wetted areas of the valves had to be made of an inert material. A six-solenoid normally closed (N.C.) hex valve and a two-way normally open (N.O.)/ N.C. switching valve were purchased from NResearch (NResearch Ltd., Northboro, MA). All wetted areas of these valves were Teflon® and the valves operated with 12 V power and 0.4 mA. These valves were not specifically designed for underwater applications, but consultation with the NResearch technicians suggested that the valves would function adequately if the individual solenoids were coated to prevent water leakage. Therefore, all exterior surfaces and wires were coated with a silicone sealant.

The flow manifold incorporated five mini-columns designed and built in-house. These columns were filled with 8-HQ on silica. The resin was synthesized in house by L. Yang (Department of Chemistry, UBC), using the method detailed by Marshall and Mottola [106]. The components of the manifold were connected with Teflon® narrow bore tubing (i.d. 0.8 mm, Cole-Parmer, Chicago, IL). The pump tubing used on the peristaltic pump head was MASTERFLEX® C-Flex tubing (size 13, Cole-Parmer, Chicago, IL).

A schematic of the flow manifold is shown in Figure 2.5. The out-flow from the filter sandwich was connected to the N.O. port of the two-way switching valve and a buffer or standard (if required) was connected to the valve's N.C. port. The switching valve's common port was connected to the common port of the six solenoid hex-valve. Five of the six N.C ports of the hex valve were connected to mini columns, the sixth one used to flush the system once in the water before sampling commenced. All the six ports were attached to a common Teflon® eight port connector (Omnifit, Rochester, NY). Of the two remaining ports on this connector, one was plugged and the other was connected to the flow meter. The out-flow from the flow meter returned to the environment.

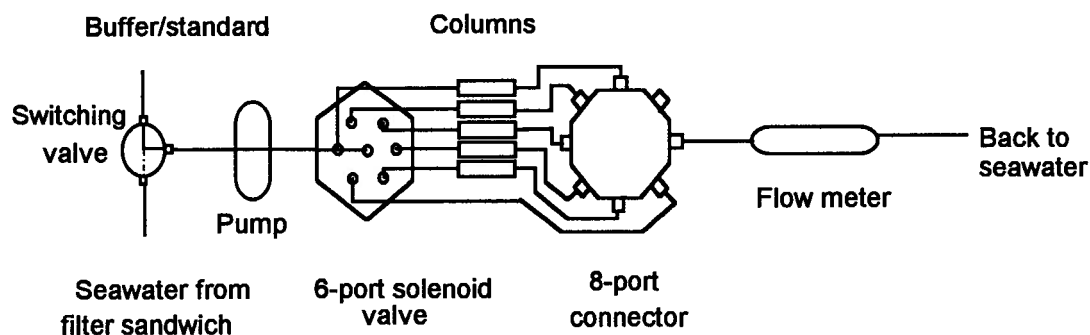


Figure 2.5 A schematic of the flow manifold used to preconcentrate metals from seawater using the new sampler.

Each solenoid had two wires, one for connecting to power and the other for connecting to ground. All wires from each solenoid that were designated ground were connected to the ground pin of one end of the 8 pin underwater cable ensemble. Each of the remaining solenoid wires were connected to the individual pins. This connected the valves to their control circuits in the interior of the casing found at the other end of the cable.

2.2.6 Battery Pack

The battery pack (Fig. 2.6) was constructed out of a Nylon polymer. It housed 45 "D-cell" batteries (each 1.5 V) in nine sets of five in series. Six of these sets of five provided the 15 V to power the motor and valves. The three remaining sets powered the computer board and the electronic circuit board. This battery configuration was necessary as the power drain of the prototype sampler was considerably more than that of the INFILTREX II sampler due to the addition of valves, the pump design and the computer board. The battery housing was attached to the top endplate by two metal supports. The computer board and electronic circuit board were also attached to these supports.

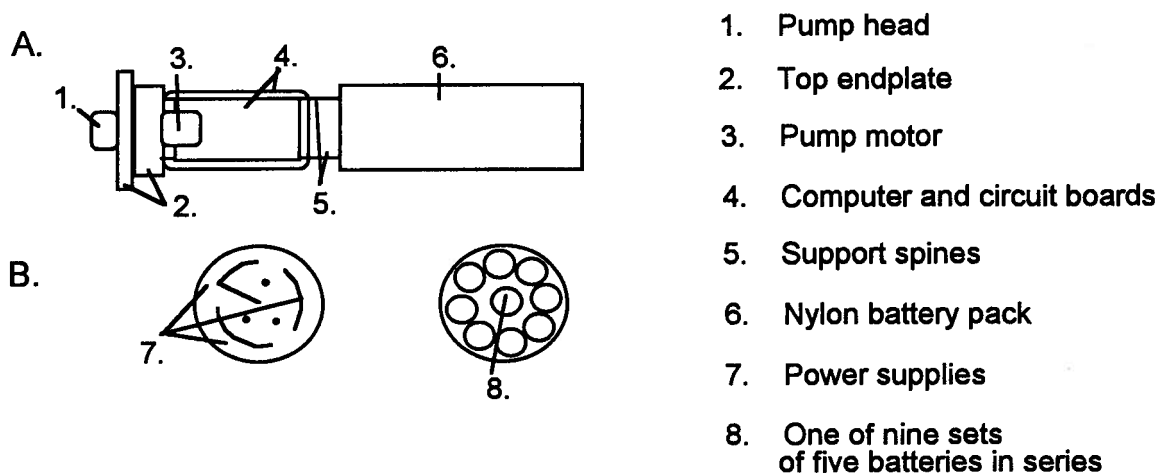


Figure 2.6 Schematic of the battery pack:
 (A) view from the side
 (B) view from the top and bottom of battery pack.

2.2.7 Casing

The aluminum casing was built in the UBC Dept. of Chemistry mechanical shop out of a 71.12 cm long, 1.27 cm thick piece of aluminum tube with an i.d. of 15.24 cm. This accommodated the computer and circuitry boards and battery pack. Calculations made by staff at the mechanical shop indicated that an aluminum tube of these dimensions would withstand the pressure at depths up to 3000 m.

The casing was attached to a 106.68 cm long, 0.635 cm thick aluminum spine, which was also built in the UBC Dept. of Chemistry mechanical shop. The valves, flow meter and underwater connector plugs were attached on the underside of the spine (Fig. 2.1B). These components were protected with a piece of sheet aluminum during transport. During deployment, the sampler was attached to the hydrowire by the two hydrowire brackets present.

The endplates which sealed the aluminum tube casing were also made of aluminum. Each endplate had double silicone o-rings to ensure a water tight

seal. The bottom endplate, once attached to the sampler, closed the circuit of the battery pack. The top endplate had the pump motor and pump shaft screwed into it. When the top endplate was removed, the whole interior was also removed.

On the exterior side of the top endplate were the pump head and three female underwater pluggable cable connectors (Impulse Enterprises, San Diego, CA). Two of the connectors were six pin with ground (model # BH-6-FS), the other was an eight pin with ground (model # BH-8-FS). The first six pin connector was used to access the computer board. Prior to deployment, this connector linked the computer board to the PC. When the sampler was to be deployed, a closed plug was attached to this connector, linking the computer board to the battery pack, and thus commencing sampler operation.

The second female six pin and the eight pin connector in the top endplate were linked to two other female underwater pluggable cable connectors (model #s BH-6-FS-SS and BH-8-FS-SS) via a 6 pin two-way male connecting cable and a 8 pin two-way connecting cable, respectively (model #s IL6-MP and IL8-MP). These other cable connectors were wired to the flow meter (using the 6 pin) and to the valves (using the 8 pin). This six pin connector ensemble linked the three thermistors in the flow meter to the flow meter circuitry. The eight pin connector ensemble linked the seven valves to the valve control circuitry.

2.2.8 Electronics Hardware

All electronic components used in the circuit boards were obtained from Active Components Ltd. (Vancouver, BC) unless otherwise specified. All the electronic circuitry incorporated into the prototype sampler was built on to a single board by the UBC Dept. of Chemistry electronics shop (see Appendix C).

2.2.9 Filter

The 0.45 µm filter sandwich was the only part of the original INFILTREX II sampler to be used in the prototype sampler. Anything passing through the filter was considered to be dissolved (this is the standard definition of dissolved, although colloidal material may be present). The filter sandwich was attached to the sampler bracket by two metal plates which also sealed the sandwich and prevented water leakage from its sides. The original in-flow tube to the filter sandwich was unchanged, but an adapter had to be built to connect the out-flow from the filter sandwich to the two-way switching valve.

2.3 Operation of the Prototype Sampler

2.3.1 General operation

The prototype sampler was programmed to pump for a specified length of time through each port of the six-way solenoid valve. While each separate valve is open, the two-way valve switches between the seawater stream and the buffer/standard stream every few seconds (typically 10 seconds in the seawater stream position and 1 second in the buffer/standard position). The flow meter recorded one measurement every 12 to 14 seconds during the total operation time of the sampler. These flow rate measurements were stored in six separate files, one for each port (and therefore column) of the six-way solenoid valve.

2.3.2 Pump Control

The computer board turned the pump on or off by sending a HI or LO signal to the pump controller on the circuit board. When the signal was HI, the pump controller connected the pump motor to +15 V dc, causing the pump motor to rotate. The pump speed changed only by fluctuations in this input voltage. Thus, the pump speed slowed as the batteries in the battery pack were drained.

Since flow rate measurements were taken regularly, this was not a problem. In addition, the operating time of the pump was less than ten minutes per column and repeated operations (greater than 10 times) did not cause a drop in the flow rate.

2.3.3 Valve Control

The seven solenoid valves, *i.e.*, six on the hex-valve and one on the 2-way switching valve, are controlled using the identical relays used for controlling the pump motor. When the computer triggers a particular relay HI, that relay connects the its valve to the 15 V dc supply. This opens the valve allowing water to flow through it.

2.3.4 Flow Meter Control

The flow meter operated as follows: A heat pulse was sent through the heating thermistor for 400 milliseconds and the timer was started. When the heat pulse was sensed, the timer was stopped. A 3.5 second wait was built into the circuit in the event that if a pulse was not sensed, the timer would still stop and another pulse would be sent out at preset time intervals. The signal was coupled with a 10 kHz frequency generator. The Ziatech computer board then counted the number of oscillations at 10 kHz for each measurement. Therefore, this measurement was the number of oscillations of the 10 kHz signal during the time the heat pulse was first pulsed to when it was detected. These values were stored in separate files in the Ziatech computer board's memory for each column. The flow rate was inversely proportional to the counts. After deployment of the prototype sampler, the flow rate files were down loaded to a PC. The series of measurements by the flow meter were then averaged and using the calibration file, described below, the volume of seawater through each column was determined.

2.4 Flow Meter Calibration

To calculate the actual flow rate, the flow meter was calibrated by collecting ca. 50 measurements at 5 to 10 different flow rates over the working range (between 0.8 to 7 ml/min) and averaging the results. An Alitea peristaltic pump (Alitea USA, Medina, WA) was used to obtain the range of flow rates needed for the calibration. Typical calibration results are shown in Figure 2.7. The calibration plots in this figure indicate that the flow meter response becomes unstable at flow rates greater than ~ 7.0 ml/min and flow rates less than ~ 1.0 ml/min.

Generally, the pulsing of the peristaltic pump is noticeable over the 50 points measured at each flow rate. Though it should be noted that it is most pronounced at the slowest of the stable flow rates. Visual inspection of the plots in Figure 2.6 indicated that the effects of pulsing decrease with increasing flow rate. Upon examination of Table 2.2, which shows the average of each of the data sets at each flow rate at the 95% confidence level, it is apparent that the fluctuations in the flow meter response is similar between the flow rates of 1.5 to 6.3 ml/min.

Plots of Flow Meter Response at Various Flow Rates

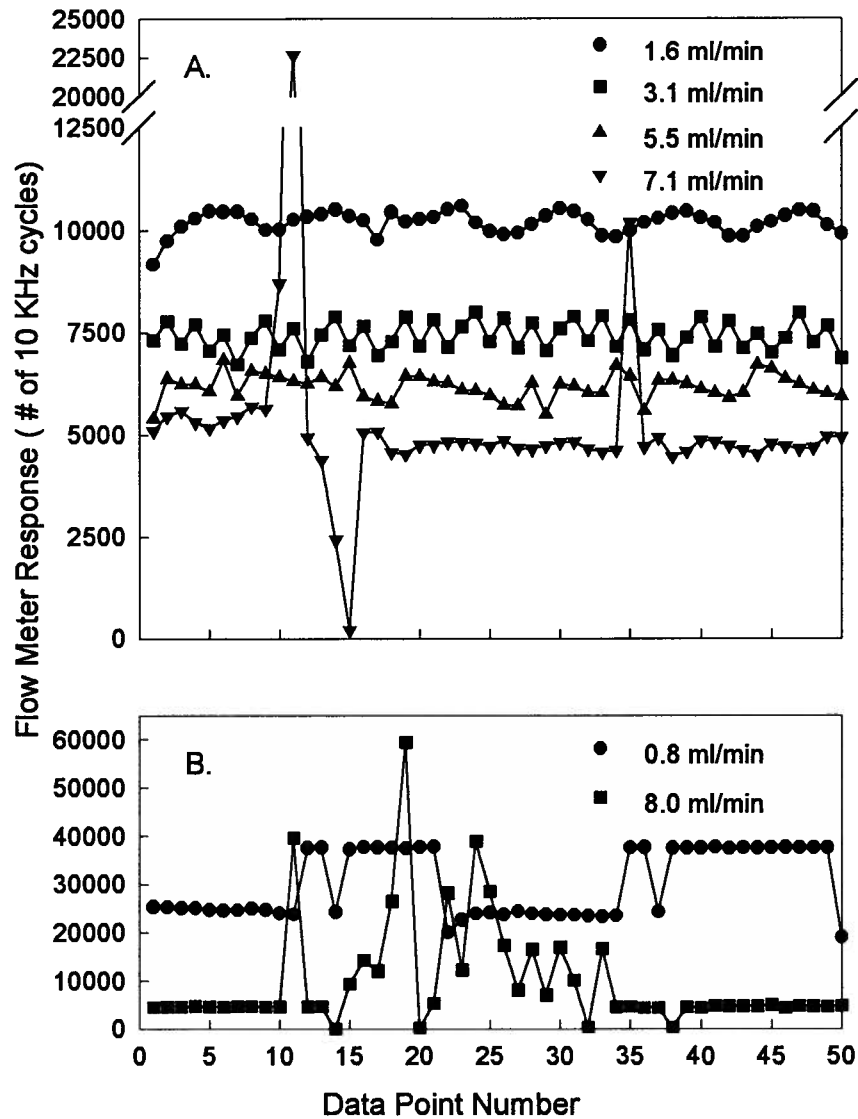


Figure 2.7 Plots of the 50 data point sets of the flow meter response over a range of flow rates between 0.8 to 8.0 ml/min:
 A. Working range of flow meter.
 B. Borderline to non-working flow meter range.
 N.B. The number of 10 kHz oscillations are inversely proportional to the flow rate.

Flow Rate	Averaged Flow Meter Response
0.81	30181 ± 1991
1.58	10188 ± 77
2.36	8193 ± 89
3.13	7417 ± 99
3.91	7085 ± 104
5.50	6182 ± 90
6.29	5653 ± 71
7.09	5264 ± 794
7.99	9935 ± 3280

Table 2.2 The average flow meter response at different flow rates at the 95% confidence limit.

A plot of the flow meter response as a function of the flow rate is shown in Figure 2.8. Excluding the two extremes, the flow meter had a linear response between flow rates of 2.3 to 7.1 ml/min (regression coefficient, $R^2= 0.991$). This relationship deviated when the lowest stable flow rate of 1.58 was included (regression coefficient, $R^2= 0.901$). The linear response between flow rates of 2.3 to 7.1 ml/min greatly simplifies the conversion between the number of counts from the flow meter to flow rate.

The pump system on the sampler had a maximum flow rate of ca. 8 ml/min when an external power supply of 15 V was used. With columns in place, the flow rate lowers to ca. 6 ml/min using the same voltage, which is well between the linear working range of the flow meter.

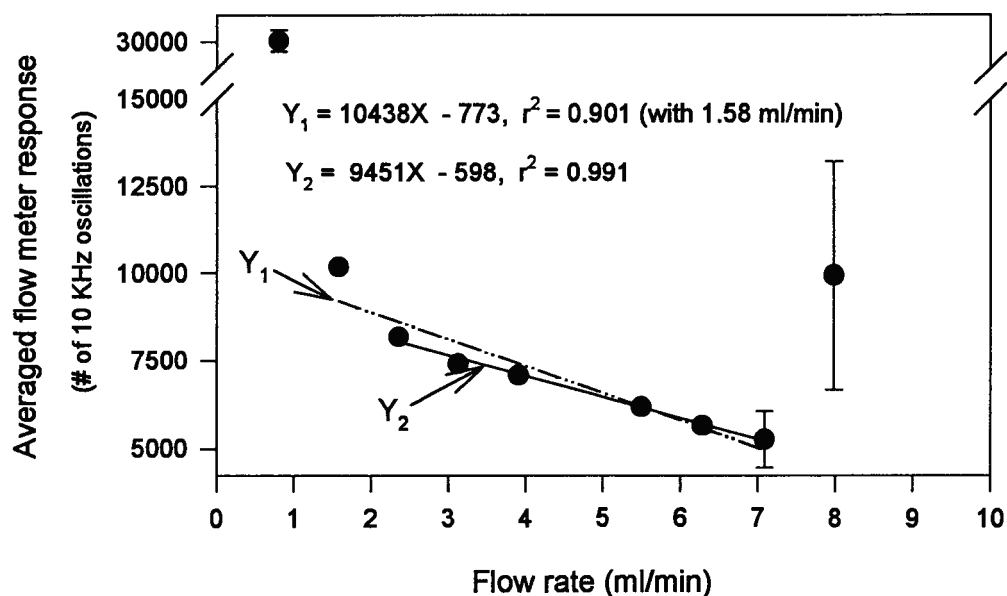


Figure 2.8 Flow meter response vs. Flow rate.

2.5 Prototype Sampler Testing

2.5.1 Preliminary Testing at Sea

The first testing of the prototype sampler involved taking the casing to sea during a "line P" cruise to station P 26 (50°N 145°W) in March 1993. At this stage of the sampler development, the valves and pump head were already attached to the casing's exterior, and the computer electronic circuit boards were in place and wired to the exterior attachments. Prior to the cruise, a prototype computer program was written to ensure the valves and pump motor worked in the correct manner. The exposed surfaces of the valves were coated with silicone sealant for protection.

The casing (particularly the pumphead interface) was tested for leakage due to pressure changes by sending the sampler to depths of 500 and 1000 m. Prior to testing, the computer and electronic boards were removed to prevent

their damage if leakage did occur. Once the sampler was retrieved from depth, its interior was checked for leakage. Less than 25 mls of seawater was found at the bottom of the casing. The water was removed, but the exposed metal surfaces, i.e. contacts on battery pack and bottom endplate, still corroded. The leakage occurred at the pump interface, but the seal was not broken when tested later. The seal, which works when pressure is applied, was not tight when first tested. The outcome was slight leakage of seawater until the pressure differential between the casing and the seawater was high enough to retighten the seal. This was remedied in later tests by tightening the seal before deployment. This was accomplished by running the motor and adjusting the current to between 0.3 and 0.4 A by tightening the metal plates which hold the seal in place.

After deployment the valves were inspected and checked by applying 15 V to each valve separately. The solenoids within each valve appeared to be working since the typical switching sound was heard. Later it was discovered that seawater had seeped into the interior of the solenoids, freezing the valves into the N.O. position. The valves were removed, disassembled and cleaned. One of six valves in the hex-valve sustained damage. A replacement solenoid valve could not be purchased and another hex-valve was not available. Instead the port of the bad valve was plugged and the sampler control program was rewritten to account for the changes in operation.

2.5.2 Submersion Testing

Once the sampler was recleaned, the flow meter was connected and tested successfully, it was subjected to a week long submersion test in house. This involved placing the sampler into a Plexiglas tank filled with tap water for five days. The on-board computer was linked to another PC in order to run the

control program and to collect the data from the flow meter. Each day the sampler operation was monitored, checking that the pump worked, the valves opened and closed properly, the flow meter operated and that the relevant flow rate data was collected by the computer. No problems were encountered, though some rust formation occurred on some of the valves.

The sampler was then removed from the tank and opened up to check its interior for any leakage. Only slight condensation was observed, which was remedied by adding a drying agent to the interior (e.g. CaO). The valves had to be disassembled and cleaned, with only the switching valve becoming inoperable.

2.5.3 Contamination Control

The seawater manifold of the sampler, without the columns, was cleaned with 2 N nitric acid for several days. High blanks were found for the elements Ni, Mn, Pb and Zn and were attributed to the flow meter. When blanks were collected from the manifold before the flow meter, they were found to be much lower. In real operations contamination of samples by the flow meter would not occur since the metals are extracted onto columns before the seawater passes through the flow meter. During blank collection, one of the thermistors in the flow meter was severely damaged and replaced with a partially repaired thermistor. The flow meter worked intermittently and hence not reliably with the replacement thermistor.

The columns which were to be used with the sampler were also tested. Each column was cleaned with acid until blank levels were low. They were then rinsed with DDI water and left for one week. The blank levels of the columns were found to be extremely high for Mn, Ni, Cu, Zn and Pb. Off-line tests were conducted on the 8-HQ on silica resin to determine its stability in 2 N nitric acid

and in DDI water over a one week period. Higher blanks were observed for the resin stored in DDI than for the resin stored in 2 N nitric acid. Though both had higher blank levels than that of the newly cleaned resin. Thus, the resin would have to be freshly cleaned before used with the sampler.

The column, without resin was also tested since some metal is present in the flangeless fitting used for the columns. High blanks were observed after storing the column for one week after cleaning. It was concluded that a new sturdy, metal free miniature column would need to be designed, or replace the FI fittings with metal free ones.

2.6 Conclusions

After consultation with the Department of Chemistry mechanical shop, it was decided that using the existing sampler to collect uncontaminated trace metal samples would not be possible after the extensive testing involved. Instead, a second generation sampler, based on the prototype, with all seawater wetted sampling components replaced, be built before contaminant-free trace metal samples could be collected in natural waters.

CHAPTER 3: EXPERIMENTAL AND TECHNIQUE DEVELOPMENT

This chapter details the development of an on-line preconcentration/matrix separation FI-ICP-MS manifold using a chelating resin of 8-hydroxyquinoline on silica to determine multiple elements from seawater under one set of conditions. The elements successfully analyzed using this system were Zn, Cd, Ni, Cu, Pb, Mn, Ga and Nb from seawater adjusted to pH 8. Other elements tested were Cr and Co. Chromium suffered from high variable system blanks due to the resin. Cobalt had low system blanks but suffered from interferences attributed to residual matrix effects caused by preconcentrating seawater.

The FI manifold was designed and built in-house. It could be operated either manually or via computer. The chelating resin column was incorporated in the sample loop in such a manner that the directions of flow of the seawater sample and eluent were opposite. This reduced column packing, prevented seawater from entering the ICP-MS, and altered the elution patterns of the trace metals such that they were all eluted simultaneously. Up to 13 isotopes were simultaneously determined using the peak jump mode of the ICP-MS. This was an improvement on other on-line FI-ICP-MS methods using "multiple elements" software of their ICP-MS which could typically measure up to 4 isotopes simultaneously [77,78].

3.1 Materials and Reagents

3.1.1 Reagents

All reagents were prepared using distilled deionized (DDI) water (18 M Ω , Nanopure, Barnstead/Thermolyne Corp., Dubuque, IA and Millipore Waters Associates, Mississauga, ON). A stock mixed metal solution was prepared by serial dilution of 1000 ppm atomic absorption standards (Johnson Matthey Inc.,

Seabrook, NH, and J.T. Baker Chemical Co., Phillipsburg, NJ) in 0.1% (v/v) nitric acid (double subboiling-distilled in quartz, Seastar Chemicals Inc., Sidney, BC) and used for standard additions. In the rest of this dissertation the prefix "Q-" will denote ultra clean acids and bases. Samples were pH adjusted using Q-ammonium and Q-acetic acid (Seastar Chemicals Inc.). Q-nitric acid was also used to make 2.0 N Q-HNO₃ for column elution and cleaning.

3.1.2 Bottles

All new polyethylene (PE) bottles used for trace metal work were first rinsed with acetone to remove any organic residue. The bottles were then rinsed with DDI water, filled with 4 N HCl (reagent grade, BDH Inc, Toronto, ON) and heated overnight at 65°C. The bottles were not completely filled to allow for any expansion of the acid during the heating. The next day, the bottles were removed from the oven, inverted and left overnight to cool. The bottles were then rinsed with DDI water and stored in 0.1% Q-nitric acid until use. Bottles which previously contained seawater were rinsed well with DDI water and stored in 0.1 to 1% Q-nitric acid prior to reuse.

3.1.3 Seawater Standards

NASS-3 Open Ocean Seawater Reference Material (National Research Council of Canada, Ottawa, ON), a seawater standard, was used to assess the accuracy and precision of the on-line method developed for trace metal analysis in seawater.

3.1.4 Resins

8-hydroxyquinoline (8-HQ) on silica resin was synthesized in-house by L. Yang (Department of Chemistry, UBC), using the methods published by Marshall and Mottola [106]. The 8-HQ on Fractogel (TSK) was synthesized

previously by Dr. K.J. Orians using the method published by Landing *et al.* [26]. The 8-HQ on XE-305 resin was purchased from Seastar Chemicals. Chelex-100 was purchased from Bio-Rad Laboratories (Richmond, VA).

3.2 Sample Collection

3.2.1 Seawater Samples

Samples were collected by the author and/or K.J. Orians, B.A. McKelvey, R.K. Mugo and H.R.C. MacLean (Departments of Chemistry and Oceanography, UBC). Trace-metal clean methods developed by Bruland *et al.* [17] were used. Acid cleaned Teflon[®]-lined "Go-Flo" bottles (30 L, General Oceanic, FL) were suspended on Kevlar[®] line. The bottles were closed prior to being lowered into the ocean to avoid potential contaminants present in the ocean's surface micro-layer. The bottles were opened once they had reached a depth of 5 to 10 m, and then lowered to the desired depths. At the depth of sampling, the bottles were allowed to flush for several minutes before they were closed, triggered by a Teflon[®] messenger (Department of Chemistry mechanical shop, UBC).

Once the bottles were brought back on board ship, they were secured next to a clean area in preparation for filtering the samples. This clean room had walls, ceiling, and all exposed surfaces covered with polyethylene sheets and duct tape. Placed inside this makeshift clean room was a high efficiency particle air (HEPA) filter which was used to create a slight positive pressure inside the room. Equipment used for filtering, collecting and acidifying samples was also inside the clean room. Samples were filtered at sea in this clean room through 0.45 μm polycarbonate membrane filters using a 10 psi N_2 over-pressure and the filtrates were collected in acid leached PE bottles. The samples were then acidified to pH 2 with 2 mls 6N Q-HCl per litre of seawater prior to storage.

Further processing and analysis was carried out in a shore-based clean laboratory.

3.3 On-Line FI-ICP-MS Instrumentation

3.3.1 Apparatus for Flow Injection Manifold

The FI manifold used for this work incorporates the chelating column in the sample loop. In this configuration, the column can be considered as a special form of a sample loop [58]. The analyte is concentrated on the column which is analogous to the filling of the sample loop in conventional FIA. The analyte is then stripped from the column and analyzed which is analogous to the injection of the sample into the carrier stream.

3.3.1.1 Valves

Two valves were used in the manifold. A 2-way switching valve (Biovalve Corp), consisting of two normally closed (N/C) solenoids, was used to switch between the column rinse solution and the seawater sample. This valve was electronically controlled through a relay allowing one to switch the valve manually, or by a computer through an IBM data acquisition and control adapter (DACA) board (Mendelson Electronics, Dayton, OH) using one digital I/O line. For the sake of clarity, this valve will be referred to as the "switching valve" for the remainder of this work.

A second valve, a 6-port injection valve with pneumatic actuator (Rheodyne Inc., Cotati, CA), which needed a pressure of 80 psi to operate, was used to switch the column between sample preconcentration (load position) and elution (inject position). Electronics designed in-house [110] were used to control the pneumatic actuator either manually or through the connected

computer. For the sake of clarity, this valve will be referred to as the "injection valve" for the remainder of this work.

3.3.1.2 Peristaltic Pump

A six channel Alitea peristaltic pump (Alitea USA, Medina, WA) was used to transport seawater or rinse solution through the column. The pump was controlled by the computer through an analog to digital (A/D) channel on the IBM DACA board. Clear Tygon pump tubing (Cole-Parmer, Chicago, IL) was used with the pump. When incorporated into the flow manifold, the pump operated at flow rates between 0 and 5 ml/min.

3.3.1.3 Design of the Extraction Column and Flow Injection Fittings

The extraction column was designed in-house. The body of the column consisted of a 5 cm length piece of 1.6 mm i.d. Teflon[®] tubing with flangeless fittings (Omnifit) at both ends. These were screwed into a Teflon[®] coupling, consisting of a plug with a 0.8 mm hole drilled into its middle. A 74 μm fluorocarbon-weave filter frit (Spectrum, Los Angeles, CA), placed between the plug and the column body, was used to keep the resin inside the column. The filter frit was cut into a small circle to fit inside of a lip machined into the plug of the coupling. The chelating resin column was incorporated into the manifold with standard flow injection fittings. The rest of the manifold was constructed out of 0.8 mm i.d. Teflon tubing using standard FIA fittings (Omnifit, Cole-Parmer, Chicago, IL) and was acid cleaned for several days prior to being used for on-line work.

Prior to assembly of the columns, the Teflon couplings and frits were acid cleaned using the procedure previously described for cleaning the PE bottles. To load the resin into a column, one end of the column body was connected to one frit/coupling ensemble and a syringe loaded with ca. 300 μl of resin

suspended in DDI water was attached to the other end. Once the resin was loaded into the column, the syringe was replaced with the other frit/coupling ensemble and the column was sealed with Teflon plugs (Omnifit). Prior to use on-line, the column was incorporated into the on-line FI-ICP-MS manifold and metal background levels were monitored while acid was run through the manifold. During this process, the column was rinsed at a flow rate of 0.75 ml/min with 2 N Q-nitric acid until the background levels matched those of the acid.

3.3.2 On-Line FI-ICP-MS Manifold used for Preconcentration

A schematic of the manifold used for on-line preconcentration and matrix separation is shown in Figure 3.1. The 2-way switching valve was placed upstream of the pump, thus either the seawater or rinse streams would be drawn into the pump. The injection valve, with the chelating resin column in the sample loop, was placed downstream from the pump. In the sample load position either rinse or seawater passes through the column and to waste.

A second peristaltic pump (Gilson), forming part of the VG PlasmaQuad sample introduction system, continuously pumped 1% nitric acid rinse into the ICP-MS. The injection valve was connected to the PlasmaQuad between this second pump and the ICP-MS. To flush the FI system, the acid rinse solution was replaced with 2 N Q-nitric acid prior to switching the injection valve to the elute position. The eluent was not continuously run through the ICP-MS to conserve the eluent and to minimize any deterioration of the sample cone and other parts of the ICP-MS. Since only one switching valve was available, switching between the 1% nitric acid rinse and the eluent (2N Q-HNO₃) was carried out manually.

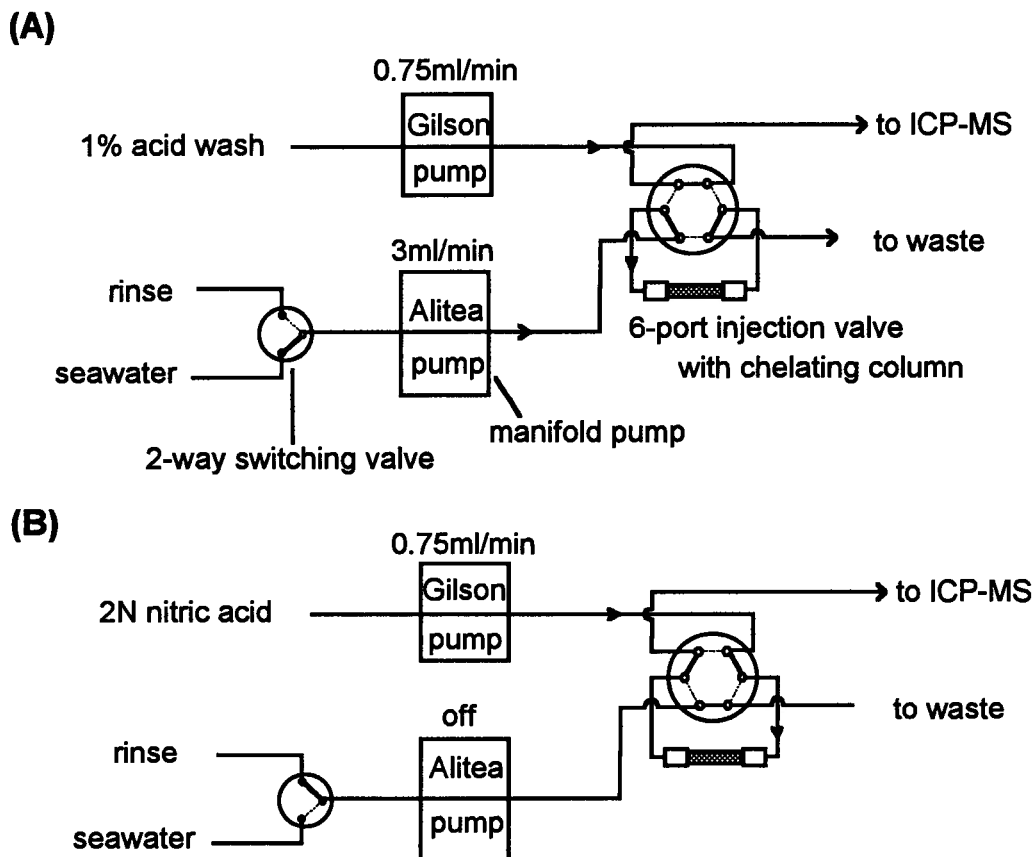


Figure 3.1 On-line FI-ICP-MS preconcentration manifold used for:
 (A) Loading: The injection valve is in the sample load position, the 2-way valve is in the seawater position. 1% nitric acid wash is going to the ICP-MS.
 (B) Elution: After the column is rinsed to remove any seawater, the injection valve is switched to the elute position and now 2 N Q-nitric acid enters through the column in the opposite direction to which the sample was loaded. During elution, the Alitea pump is off, and the 2-way switching valve is left in the rinse position, ready for the next sample.

A typical operation is described in detail: The 2-way switching valve is set to the rinse position, the pump turns on and the rinse solution is pumped through the column for a pre-determined time interval. The 2-way switching valve then switches to the seawater position to pump the seawater through the column. Finally, the switching valve returns to the rinse position to remove any traces of seawater. After rinsing, the manifold pump stops and the injection

valve switches to the elute position, allowing the eluent to enter the column in the opposite direction to the loading of sample. The eluent, now containing the trace metals stripped from the resin, enters the ICP-MS for metal determination. During the sample detection, the eluent continues flowing through the column, cleaning it and readying the column for another sample.

3.3.3 Automation of the FI manifold and Data Collection

The FI manifold was controlled using a 386 SX computer via an IBM DACA board. The computer controlled the operation of the 2-way switching valve, the injection valve and the Alitea pump. The original program FIARun, written in BASIC 7.0 (Microsoft) by Dr. O. Lee as a more complex version of the flow injection development and optimization (FIDO) system software [110], was modified for this task.

3.3.3.1 Pump Calibration

The Alitea pump was calibrated using a subprogram within the control program before use. Before running the calibration subprogram, the manifold was configured with the 2-way valve in the seawater stream position and the injection valve in the sample load position with the chelating resin column in place. The pump was manually set to its maximum speed. The pump speed was controlled by adjusting the voltage to the pump via the computer through the A/D channel.

The calibration subprogram required the input of liquid density, length of time to run the calibration, the pump speed setting (between 0 and 4095) and the initial weight of the flask which the water is collected in. The program then runs the pump at the speed chosen for the appropriate time and then asks for the final weight of the flask. The subprogram then extrapolated a working flow rate range in ml/min for the on-line system from the data entered. These results

were then saved to a file which was accessed each time the manifold control program was initiated. This calibration was repeated whenever modifications were made to the system (i.e., replacing column, pump or Teflon tubing).

3.3.3.2 Automation and Manifold Control

The FI manifold was computer controlled when used on-line with the ICP-MS. The system was first incorporated into the ICP-MS sample introduction system and the subprogram which controlled the manifold was selected from the menu of the control program FIArun. The correct calibration file was chosen and the flow rate (usually 3 ml/min) was selected.

Variables for each preconcentration/elution cycle were the length of time needed to rinse the column (at the preset flow rate) and the volume of sample to be loaded.

3.3.3.3 Data Collection

The computer of the FI manifold was not interfaced to the ICP-MS, thus data were collected by the computer and software which controlled the ICP-MS (section 3.3.4.2). The sample acquisition time was manually set such that data was collected during the time the eluted metal concentrations were highest. This was determined by monitoring a mass of one of the metals during elution using single ion monitoring mode (SIM). More detail about SIM and general ICP-MS operations are given in the following paragraphs.

3.3.4 ICP-MS

A VG "PQ2 Turbo Plus" ICP-MS was used for both on-line and off-line work. A schematic of this instrument was shown previously in Chapter 1 as Figure 1.4. The system was equipped with a VG ICP torch and extraction system, an SX 300 quadrupole mass analyzer, and a channel electron multiplier

(Galileo Electro-Optics Corp). Data were collected with a Dell 486 computer equipped with O/S2 and PQ Vision 4.1.1 software. Pure (99.998 %) argon gas (Medigas, Vancouver, BC, Canada) was used as both plasma and carrier gas.

3.3.4.1 Operating Conditions

The ICP-MS was ignited and allowed to warm up for a minimum of 30 minutes before optimizing the operating parameters. The mass analyzer was manually tuned to either m/z 115 or 238 to monitor either In or U in a 10 ppb tune solution containing these two elements, Ba, Co, Pb and Bi. The tune solution was run through the ICP-MS and the signal to the mass analyzer was optimized by adjusting the argon gas flow rate(s), the distance between the sampling cone and the load coil, the torch position and the lens settings. Table 3.1 shows the typical parameter ranges used for the quantitative work. Once optimized, the short term stability of the ICP-MS was checked using the scanning mode to measure the response of all elements in the tune solution for a 60 second acquisition time, repeated 10 times. The full mass range was scanned continuously except for masses affected by the plasma (e.g. $^{40}\text{Ar}^+$, $^{40}\text{Ar}^{16}\text{O}^+$ and $^{40}\text{Ar}_2^+$). The smoothness of the peak shapes were ascertained by visually inspecting one of the full scans. Peak resolutions were checked by examining the extent of separation between the ^{10}B and ^{11}B isotopes and the ^{206}Pb , ^{207}Pb and ^{208}Pb isotopes. To achieve a good separation of the isotopes and still maintain the best possible sensitivity, the resolution (R) dial and the peak shape (ΔM) dial (which adjusts the peak width at 5 % peak height) were used.

Parameter	Typical Value(s)
RF power (W)	1350
Argon gas flow rate (L/min):	
Cooling gas	13.72 to 13.85
Auxiliary gas	0.494 to 0.505
Nebulizer gas	0.800 to 1.000
Sampling position (mm above load coil)	13
Sampler cone (nickel) orifice (mm)	1.0
Skimmer cone (nickel) diameter (mm)	0.7
Ion lens settings (V):	
Extraction lens	-160 to -210
Collector lens	-2.0 to 0
L1	-2.5 to 0
L2	-60 to -30
L3	0 to +5
L4	-50 to -42
Pole Bias	-3 to -4
Operating pressure (mbar):	
Interface running pressure	$<0.1 \times 10^{-4}$
Expansion pressure	2.2 to 2.9
Analyzer pressure	$(2.2 \text{ to } 2.8) \times 10^{-6}$

Table 3.1 ICP-MS Operation Conditions

In the work presented here, the instrument was used in multichannel peak jump mode. In peak jump mode, the quadrupole jumps from selected mass to mass, and stays at each mass for a set dwell time. This mode was used with a 10.24 millisecond dwell time, one point per peak and a 20 second acquisition time.

3.3.4.2 PlasmaQuad Control and Software

The computer control of the in-house automated FI manifold was not interfaced to the PlasmaQuad (PQ) system due to the incompatibility of the two systems. The VG system had a very complex interface which was not intended to be altered. A RS-232 connection exists on the VG instrument for the interfacing of the commercial FI system that VG markets, but it was not suitable for any other systems, including the FI system developed for this work.

The PQ program was manually controlled to make the desired measurements across the eluent peak area. As soon as the injection valve switched to the elute position, the program was triggered, and measurements were made after a preset interval which allowed the eluent peak time to enter the mass spectrometer. The time interval between triggering the PQ and taking the measurement had been predetermined using the single ion monitoring mode of its program.

In the single ion monitoring mode (SIM), a single mass is continuously monitored over time, with the resulting measurement in the form of a peak. Thus, the elution peak can be observed and from this, the time the peak takes to reach the ICP-MS and the width of the peak can be determined. Once the time between elution and detection was determined, the SIM mode was used to detect any changes only when either the ICP-MS sample introductory system or the FI manifold had been altered, e.g. pump tubing replaced.

In this work the Cd signal was monitored in SIM mode to determine the length of time between the switching of the injection valve to the elution position and peak maximum reaching the ICP-MS mass analyzer. A typical response is shown in Figure 3.2. SIM scans of other elements are shown in APPENDIX D. From this, the PQ was triggered to wait for 25 seconds before collecting data for 20 seconds (over the peak maximum). A longer collection acquisition resulted in lower total counts per second (cps), while shorter times resulted in larger variations in the responses of replicate analyses.

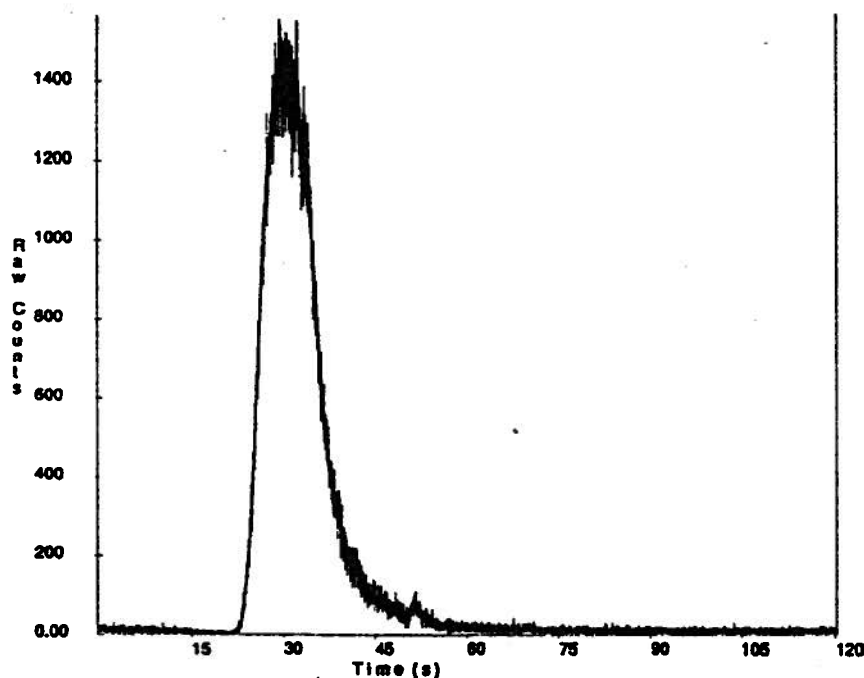


Figure 3.2 A two minute SIM mode scan of ¹¹⁴Cd.

3.4 Method Development

The work presented in this section was performed to optimize the operation of the on-line FI-ICP-MS system.

3.4.1 Chelating Resins

Several resins were studied to determine their potential for on-line multi-elemental preconcentration using the FI manifold with ICP-MS detection. This on-line work was also necessary to find the ideal resin to use in the *in situ* sampler discussed in Chapter 2. The chelating resin of choice would:

1. Preconcentrate many metals over a broad pH range.
2. Extract metals from seawater at flow rates between 2 and 5 ml/min.
3. Not suffer any back-pressure effects at these flow rates.
4. Not change size with a change in pH.
5. Have no or minimal degradation of the functional group over time.
6. Have a high metal complexing capacity to minimize resin volume and risk of column break through.
7. Have quick exchange kinetics with the metals in seawater.
8. Be easy to synthesize, or be relatively inexpensive if available commercially.

The four resins chosen for study were 8-hydroxyquinoline (8-HQ) on silica, 8-HQ on XE-305, 8-HQ on TSK and Chelex-100. Studies were carried out on-line using unspiked and spiked seawater samples, divided into subsamples with each subsample adjusted to a different pH between 3 and 8. Half of the seawater samples were spiked with 0.5 ppb of Cd, Cu, Pb, Mn, Ni and Zn. Approximately 350 μ l of each resin was loaded into the individual columns. As a result of these studies, 8-HQ on silica was used for all further work. Explanations for this choice are given below.

3.4.1.1 Chelex-100

Chelex-100 is known to shrink and swell with changing pH, being largest in its ammonium form and smallest in its hydrogen form. Chelex-100 consists of a polystyrene matrix with iminodiacetic acid functional groups. It has slow exchange kinetics with trace metals, which may result in less than complete recoveries when used at flow rates greater than 0.5 ml/min [105]. This resin was loaded in a column in its ammonium form to ensure that the Chelex-100 would not exceed the column volume with changing pH. During the preconcentration there was no leakage of the column nor any problems with back pressure. When eluting the column with the acid, the resin compacted into one corner of the column causing enormous back pressure on the system, and attempts to redistribute the resin by agitation of the column and by passing a higher pH solution through the resin did not work.

3.4.1.2 8-HQ on TSK

This resin was considered since its use with on-line FIA systems for trace metals has been widely reported [73, 75, 76]. In the current work, severe problems with the back pressure, experienced when using flow rates greater than 2 ml/min, curtailed further study. This was attributed to the age and previous usage of the resin, resulting in the resin backbone breaking up into finer particles. Attempts to synthesize the resin in-house resulted in break-up of the polymer backbone during synthesis. Other reasons were attributed to the column design and volume used. In other work published [73, 75, 76], resin volumes used were approximately 100 μ l (cf. 350 μ l used here). The resin was loaded into columns made of Tygon pump tubing held in place by glass wool at each end. Glass wool was not used here since it could be a potential contamination source for metals such as Zn and Pb.

3.4.1.3 8-HQ on XE-305

This resin was studied since it is marketed by the Axys Group for trace metal work and for use with the INFILTREX II sampler. Chemically, this resin has the 8-HQ coupled to a styrene-divinylbenzene backbone [28]. The 8-HQ on XE-305 has a much larger bead size than the other resins used here (1 mm diameter vs. <200 μm) which results in fewer chelating sites per unit volume.

This resin did not change size with pH, nor did it suffer from backpressure. However, using this resin in the on-line system resulted in low signal response for of the most trace metals studied, compared to 8-HQ on silica (section 3.4.1.5).

3.4.1.4 8-HQ on silica

This resin has been successfully used to extract Cr, Mn, Co, Ni Cu, Zn, Cd and Pb at pH between 6 to 8 in the NASS-3 and CASS-2 seawater reference materials and it has been used for on-line work with both ICP-AES and ICP-MS [27, 77, 78, 81]. Furthermore, this resin is simple to synthesize in comparison to 8-HQ on XE-305 [28,106]. However, potential problems with the resin included the possibility of metals being leached from the silica and the likelihood that extended exposure of the resin to pH of 7 and higher could cause the chelate to hydrolyze off.

3.4.1.5 Comparing 8-HQ on XE-305 and Silica Backbones

A comparison was made between the 8-HQ on XE-305 and silica backbones with respect to their suitability for on-line work. Both resins, in identical on-line configurations were used to measure seawater adjusted to pH 8 and spiked with 0.5 ppb of Mn, Ni, Cu, Cd and Pb, using Ga as an internal standard. A flow rate of 3 ml/min was used, though in further studies the 8-HQ on XE-305 resin was also evaluated at a flow rate of 1.5 ml/min. The results

shown in Table 3.2 were corrected with the internal standard and blank subtracted.

At 3 ml/min, the use of the silica based 8-HQ resin resulted in higher signals for all the elements measured. When the responses of the XE-305 resin at 3 ml/min and at 1.5 ml/min were compared, a marked increase for five of the six elements is apparent (not Cd) at the slower flow rate. The results shown in Table 3.2 were used only to decide on the suitability of each resin for further work on-line and for use with the *in situ* sampler. As a result of these studies, the remainder of the on-line work proceeded using the 8-HQ on silica resin.

Isotope	Silica resin 3 ml/min	XE-305 resin 3 ml/min	XE-305 resin 1.5 ml/min
Mn 55	2770	1907	2767
Ni 58	2088	155*	1116
Cu 65	6958	2681	3621
Zn 66	4193	1671	2414
Cd 114	2387	1440	973
Pb 208	8589	6288	7266

Table 3.2 Response of the 6 metals from 6 mls of a 0.5 ppb spiked seawater sample adjusted to pH 8. The average of two trials are shown for all results using 3 ml/min flow rate except where denoted by an * (one bad result for that element). All results are in integrated counts per second (CPS).

The drawbacks to the 8-HQ on silica resin, i.e., leaching of metals from the silica backbone and hydrolysis of the 8-HQ functional group, were not found to be a problem. The resin was cleaned before analysis, and column blanks measured throughout the day showed no increase. The same column was used

for up to 4 months at a time with no visible signs of resin and performance degradation.

3.4.2 Silica based 8-HQ pH Studies and Recovery Tests

On-line experiments using the FI manifold were used to determine the optimum pH for the metals of interest and to determine the best pH to use for multi-elemental analyses.

3.4.2.1 On-Line Studies

Seven 100 ml aliquots of seawater were adjusted to pH values between 2 and 8. Each pH adjusted sample was divided into two subsamples, one left unspiked and the other spiked with 1000 μ l of the mixed metal stock solution listed in Table 3.3. For each subsample, three 6 ml seawater volumes were preconcentrated and eluted on-line for each sample using the general on-line FI-ICP-MS procedures described earlier in section 3.3.2. The eluent contained 0.5 ppb Rh as an internal standard. The results, shown in Figure 3.3, are normalized to the highest value as the absolute recoveries cannot be determined with this type of system. Since this system incorporated FIA with its benefits including reproducible timing, 100% recoveries were not necessary as long as the metal-resin interactions stayed constant throughout a set of experiments (*i.e.*, under identical pH and flow rates).

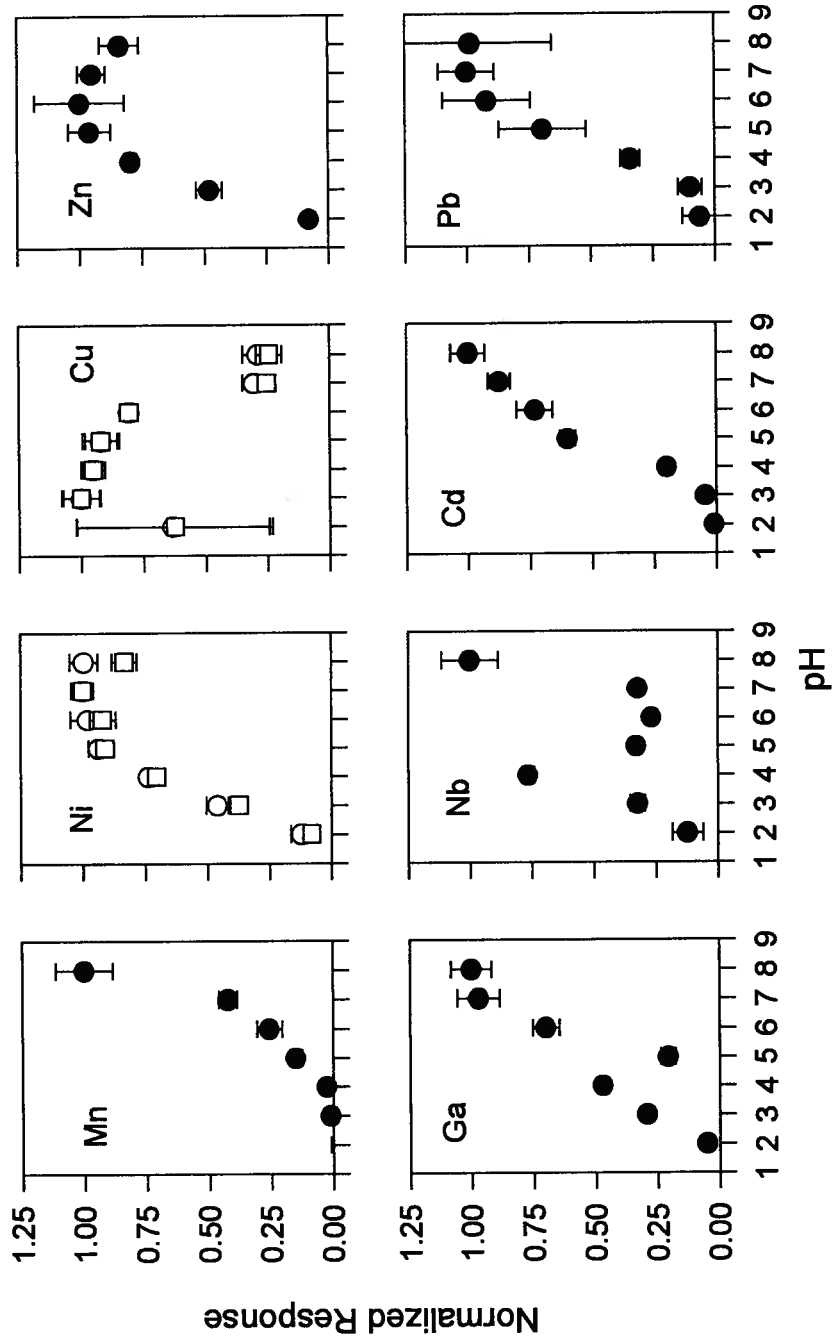


Figure 3.3 Plots of the pH dependency of the elements using the on-line system. Points are the average of three measurements and error bars represent 1s. Responses were normalized to the maximum signal of each element (in CPS). Two isotopes of Ni and Cu are shown.

Metal	Concentration (ppb)
Cd	10
Cu	100
Ga	1
Mn	20
Nb	10
Ni	100
Pb	2
Zn	100

Table 3.3 Concentration of metals in the mixed standard solution used for standard additions.

All elements showed smooth responses with pH except for Nb. The Nb response at pH 4 and 8 seem suspect since there was no gradual increase in signal response with changing pH, possibly indicating contaminated bottles for the spiked samples at these two pH. If these points are ignored, it can be seen that the recovery of Nb at pH 3, 5, 6 and 7 are similar, indicating a broad working pH range for Nb, suggesting that the response of Nb at pH 4 should be similar to that of the working range. At pH 8, the on-line results of Nb in the seawater samples indicated that all the samples analyzed, spiked and unspiked, gave consistent results with good calibration curves. The pH chosen for subsequent studies was pH 8, since all elements had optimal or near optimal responses at this pH, except Cu.

Absolute responses at optimum pH and at pH 8 for the added spiked metals after preconcentrating 6 mls are shown in Table 3.4. All responses were

greater than 10^4 cps, even for the elements Mn, Cd, Pb, Ga and Nb, which were present in sub ppb concentrations.

Isotope	Spiked seawater (ppb)	Optimum pH	Response at optimum pH ($\times 10^3$ CPS)	Response at pH 8 ($\times 10^3$ CPS)
Mn 55	0.4	8	109 \pm 12	109 \pm 12
Ni 58	2.0	5-8	499 \pm 23	497 \pm 27
Ni 60	2.0	5-8	260. \pm 11	217 \pm 12
Cu 63	2.0	3-6	472 \pm 37	137 \pm 29
Cu 65	2.0	3-6	292 \pm 21	71 \pm 2
Zn 66	2.0	5-8	308 \pm 56	259 \pm 24
Ga 71	0.02	7-8	12.4 \pm 1.0	12.4 \pm 1.0
Nb 93	0.2	3-7	5.2 \pm 0.4	16.1 \pm 1.8**
Cd 114	0.2	8	80.6 \pm 5.6	80.6 \pm 5.6
Pb 208	0.04	7-8	58.3 \pm 6.6	57.4 \pm 2.0

Table 3.4 Results of the on-line pH studies. The response at optimum pH and pH 8 for each element is the average of the three analyses \pm 1s. All measurements were corrected for instrument drift using Rh as the internal standard. NB. **Samples believed to be bad.

3.4.3 Flow Rate

The extraction efficiency of a resin is dependent on the flow rate used to preconcentrate the sample onto a resin column. Slowing the rate of flow of a sample can increase the extraction efficiency of a resin, but the length of time required to perform this extraction may make the use of this flow rate impractical. In on-line FI manifolds used for the preconcentration of sample onto a resin, use

of the optimal flow rate is not necessary to obtain good results, as long as the flow rate stays constant throughout the entire experiment. When using an FI manifold on-line with an instrument such as an ICP-MS, the time taken for each analysis is an important consideration since the ICP-MS is operating during the preconcentration cycle of the FI manifold. A lengthy preconcentration time, where no analyses are being made, not only reduces sample throughput but also increases operating costs, defeating the purpose of an on-line system.

The maximum flow rate of the preconcentration manifold was 5 ml/min, however flow rates between 1 and 4 ml/min were examined using 6 mls of spiked seawater adjusted to pH 8 for sample loading and 2 mls of DDI to rinse the column between sample loading and eluting. The time needed for each preconcentration cycle at each of these flow rates are shown in Table 3.5. The results are displayed in Figure 3.4. For all elements, the best extraction efficiency was achieved at 1 ml/min, with the extraction efficiency leveling to ~ 60% of the optimum response between flow rates of 2 and 4 ml/min.

Flow rate (ml/min)	Preconcentration cycle
1	10 min
2	5 min
3	3 min 20 sec
4	2 min 30 sec

Table 3.5 Time per preconcentration cycle using 6 mls of seawater and rinsing with 2 mls of DDI before and after sample loading. N.B. Add 2 minutes for elution to obtain time of 1 analysis.

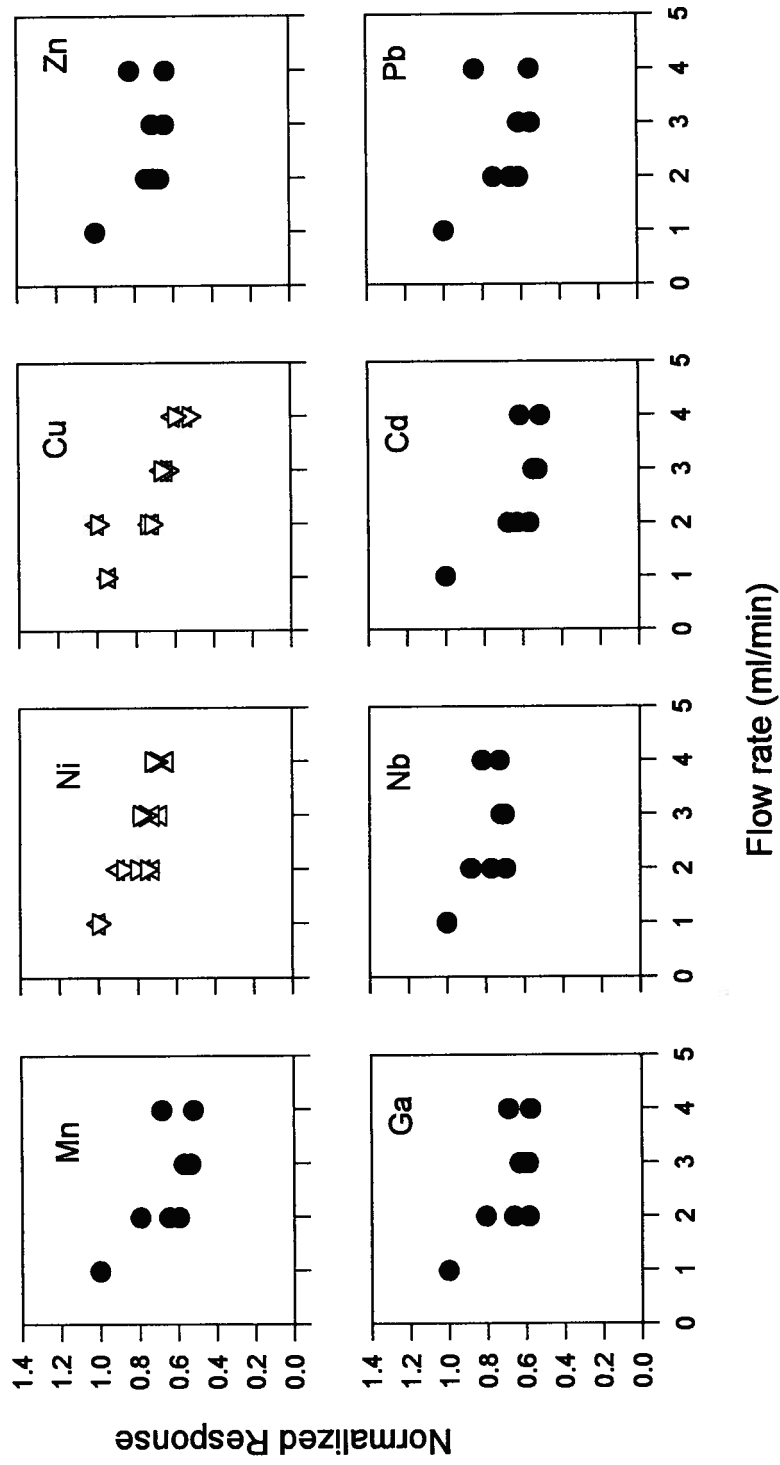


Figure 3.4 Metal response vs. flow rate for the 10 elements. 1, 3, 2 and 2 measurements were made for flow rates of 1, 2, 3 and 4 ml/min, respectively. Responses were normalized to the maximum signal of each element. Two isotopes of Ni and Cu are shown.

For the work presented in this dissertation, the maximum time per analysis using the on-line FI-ICP-MS method was chosen to be 10 minutes, resulting in a minimum throughput of 6 analyses per hour. From Table 3.5, using a 1 ml/min flow rate would result in less than the six analyses per hour, for 6 mls of sample. For depth profiles, volumes of samples preconcentrated were between 12 and 18 mls for each analysis. Therefore a flow rate of 3 ml/min was chosen since the time per analysis was decreased and it was the middle of the flow rate range of the manifold.

3.4.4 Interelement Interferences

The ICP-MS does not suffer from line interferences as does the ICP-AES, but it does suffer from overlapping mass to charge ratio (m/z) for some elements as a result of isobaric interference, doubly charged ions, and formation of oxide- and hydroxide- species [111]. Potential interferences are listed in Table 3.6.

Of the possible interfering species listed in Table 3.6, Ca oxides and hydroxides would appear to be the most serious potential interferent since Ca is present in mM levels in seawater. During the preconcentration step, the major seawater ions, including Na, Mg and Ca are almost totally not extracted from seawater and are in effect separated from the trace elements. The effect of TiO on either Cu or Zn would not be noticeable since Ti is present in the pM range while Cu and Zn are present in the nM range. Chromium and V have isotopes that as oxides, can interfere with ^{66}Zn . The effects of their oxides should be minimal since V is not significantly retained on the resin and total dissolved Cr is present in seawater at concentrations similar to than total dissolved Zn. Furthermore, the natural abundances of ^{50}Cr and ^{50}V are much lower than for ^{66}Zn (4.35%, 0.24 % and 27.81%, respectively), and even assuming that 50% of Cr and V existed as oxides in the plasma, their effects would be less than 10% of

the ^{66}Zn signal. On-line work has shown that neither Sn nor Mo are significantly extracted by the resin column during seawater preconcentration (< 10% of the Cd signal), hence their effects, if any, are minimal with respect to Cd. Finally, the effect of doubly charged ions can be minimized by tuning the ICP-MS to decrease their formation in the plasma.

Isotope	Potential Interferents
^{55}Mn	
^{58}Ni	^{58}Fe , $^{42}\text{Ca}^{16}\text{O}$
^{60}Ni	$^{44}\text{Ca}^{16}\text{O}$
^{63}Cu	$^{47}\text{Ti}^{16}\text{O}$
^{65}Cu	$^{49}\text{Ti}^{16}\text{O}$, $^{130}\text{Ba}^{2+}$
^{66}Zn	$^{50}\text{Ti}^{16}\text{O}$, $^{50}\text{V}^{16}\text{O}$, $^{50}\text{Cr}^{16}\text{O}$, $^{132}\text{Ba}^{2+}$
^{71}Ga	$^{141}\text{Pr}^{2+}$, $^{142}\text{Ce}^{2+}$, $^{142}\text{Nd}^{2+}$, $^{143}\text{Nd}^{2+}$
^{93}Nb	
^{114}Cd	^{114}Sn , $^{98}\text{Mo}^{16}\text{O}$
^{208}Pb	

Table 3.6 Potential interferents of the 10 isotopes. From reference [111].

3.4.5 System Blanks and Detection Limits

The system blank was determined by subjecting 1 ml of pH 8 adjusted DDI to the same seawater loading and eluting procedure five separate times and averaging the result. The detection limit of the system was determined as three times the standard deviation (3s) of the five system blanks. A calibration curve using 12 mls of unspiked and spiked seawater adjusted to pH 8 was used to

convert these results to nmol/kg. The system blanks and detection limits of the isotopes are shown in Table 3.7. For some elements, the lowest concentration in seawater is less than three times the system blank, e.g. Cd. To measure these elements, a larger volume of seawater would have to be preconcentrated.

Isotope	System Blank (nmol/kg)	Detection Limit (nmol/kg)	Seawater Range (nmol/kg)
Mn 55	0.169	0.017	0.1-3
Ni 58	0.298	0.047	2-12
Ni 60	0.212	0.040	see Ni 58
Cu 63	0.105	0.016	0.5-4.5
Cu 65	0.109	0.020	see Cu 63
Zn 66	0.191	0.095	0.1-8.2
Ga 71	0.006	0.001	0.012-0.030
Nb 93	0.075	0.008	0.010-0.200
Cd 114	0.007	0.002	0.001-1
Pb 208	0.024	0.001	0.003-0.150

Table 3.7 The average of five system blanks and detection limits (3s) for 6 mls of seawater in nmol/kg. Quoted concentration range of metals in seawater are from reference [94], except for Nb which was determined in this work.

3.4.6 Precision and Accuracy

It was particularly important to evaluate the precision of this method since the peak jump mode was used to measure the eluent peak maximum. Other ICP-MS instruments were able to monitor up to six individual mass settings in SIM mode simultaneously. The VG PlasmaQuad did not have this capability. In

the majority of off-line preconcentration studies, enough eluent was collected to permit the continuous aspiration of the solution into the ICP-MS. On-line methods allowed only one measurement per elution, thus multiple measurements required multiple processing per sample.

The accuracy and precision of this technique was assessed by the analyses of dissolved Mn, Ni, Cu, Zn, Cd and Pb in seawater reference standards from the National Research Council of Canada. The reference seawater sample used was the Open Seawater Reference material (NASS-3). A 300 ml portion of this water was adjusted to pH 8 and then subdivided into four unequal aliquots: a 150 ml sample left unspiked and three separate 50 ml samples, spiked with 50, 100 and 250 μl s of the mixed metal stock solution (Table 3.3). Sample volumes of 12 ml were used for each analysis with 10 measurements made on the unspiked subsample and three measurements made on each spiked subsample, all using the on-line FI-ICP-MS method.

The results from this study are shown in Table 3.8. Using Student's t-test, the data show no significant differences between the found and certified results for these metals at the 95 % confidence limit.

The precision of this on-line method for Mn, Ni, Cu, Zn, Cd and Pb was evaluated by examining the relative standard deviations (RSDs) determined for 10 replicate analyses on the NASS-3 seawater standard. The RSDs were between 5 and 12 % for all elements, except for Cu, which was higher. The precision of this method for dissolved Ga and Nb was also determined, but the accuracy could not be ascertained in the same manner for the other elements, since no certified values of these two elements exist in seawater standards.

Element	NASS-3 _{certified} (ng/l)	NASS-3 _{found} (ng/l)	RSDs (%)
Mn	31 ± 12	25 ± 1	5
Ni	263 ± 63	247 ± 11	6
Cu	93 ± 9	88 ± 17	25
Zn	218 ± 30	190 ± 12	9
Cd	22 ± 4	29 ± 1	5
Pb	31 ± 10	32 ± 3	12
Ga	--	1.54 ± 0.01	5
Nb	--	37 ± 3	5

Table 3.8 The determination of dissolved Mn, Ni, Cu, Zn, Cd, Pb, Ga and Nb in NASS-3 seawater reference material.

To evaluate the accuracy of the Ga response of this on-line FI-ICP-MS method, a profile of dissolved Ga at station P26 previously reported [3] is compared with the Ga profile obtained in this study (Figure 3.5). The dissolved Ga distributions obtained with the method developed here is similar to that observed previously at station P26, except that the sub-surface maximum is deeper and more pronounced. Scatter exists in the profile using the on-line method, but the method was not optimized when these samples were analyzed. Therefore, the new Ga results are in reasonable agreement with the previously published data.

The only seawater data published for Nb comprise two surface water samples from the English Channel in 1958. These results may not be accurate since they predate the advent of contamination controls for seawater sampling and handling. Therefore, they cannot be compared to the results obtained in the

North Pacific. Generally, standard addition methods for mono-isotopic elements such as Nb are the most accurate.

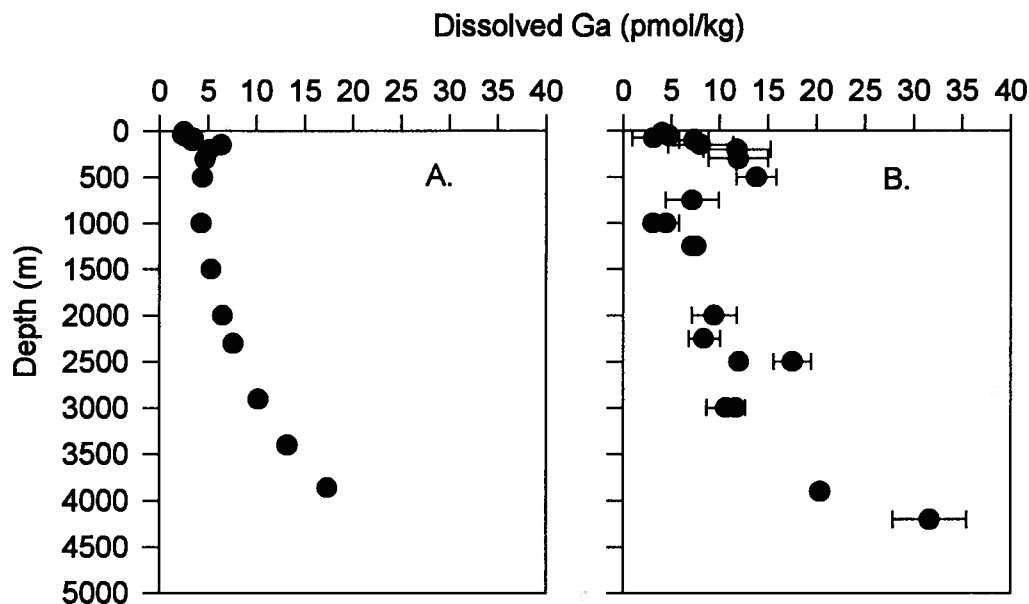


Figure 3.5 Dissolved Ga at station P26.
 A. Data from reference [3]. B. Results from this work, error bars represent the range of duplicate analyses.

3.5 Sample Preparation

Once the parameters were optimized, the procedure for all samples and standard additions analyzed by the on-line FI-ICP-MS work involved taking 50 to 250 ml subsamples from acidified seawater samples. The 50 ml subsamples of seawater were placed in acid cleaned PE bottles (60 ml), and adjusted to pH 8 using Q-ammonia and Q-acetic acid. Calibration curves were run using the method of standard addition every 3 to 5 samples. For each standard addition calibration, a 250 ml subsample of seawater was first pH adjusted, and then subdivided into four acid cleaned DE bottles (60 ml). Three of the bottles were spiked with 50 to 1000 μ l of a mixed standard solution (Table 3.3) while the

fourth was left unspiked. All the pH-adjusted bottles, both spiked and unspiked samples, were then left for 24 hours to allow equilibration.

The eluent used to strip the metals off the resin (2 N Q-nitric acid) was spiked with 0.5 ppb of Rh which acted as an internal standard. This internal standard was used to correct for any drift in the instrument response during the course of the day.

Calibration curves for all elements were linear and gave correlation coefficients, R^2 , between 0.950 to 0.999 (n= 6 to 12).

CHAPTER 4: OCEANOGRAPHIC RESULTS AND DISCUSSION

4.1 Characteristics of the Ocean Stations Sampled

The stations sampled in the North Pacific study area are shown in Figure 4.1. The surface waters of these stations span five distinct water masses which are characterized by their temperature and salinity values. The Oyashio Current (Station 1) is characterized by low temperature (T) and low salinity (S) as it carries water from the Bering Sea and Sea of Okhotsk in the north to the Japanese Islands in the south. The Kuroshio Current (Station 5) flows from south to north along the Asian coast from the equatorial Pacific and is characterized by high T and S. Station 10 is in the southern part of the central gyre and is higher in both T and S as it is located at a lower latitude than the previous two stations. The North Equatorial Current (Stations 15 and 16) brings high T and low S water from North America west across the Pacific Ocean. Station P26 lies at the convergence of the Alaskan Gyre and the North Pacific Current and has low T and S water. As the North Pacific Current approaches the North American coast, it begins to flow south creating the California Current.

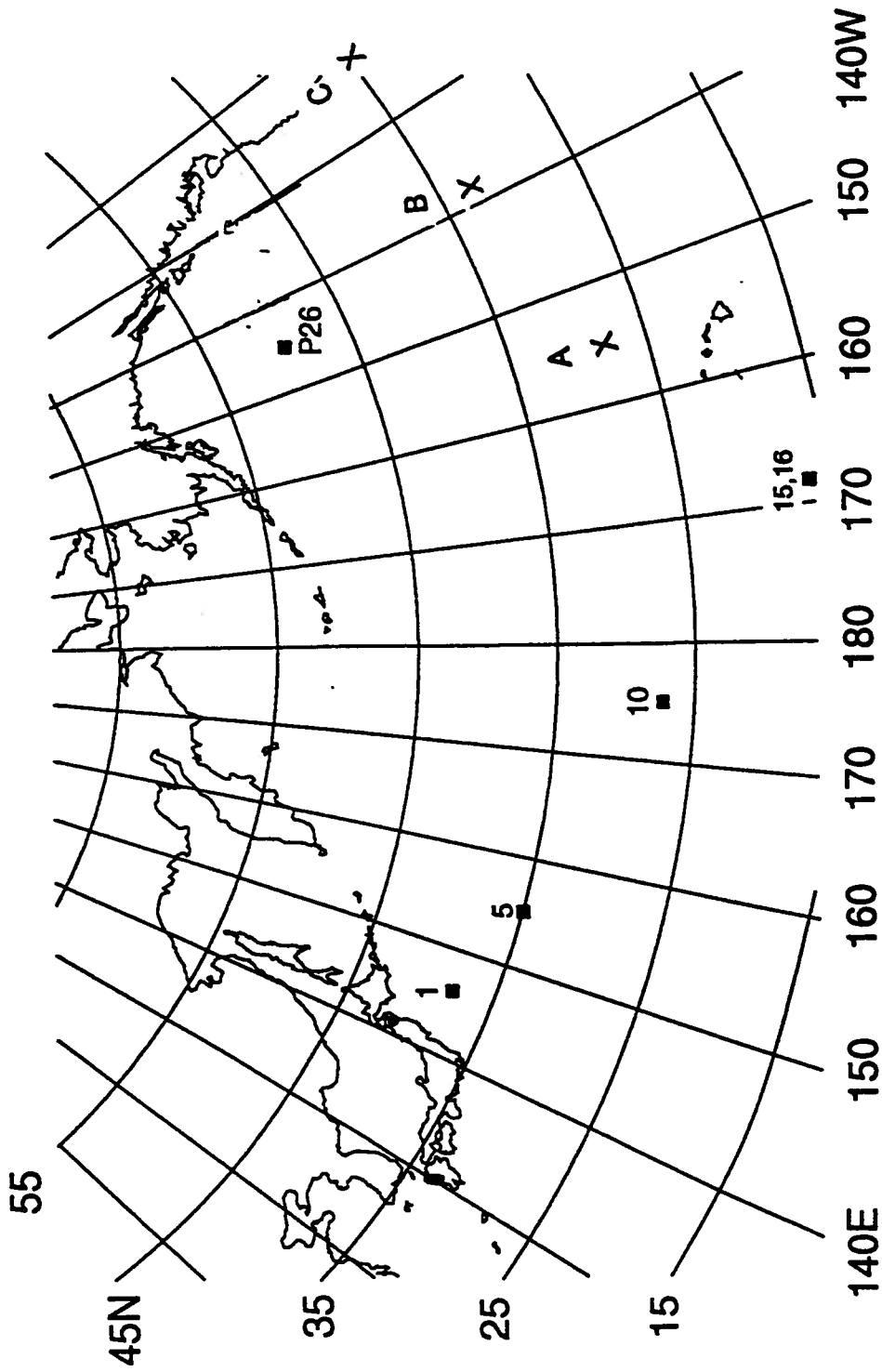


Figure 4.1 North Pacific study area.

- : Stations where vertical profiles were collected.
- x: Stations from previous work [3] used for comparisons in this dissertation.
- A. VERTEX IV. B. VERTEX VA. C. VERTEX VC.

4.2 Dissolved Zn, Cd, Ni, Pb, Cu and Mn in the North Pacific Ocean

Profiles of Zn, Cd, Ni, Pb, Cu and Mn at Stations 1,5,10, 15 and 16 have been previously determined by off-line preconcentration with ICP-MS detection and have been discussed in detail elsewhere [112]. These six elements at the same stations were analyzed using the on-line FI-ICP-MS method described in Chapter 3 with good results, indicating that this method can be used to preconcentrate and analyze full depth profiles of these elements in one day compared with up to 2 weeks with conventional processing.

4.2.1 Nutrient-type Elements (Zn, Cd and Ni)

Nutrient-type elements can have one of three distribution types. One type results in deep water regeneration with a deep water maximum similar to that of Si, which is used by organisms in skeletal structures (*e.g.* Zn). A second type shows a shallow regeneration leading to a mid-depth maximum, similar to that found for phosphate and nitrate, which are labile soft tissue nutrients (*e.g.* Cd). The third type results from a combination of shallow and deep regeneration (*e.g.* Ni).

4.2.1.1 Dissolved Zn in the North Pacific

Depth profiles of dissolved Zn at Stations 1,5,10, 15, 16 and P26 are shown in Figures 4.2, 4.3 and 4.4. The profiles at these stations agree well with previous Zn profiles in the North Pacific [35, 112]. Generally, the profiles (Figures 4.2, 4.3 and 4.4) follow those of the "hard-part" nutrient silicate, showing depleted Zn concentrations in surface waters which slowly increase with depth to broad maxima between 1000 and 1500 m. This is a result of Zn being removed from surface waters by phytoplankton and incorporated into skeletal structures (*e.g.* diatoms), which then sink and are regenerated in deep waters.

At Station 1, surface water levels of Zn are higher than at the other five stations (2.5 nmol/kg versus 0.4 - 0.6 nmol/kg at Stations 5, 10, 15 and P26 and 0.9 nmol/kg at Station 16). A deep water maximum at the same site is shallower (9 nmol/kg at 1000 m) compared to the other stations (7 - 9 nmol/kg at 1500 to 2000 m). Below this depth the profiles are similar. There is considerable scatter in the Zn data at Station P26 due to the non-optimized procedure used for the analysis. Allowing for the scatter in the data, the profile agree fairly well with previous work at this location which showed a deep water maximum between 1400 and 1800 m [113].

The correlation between dissolved Zn and silicate is estimated by plotting dissolved Zn versus silicate from Stations 1, 5, 10, 15 and 16 (Figure 4.5). A linear relationship is observed with a slope of 0.0523 Zn/Si ($\text{nmol kg}^{-1} \mu\text{M}^{-1}$) and a regression coefficient, R^2 of 0.947. The Zn/Si ratio obtained here is not significantly different to ratios observed previously at these stations (*i.e.*, 0.0544) [112] and reported for east Pacific Ocean sites (*i.e.*, 0.0535) [18].

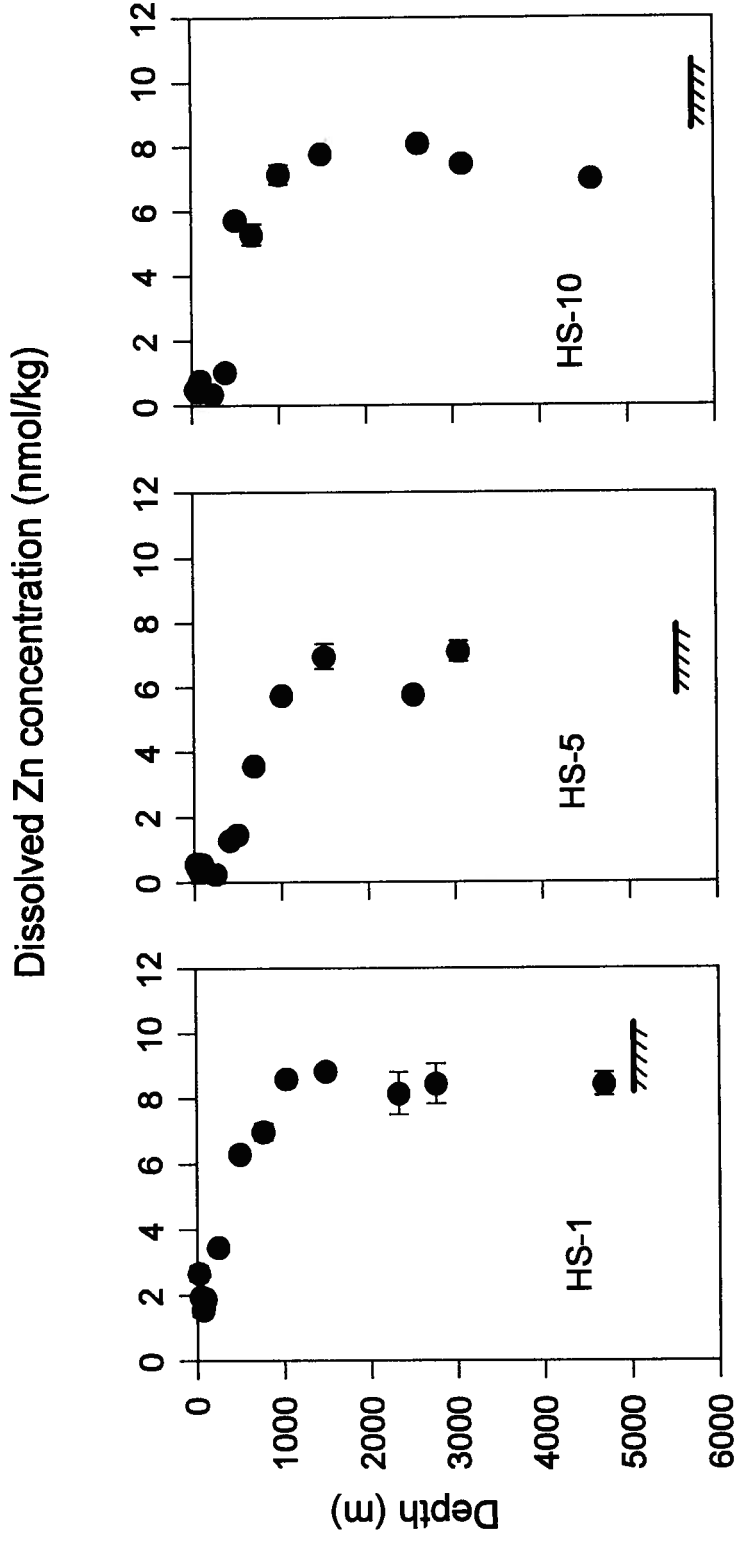



Figure 4.2 Dissolved Zn in the western North Pacific. Each point is the average of two analyses. The error bars indicate the range. The symbol  represents the seafloor bottoms at all stations.

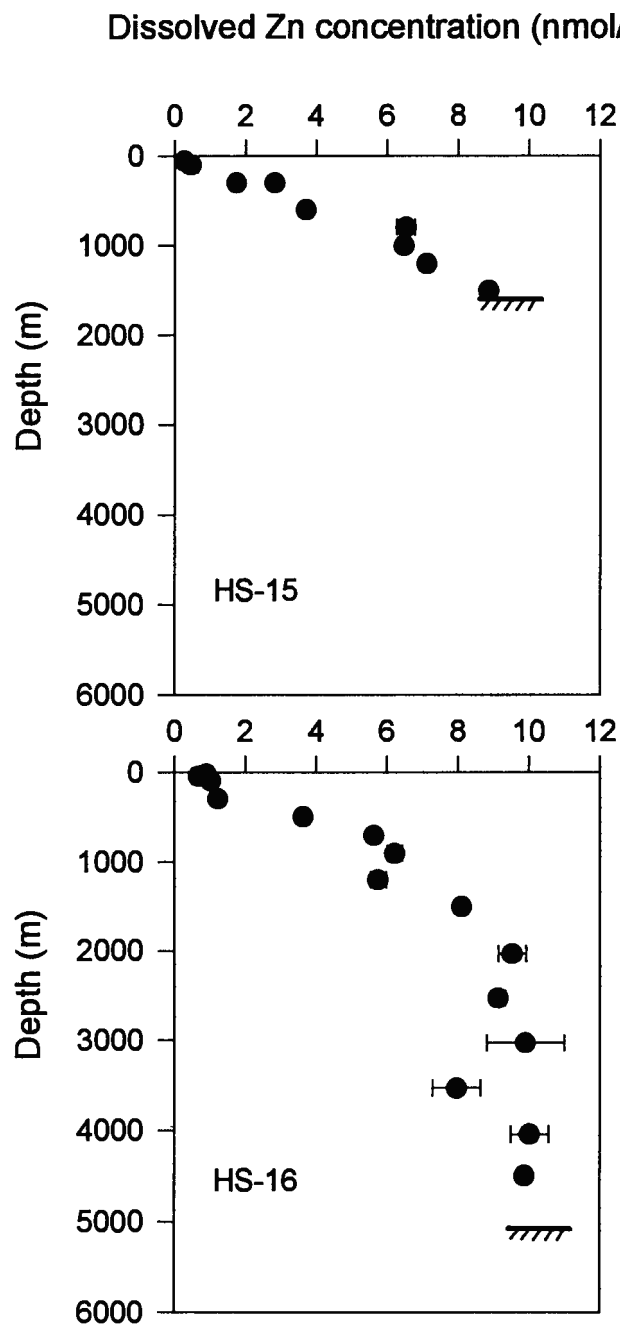


Figure 4.3 Dissolved Zn in the central North Pacific. Each point is the average of two analyses. Error bars indicate the range.

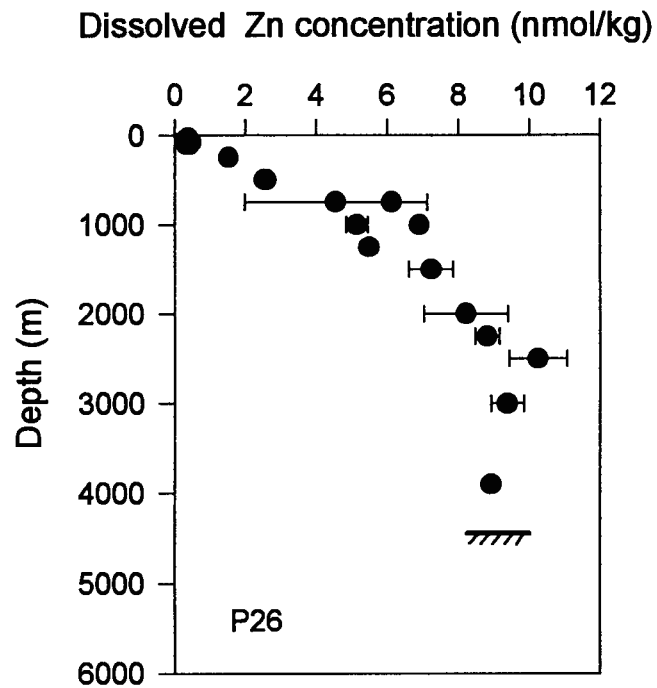


Figure 4.4 Dissolved Zn in the eastern North Pacific in the sub-Arctic gyre. Each point is the average of two analyses. Error bars indicate the range.

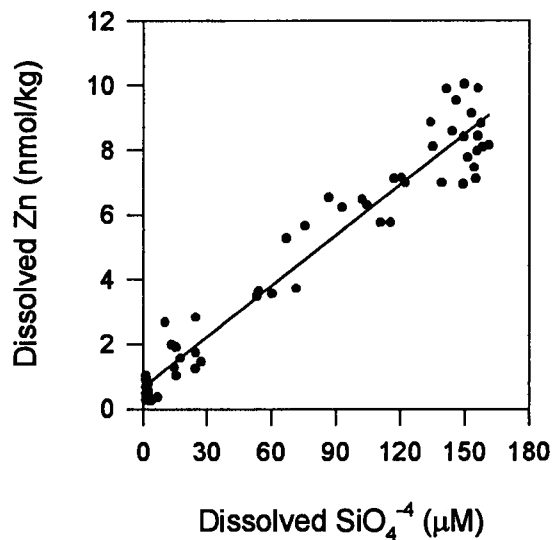


Figure 4.5 Dissolved Zn vs. the nutrient silicate. Silicate data provided by IOS (Institute of Ocean Science, Sidney, BC)

4.2.1.2 Dissolved Cd in the North Pacific

Profiles of dissolved Cd at Stations 1, 5 and 10, 15, 16 and P26 are shown in Figures 4.6, 4.7 and 4.8. The dissolved Cd distributions at all these stations agree well with previous Cd profiles in the North Pacific [18, 39, 41, 112, 113]. Generally, Cd concentrations follow the "soft-part" nutrients, phosphate and nitrate, showing depleted Cd levels in surface waters which rapidly increase with depth to broad maxima between 600 and 1000 m. The surface waters show high dissolved Cd at Station 1 (0.25 nmol/kg) which decreases to much lower levels in the Kuroshio Current (HS 5) and central gyre (HS 10) stations (0.03 and 0.01 nmol/kg, respectively). Cadmium values in the North Equatorial Pacific surface waters (Stations 15 and 16) are also lower than at Station 1 (0.01 and 0.015 nmol/kg, respectively) and are intermediate (0.15 nmol/kg) in the sub-Arctic gyre (P26). The elevated nutrient levels which occur at Stations 1 and P26 may be due to isopycnal mixing and outcropping isopycnal surfaces at these sites. This result may be enhanced at Station 1 due to a higher aeolian (wind-borne dust) input of Cd at this site [6, 113].

As for Zn, the mid-depth maximum at Station 1 occurs at a shallower depth (~1.0 nmol/kg between 500 and 1000 m) than at Stations 5, 10, 15 and 16 (~0.9 nmol/kg between 800 and 1500 m). At Station P26, the mid-depth maximum of ~0.9 nmol/kg is shallowest, occurring between 200 and 1500 m, also indicating isopycnal mixing with deeper waters further south which have higher Cd levels. Below 1000 m all profiles are similar, showing slight decreases in Cd below 1500 m. These observations agree well with previous studies in these areas.

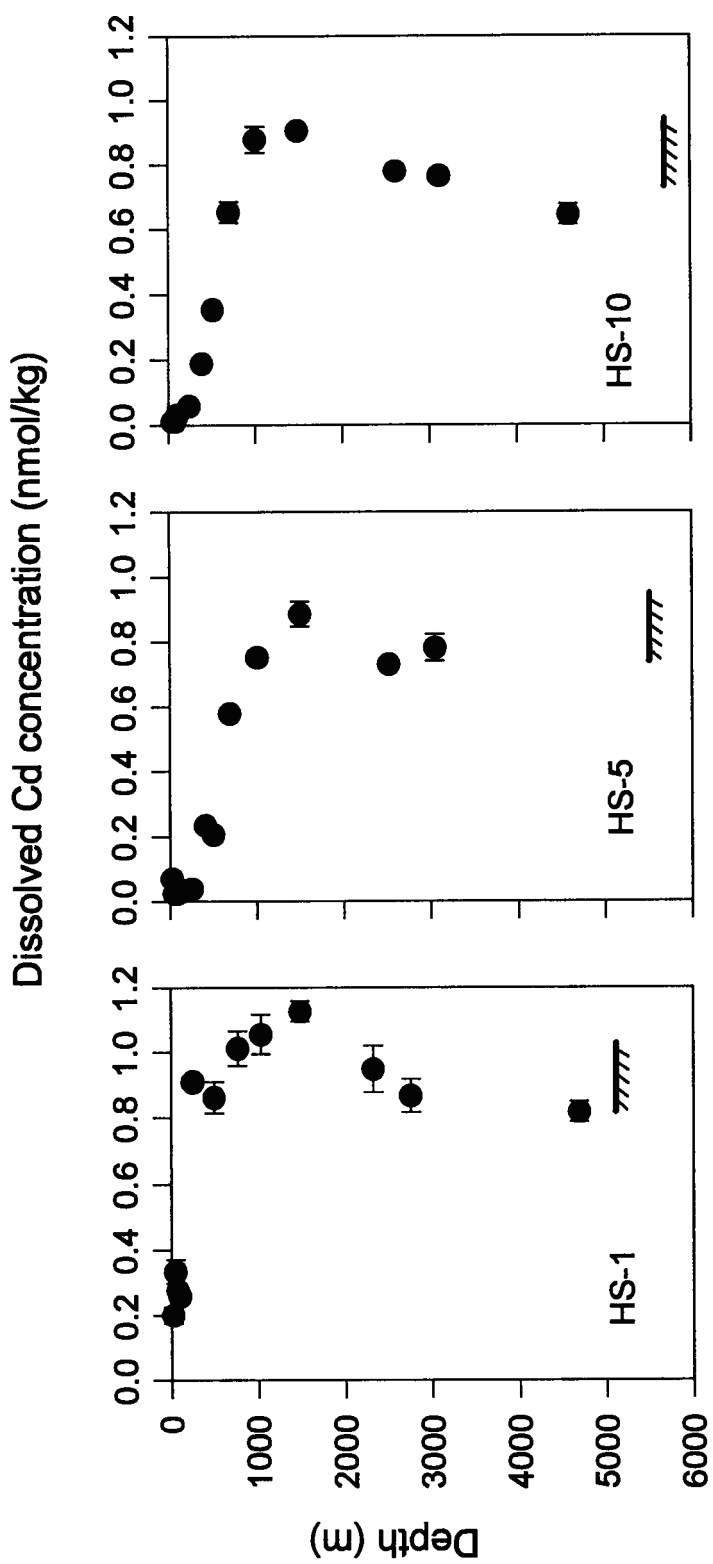


Figure 4.6 Dissolved Cd in the western North Pacific. Each point is the average of two analyses. The error bars indicate the range.

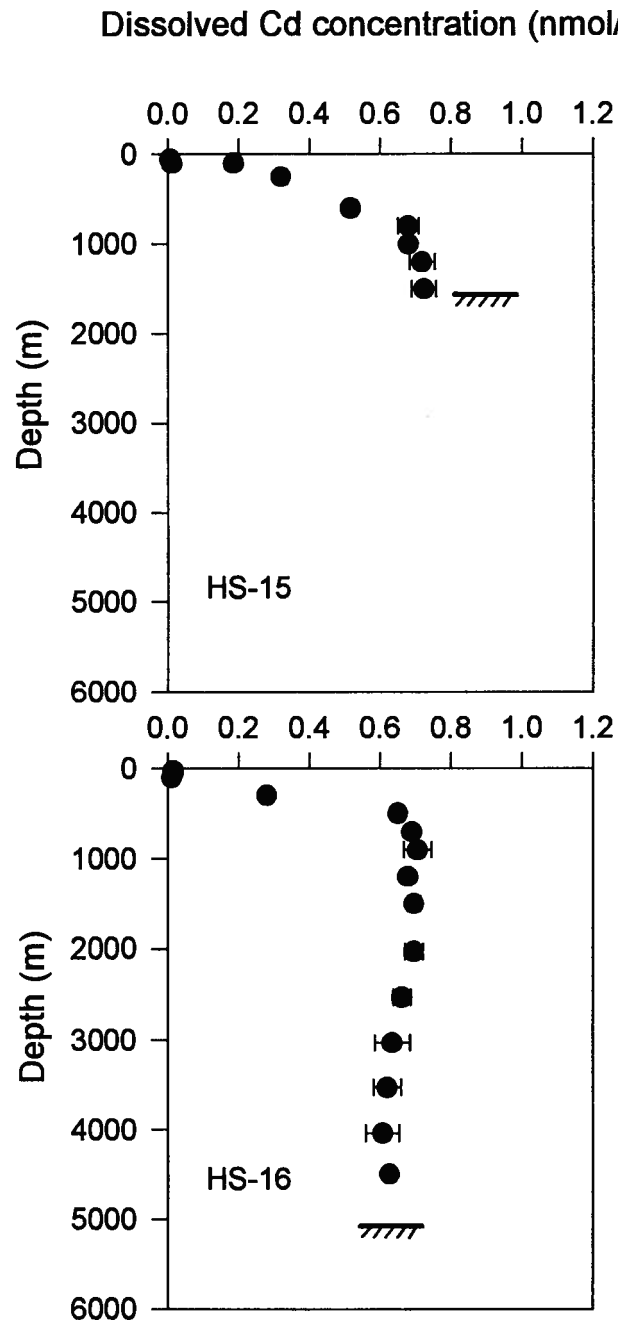


Figure 4.7 Dissolved Cd in the central North Pacific. Each point is the average of two analyses. Error bars indicate the range.

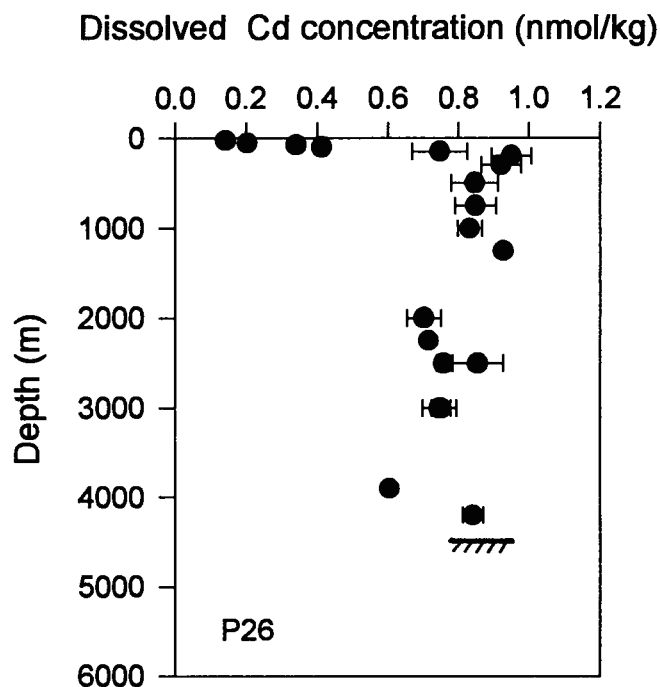


Figure 4.8 Dissolved Cd in the eastern North Pacific in the sub-Arctic gyre. Each point is the average of two analyses. Error bars indicate the range.

The correlations between dissolved Cd and nitrate and phosphate have been observed previously [18, 39, 41]. A plot of dissolved Cd versus phosphate from Stations 1, 5, 10, 15 and 16 is shown in Figure 4.9. The relationship is linear with a slope of $0.302 \text{ Cd/P (nmol kg}^{-1} \mu\text{M}^{-1})$ and a regression coefficient, R^2 of 0.943. The slope determined here is lower than that observed at these stations in previous work (0.325 Cd/P) [112] and to those reported in the east Pacific Ocean (*i.e.*, $0.33 - 0.37$) [17, 38].

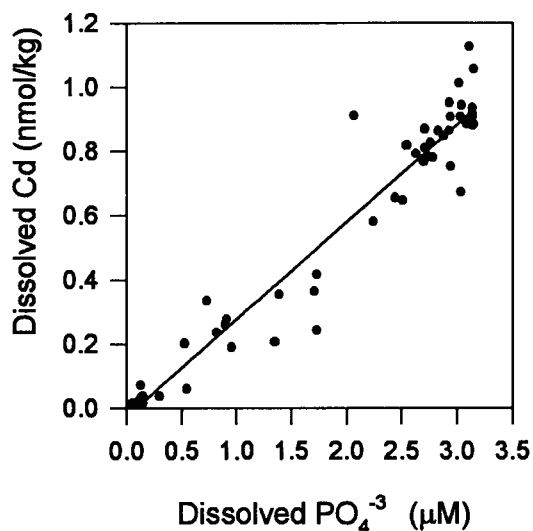


Figure 4.9 Dissolved Cd vs. the nutrient phosphate. Phosphate data provided by IOS

4.2.1.3 Dissolved Ni in the North Pacific

Profiles of dissolved Ni at Stations 1, 5, 10, 15, 16 and P26 are shown in Figures 4.10 4.11 and 4.12 and agree well with previous observations of Ni distributions in the North Pacific [18, 42, 112]. Generally, Ni in seawater has a biointermediate nutrient-type distribution with partial depletion in surface waters, a rapid increase in concentration in mid-depth waters similar to "soft-part" nutrients, phosphate and nitrate, and a broad maximum in deeper waters similar to "hard-part" nutrient, silicate.

At Station 1, the surface concentration of Ni is slightly higher than at Stations 5, 10 and P26 (3.5 versus 3 nmol/kg) and considerably higher than at Stations 15 and 16 (~1.5 nmol/kg). The Ni concentration increases rapidly to ~8 nmol/kg at 700 m, and then slowly to a broad maximum of 9-11 nmol/kg between 1500 and 3500 m, except at Station 1, which occurs between 1000 m and 2500 m and thus is shallower. This shallowing of the maximum, as for Zn and Cd, indicates isopycnal outcropping of high nutrient waters at this station.

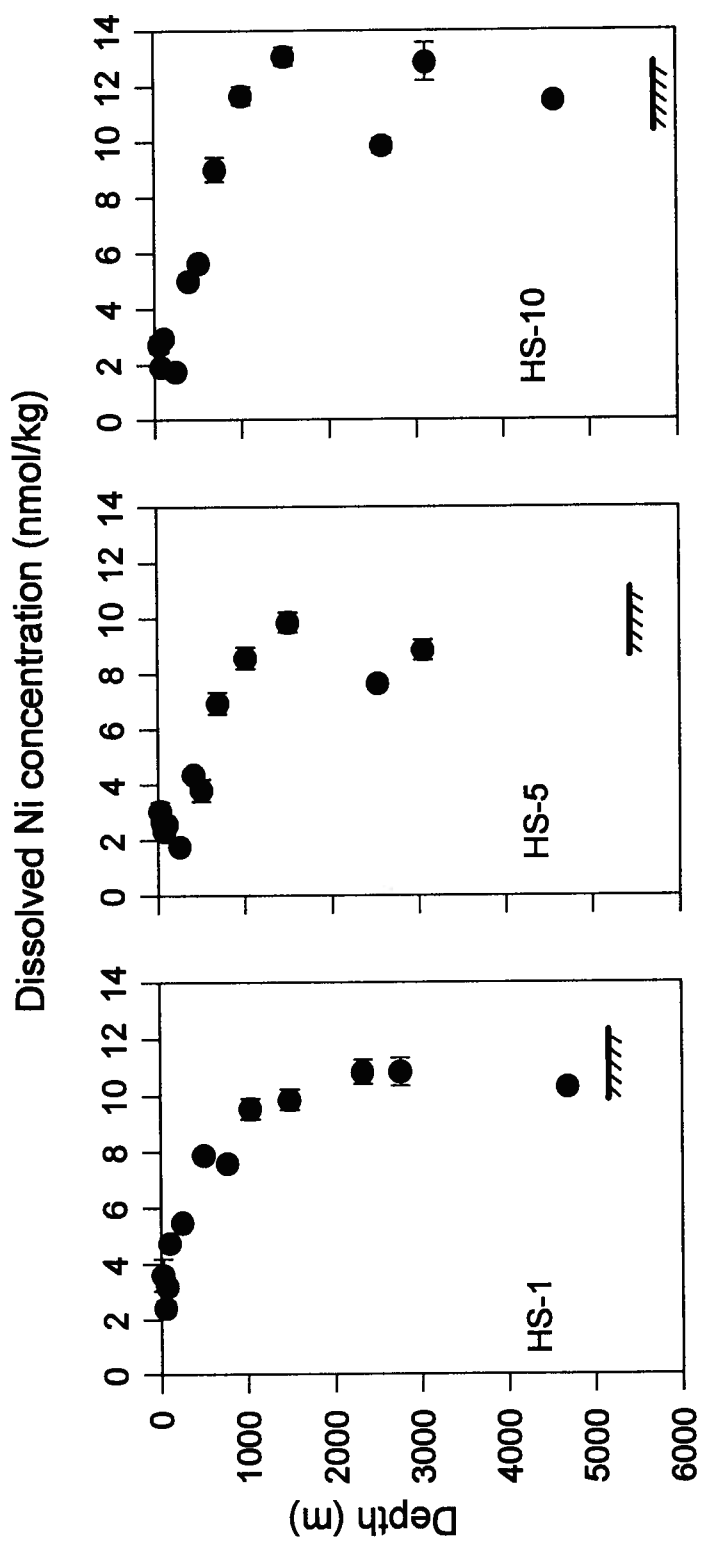


Figure 4.10 Dissolved Ni in the western North Pacific. Each point is the average of two analyses. The error bars indicate the range.

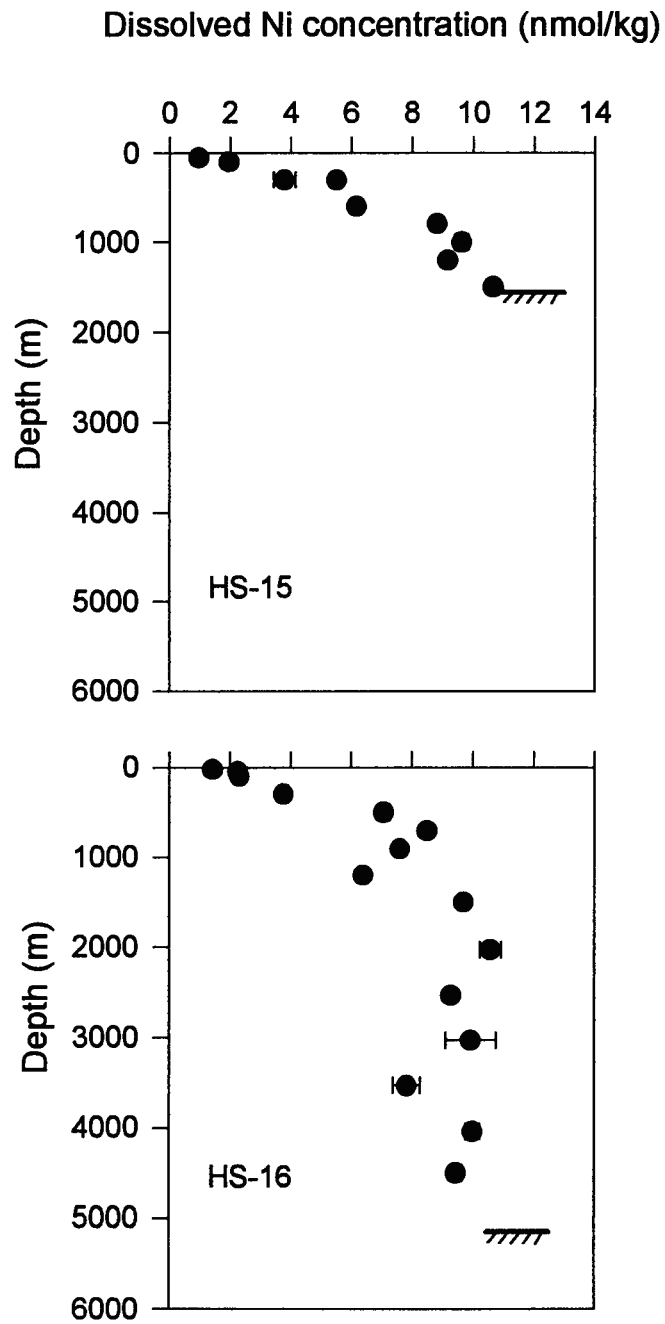


Figure 4.11 Dissolved Ni in the central North Pacific. Each point is the average of two analyses. Error bars indicate the range.

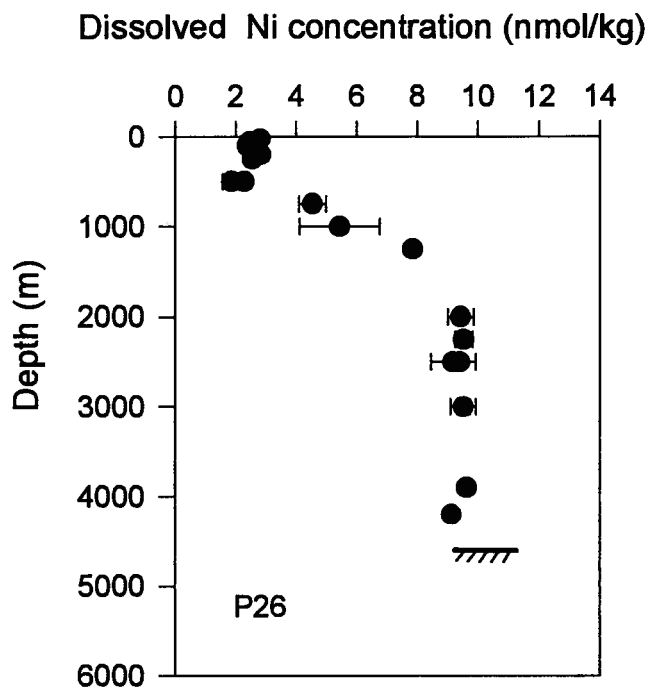


Figure 4.12 Dissolved Ni in the eastern North Pacific in the sub-Arctic gyre. Each point is the average of two analyses. Error bars indicate the range.

Dissolved Ni versus phosphate and silicate at Stations 1, 5, 10, 15 and 16 are shown in Figure 4.13. The correlation between Ni and phosphate (regression coefficient, $R^2 = 0.804$, Figure 4.13A) visually looks better than that between Ni and silicate ($R^2 = 0.855$, Figure 4.13B). The Ni-phosphate relationship in the upper 800 m (Figure 4.13C) is stronger ($R^2 = 0.845$) than that of Ni-phosphate at all depths and the relationship between Ni and silicate below 800 m (Figure 4.13D) is much worse. The improvement in the Ni-phosphate relationship in the upper 800 m agrees with Bruland's observations [18], though he also observed that the Ni-silicate relationship improved below 800 m, which is clearly not the case in this work.

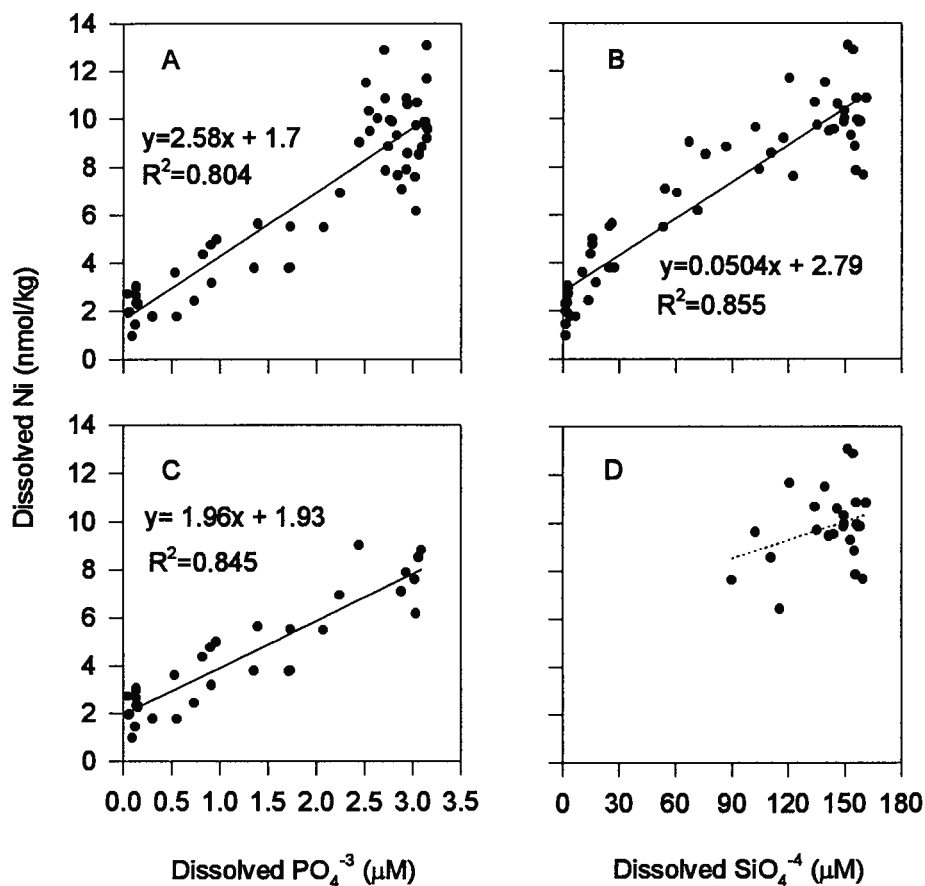


Figure 4.13 Ni versus phosphate (A, C) and silicate (B, D).
A and B: At all depths. C: Upper 800 m. D: Below 800 m.

4.2.2 Nutrient Type with Scavenging Element (Cu)

Profiles of dissolved Cu at Stations 1, 5, 10, 15, 16 and P26 are shown in Figures 4.14, 4.15 and 4.16 and agree reasonably well with Cu distributions previously observed in the North Pacific [18, 29, 43, 112, 113]. There is more scatter in these plots, possibly as a result of the poor precision for obtained for Cu with the manifold due to the pH used, which was not optimal for Cu extraction from seawater (section 3.4.6). Generally, the distribution of Cu is unique, with low levels in surface waters as it is a required biointermediate nutrient and

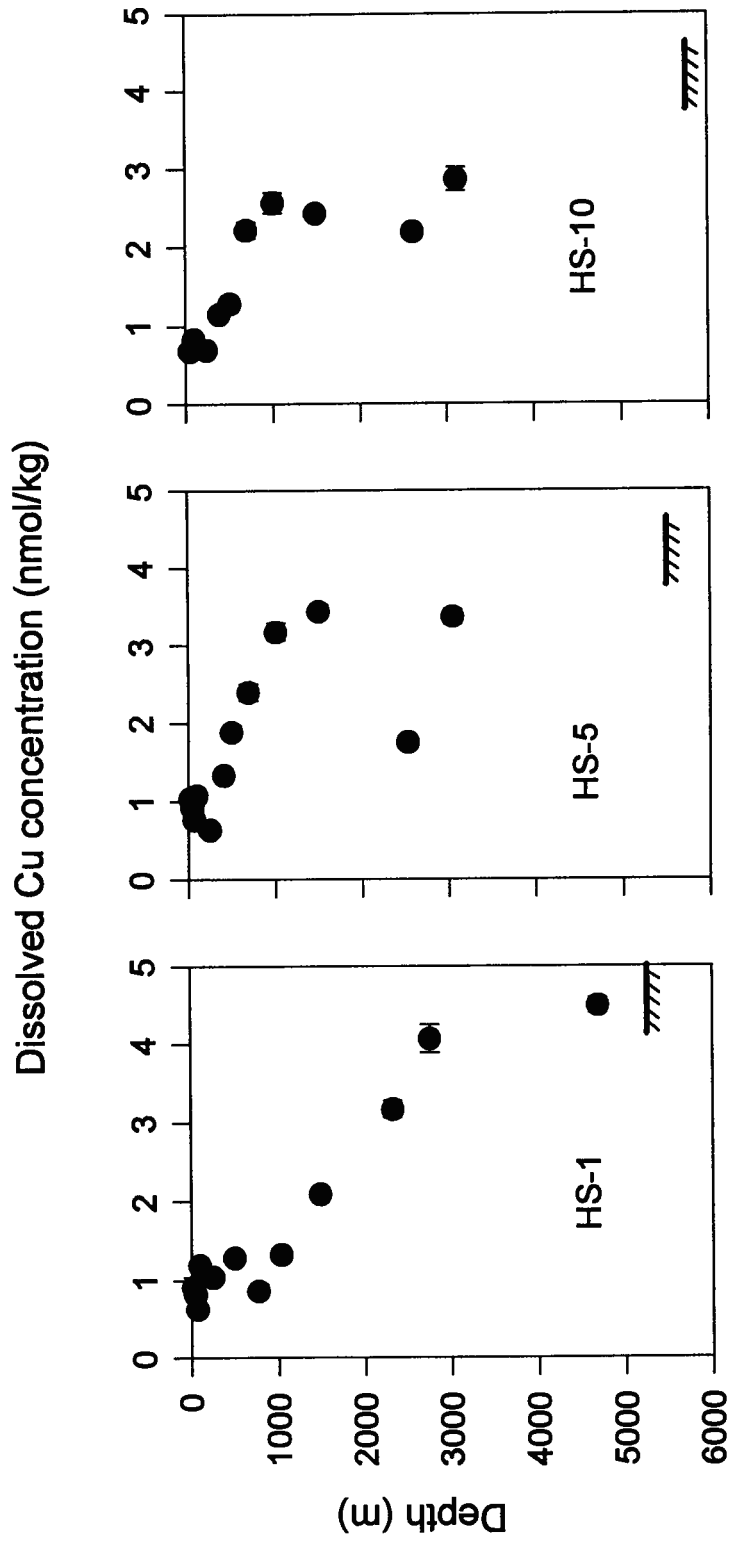


Figure 4.14 Dissolved Cu in the western North Pacific. Each point is the average of two analyses. The error bars indicate the range.

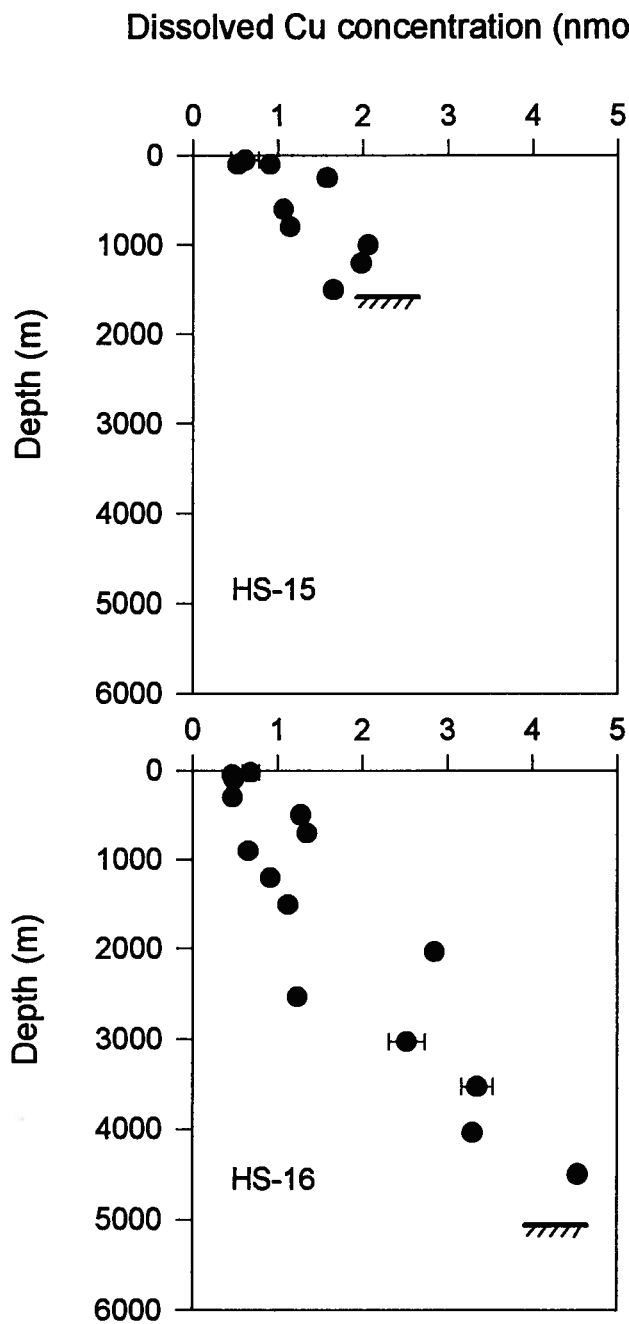


Figure 4.15 Dissolved Cu in the central North Pacific. Each point is the average of two analyses. Error bars indicate the range.

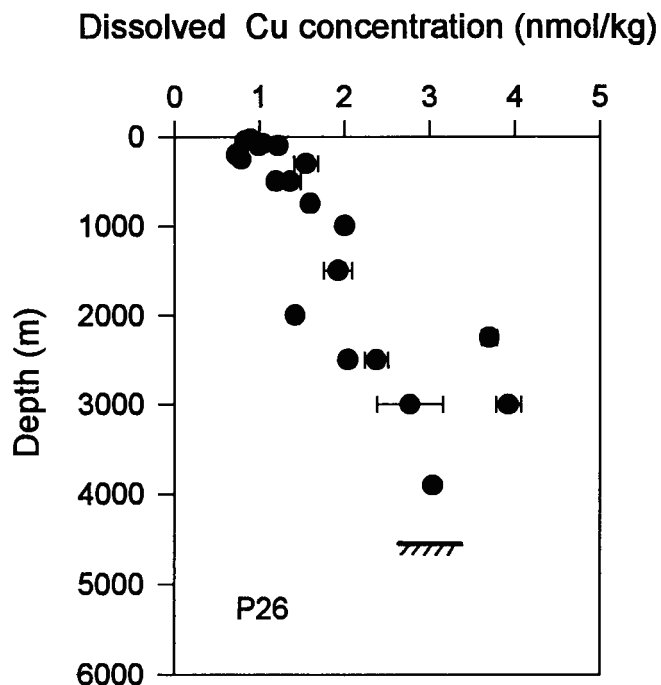


Figure 4.16 Dissolved Cu in the eastern North Pacific in the sub-Arctic gyre. Each point is the average of two analyses. Error bars indicate the range.

gradual increase with depth as a result of removal in intermediate and deep waters and a bottom source [18, 29].

Copper levels in the surface waters at all stations are similar, with dissolved Cu at Stations 1 and 5 (~1 nmol/kg) being slightly higher than at Stations 10, 15, 16 and P26 (~0.7-0.8 nmol/kg). Values increase with depth to levels between 3.5 and 4.5 nmol/kg at Stations 1, 10, 16 and P26 (the bottom water value at Station 10 was bad for this element). Station 15 is only 1550 m deep and the concentration in bottom water is 1.7 nmol/kg; samples below 3500 m at Station 5 were not collected. A first order vertical advection diffusion model has been previously used to calculate Cu residence times in the deep water (below 1000 m) at these stations. These estimates ranged from 830 to 1100

years [112], similar to previous studies [18, 29]. An explanation of the model is given in section 4.3.4.

4.2.3 Scavenged Type Element with an External Source (Pb)

Profiles of dissolved Pb from Stations 1, 5, 10, 15, 16 and P26 are shown in Figures 4.17, 4.18 and 4.19 and agree well with those observed previously for Pb in the North Pacific [45, 46, 112, 113]. Generally, Pb distributions have high surface values and decreasing concentrations with depth, though some exhibit a sub-surface maximum between 300 and 500 m. These profiles verify that the distribution of Pb in seawater is driven by scavenging removal processes and external inputs via aeolian transport.

Surface levels of Pb are highest at Station 1 (~ 60 pmol/kg) and decrease with distance from the Asian coast (30 and 40 pmol/kg at Stations 5 and 10, respectively). Surface Pb levels are low at Stations 15 and 16 (10 and 15 pmol/kg, respectively) and intermediate at Station P26 (30 pmol/kg). At Stations 1 and 5 the Pb concentrations decrease with depth to less than 20 pmol/kg, and no sub-surface maximum is observed. Stations 10, 15 and 16 all show sub-surface maxima. Stations 10 and 16 have sub-surface maxima of 40 pmol/kg between 200 and 500 m, while at Station 15, a sub-surface maximum of 25 pmol/kg at 300 m is observed. The scatter in the Pb data at Station P26 has obscured the profile, though even with scatter a suggestion of a sub-surface maximum is evident. Previous Pb from Station P26 has suggested a sub-surface maximum occurring between 300 and 500 m [113]. Below 500m at all stations, the Pb profiles become indistinguishable with Pb levels around 10 to 15 pmol/kg in deep waters.

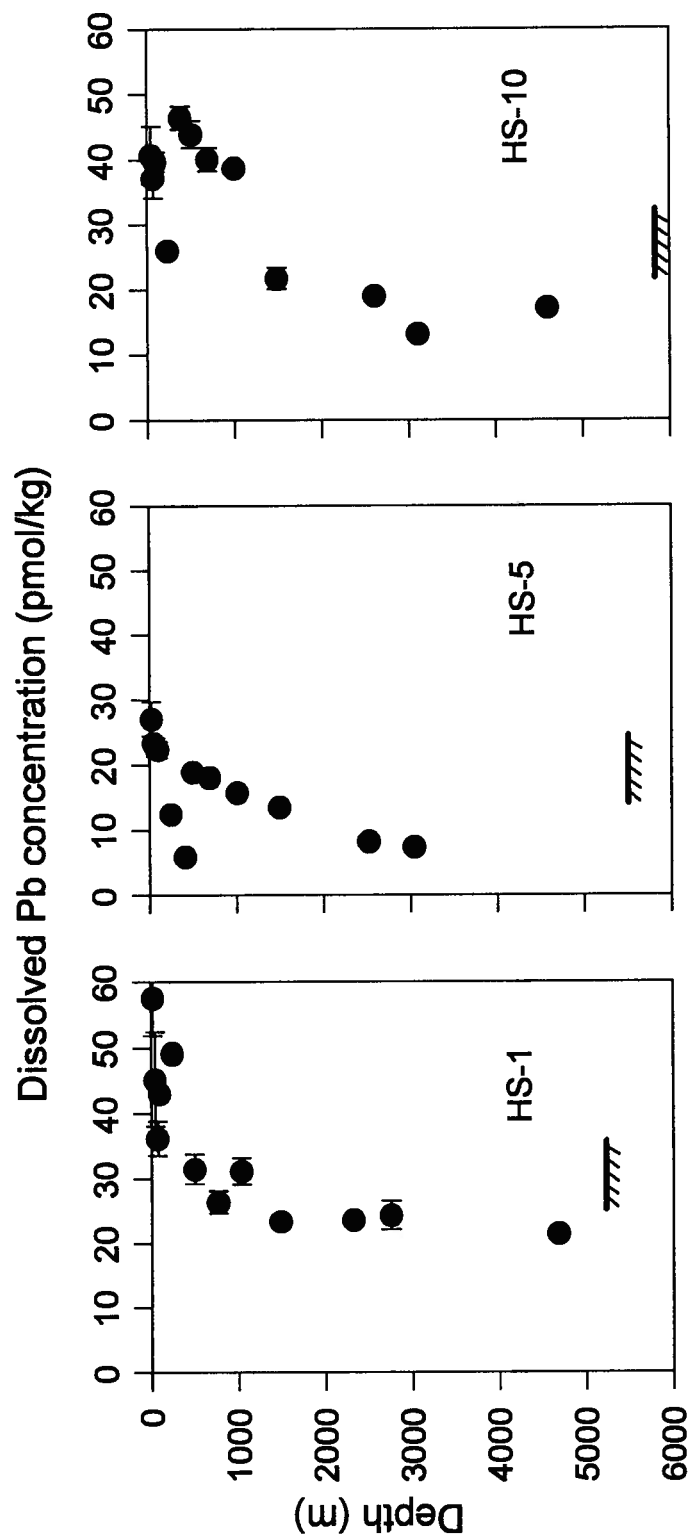


Figure 4.17 Dissolved Pb in the western North Pacific. Each point is the average of two analyses. The error bars indicate the range.

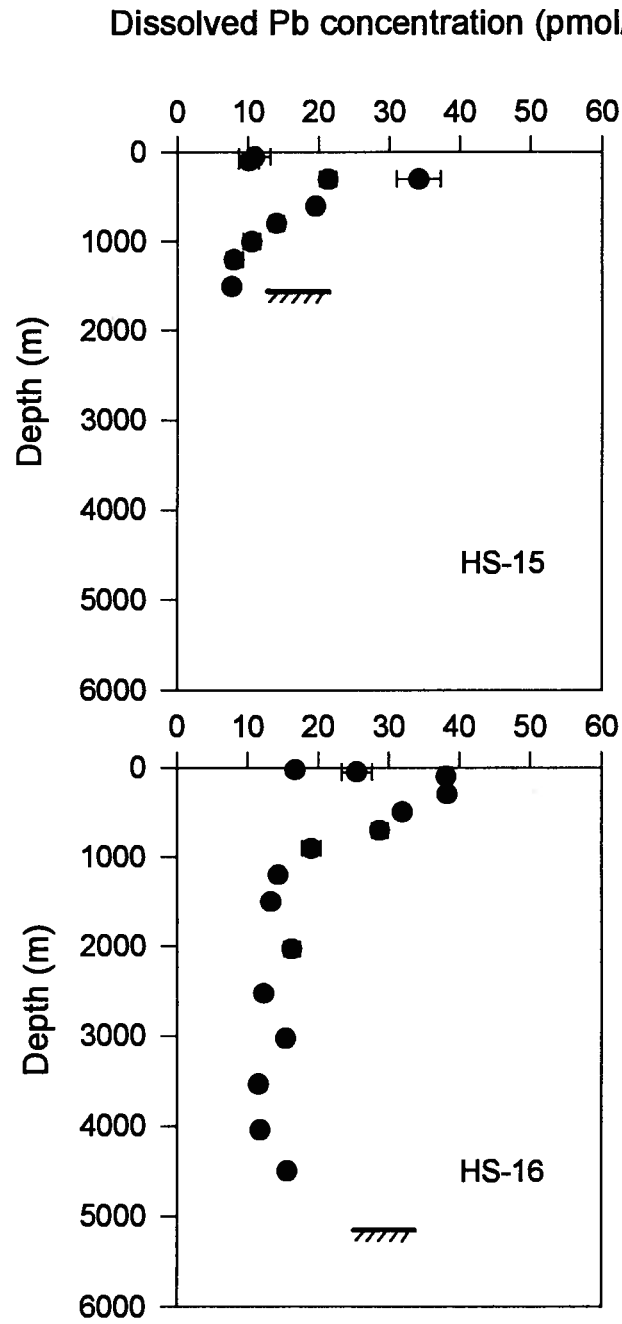


Figure 4.18 Dissolved Pb in the central North Pacific. Each point is the average of two analyses. Error bars indicate the range.

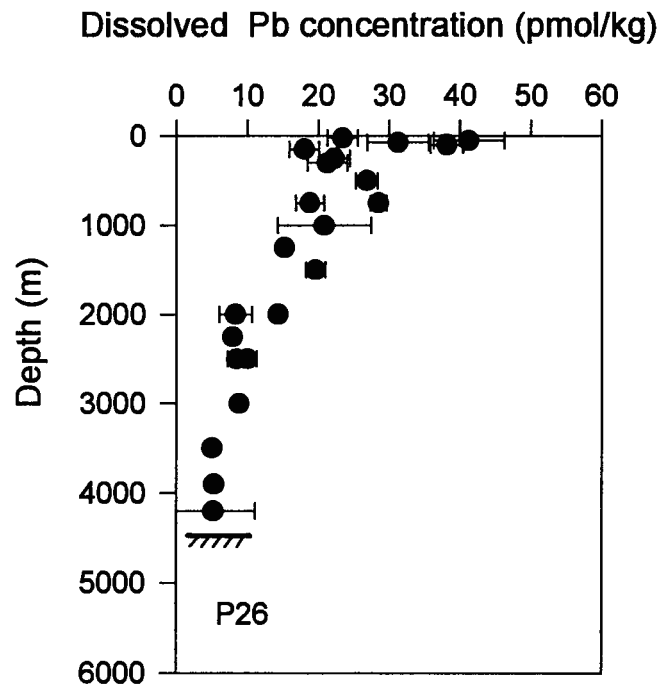


Figure 4.19 Dissolved Pb in the eastern North Pacific in the sub-Arctic gyre. Each point is the average of two analyses. Error bars indicate the range.

Explanations have been proposed to explain the sub-surface maxima observed at Stations 10, 15 and 16. The most commonly accepted is that the aeolian Pb input decreased due to reduced consumption of leaded gasoline since 1974 which may have induced a sub-surface maximum in most regions [9]. The data presented here supports this, since the mid-depth maxima of Pb are much greater in concentration than surface levels of Pb. Other possibilities have been argued for the mid-depth maxima [45], and if they are a factor, their role would be minor. One is that the Pb that is released from falling particles is greater than the scavenging flux at the depth of the mid-depth maximum, resulting in the accumulation of Pb in the water column until the scavenging flux equals or exceeds the decomposition flux as in deeper waters. Another is that

physical transport might supply Pb to the areas by isopycnal ventilation (i.e. movement of water of the same density from different locations).

4.2.4 Oxidative Scavenging Type Elements (Mn)

Profiles of dissolved Mn from Stations 1, 5, 10, 15, 16 and P26 are shown in Figures 4.20, 4.21 and 4.22 and agree well with previously observed Mn distributions in the North Pacific [47, 112, 113]. Generally, Stations 5, 10, 15 and 16 have high surface values between 0.8 and 1 nmol/kg, decreasing to a sub-surface minimum of 0.15 to 0.7 nmol/kg between 300 and 500 m, coincidental to the zone where dissolved O₂ is decreasing, and then increasing to a mid-depth maximum of 0.3 to 1.2 nmol/kg between 1000 and 1500 m in the O₂ minimum zone. Stations 1 and P26 have similar surface and sub-surface minima and mid-depth maxima values though the sub-surface minima and mid-depth maxima signals were shallower, occurring between 100 and 300 m and between 500 and 1000 m, respectively. Below 1500 m, all stations show Mn decreasing with depth.

Previous work has shown that the sources of Mn into the ocean are riverine, either directly or via reducing shelf sediments, atmospheric and submarine hydrothermal [48-50]. Manganese participates in a wide range of biogeochemical processes, including release from aeolian particles in surface waters and adsorbed onto particles. It is also a required micro-nutrient.

The Mn sub-surface minimum and mid-depth maximum has been found to be due to a combination of horizontal advection of waters from reducing shelf sediments and the cycling of dissolved Mn(II) and particulate Mn(III, IV) oxyhydroxides cycling in O₂ minimum zone [51]. Profiles of O₂ in seawater show high surface values, decreasing with depth due to its utilization during respiration and then increasing gradually due to upwelling of younger waters

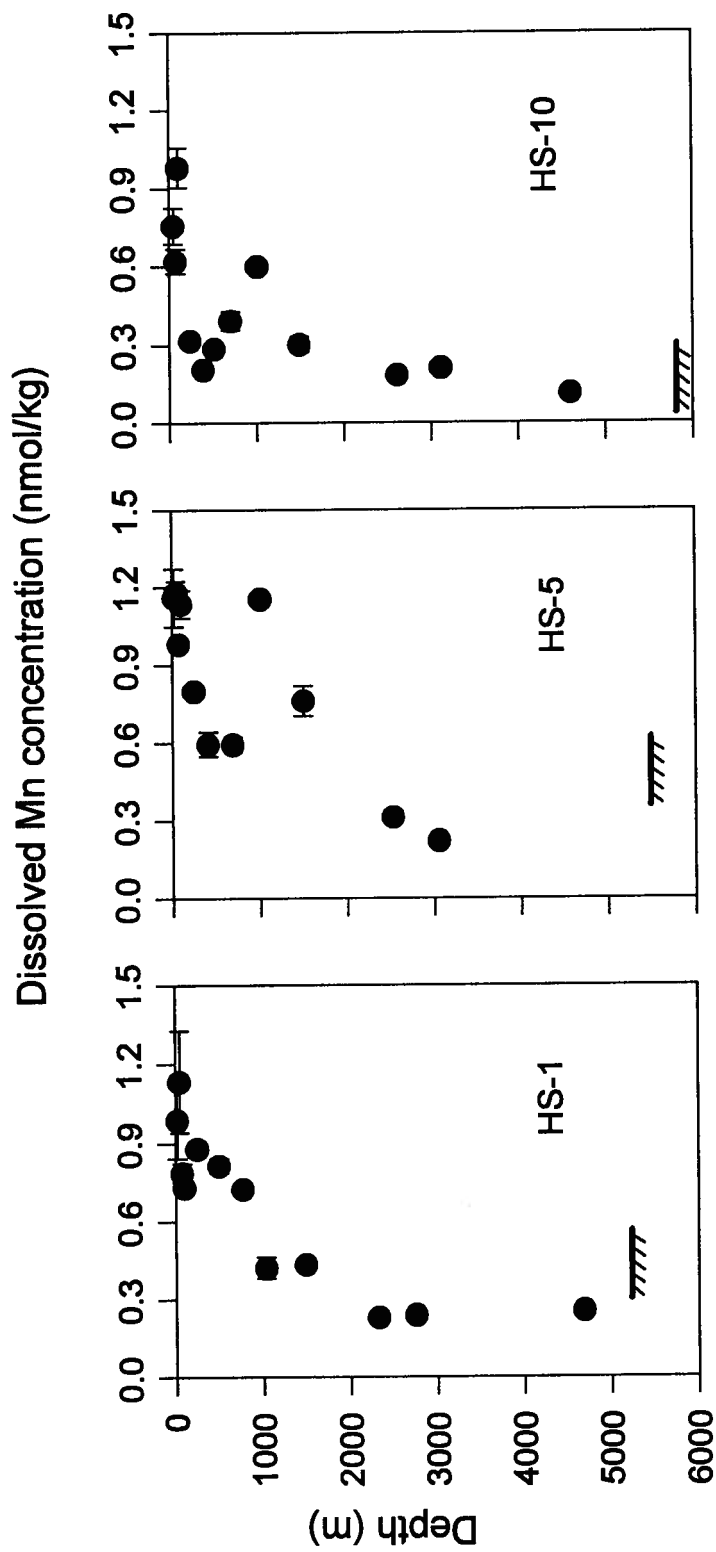


Figure 4.20 Dissolved Mn in the western North Pacific. Each point is the average of two analyses. The error bars indicate the range.

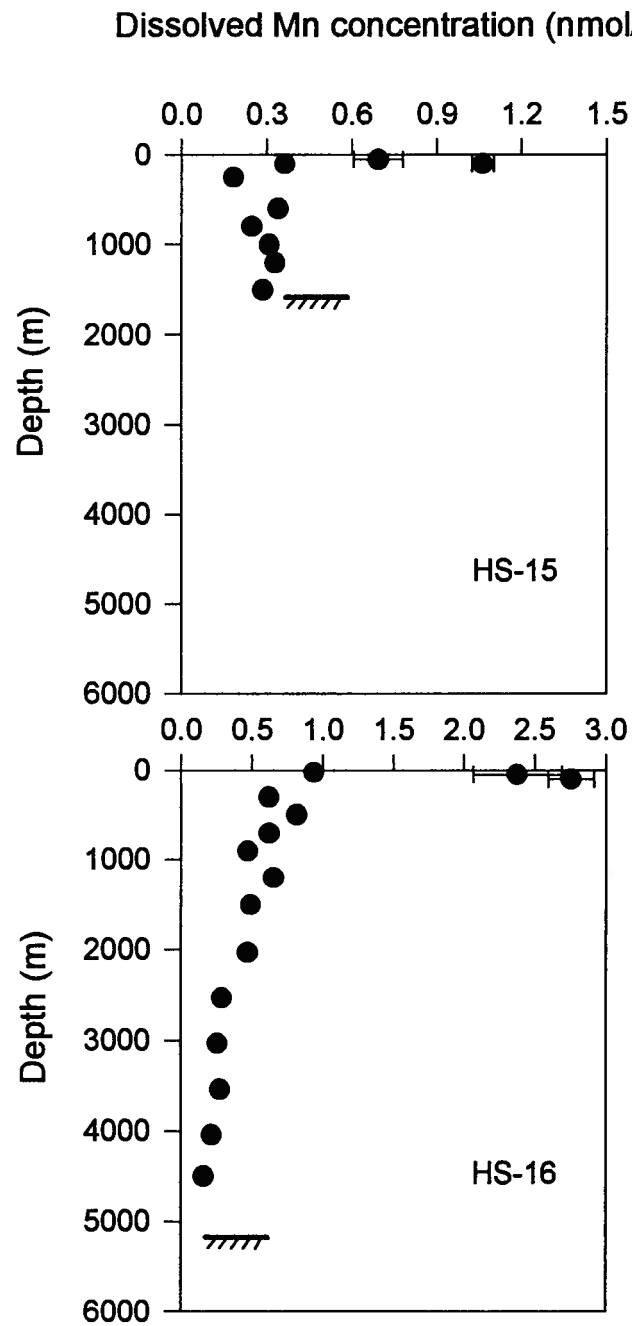


Figure 4.21 Dissolved Mn in the central North Pacific. Each point is the average of two analyses. Error bars indicate the range. N.B. The change in scale of the abscissa.

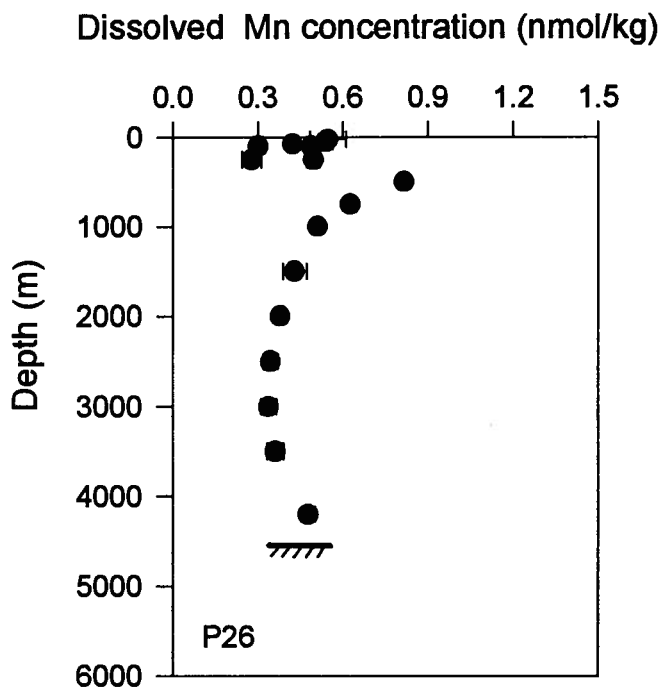


Figure 4.22 Dissolved Mn in the eastern North Pacific in the sub-Arctic gyre. Each point is the average of two analyses. Error bars indicate the range.

higher in O_2 originating in the North Atlantic and Antarctic regions. In sub-oxic waters, particulate Mn(III, IV) oxyhydroxides are reduced to Mn(II) giving rise to a dissolved Mn maximum at the O_2 minimum [49]. In waters with higher O_2 concentrations, dissolved Mn is oxidatively scavenged in its particulate form. Plots of dissolved Mn and dissolved O_2 are at Stations 1,5,10, 15,16 and P26 are shown in Figure 4.23.

The data shown in Figure 4.23 agree with previous results [47-50, 112, 113]. In surface waters, dissolved Mn is thought to be high due to desorption from aeolian detritus. Beneath the surface, but before the O_2 concentration begins to decrease, a sub-surface minimum in the Mn signal is observed which probable reflects a combination of oxidative scavenging and horizontal

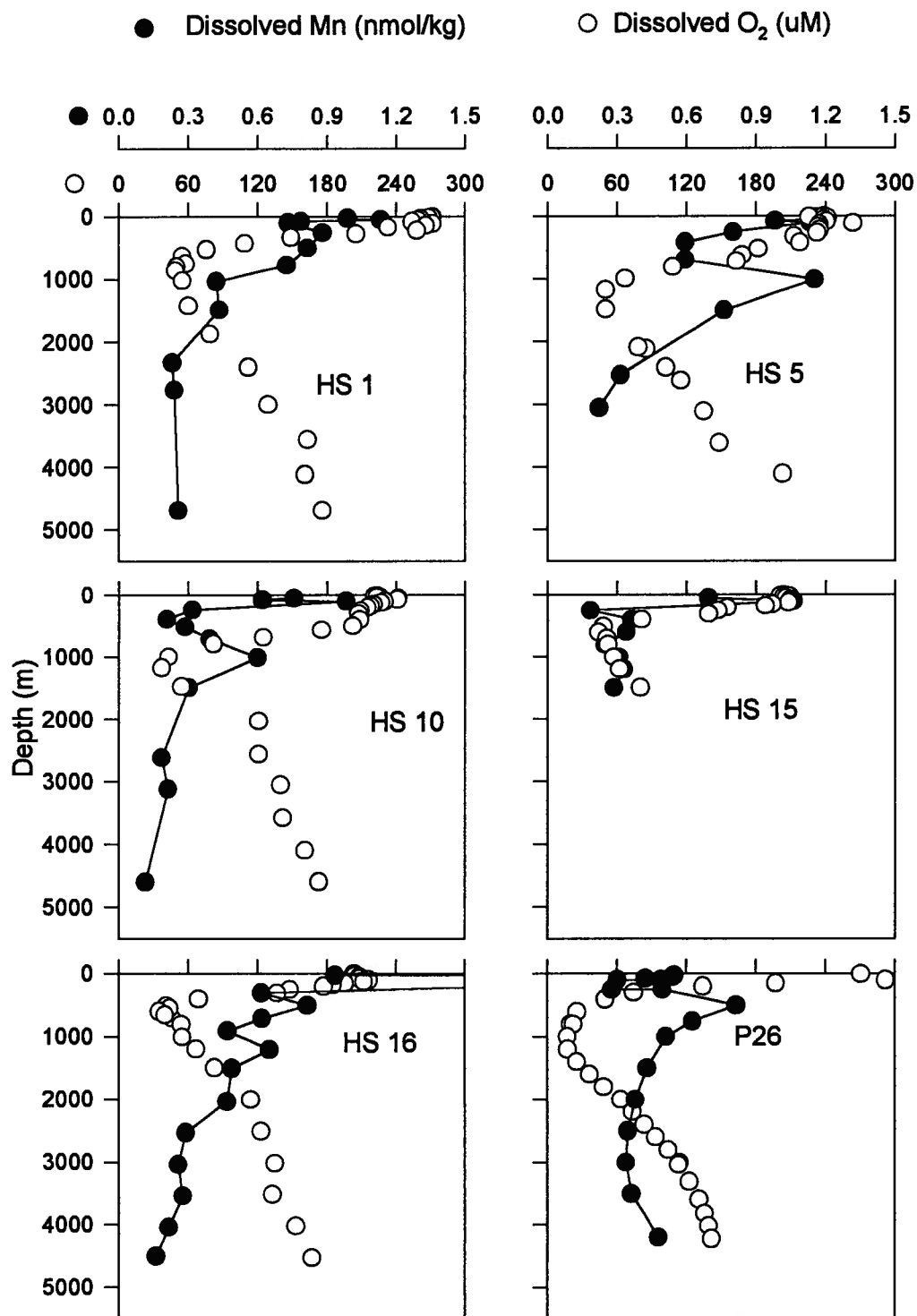


Figure 4.23 Dissolved Mn and O₂ versus depth at Stations 1, 5, 10, 15, 16 and P26.

advection of waters low in dissolved Mn. At the O₂ minimum, a mid-depth maximum in the Mn signal is observed. This has been attributed to a combination of *in situ* reduction of particulate Mn (III, IV) to dissolved Mn (II) and horizontal transport of water which has been in contact with reducing slope sediments and is consequently depleted in O₂ and enriched in Mn. As O₂ levels increase slowly with depth, the dissolved Mn concentration decreases, again due to oxidative scavenging. In deeper waters, between 2500 and 3500 m the relative increase may be attributed to waters enriched in Mn (II) from a nearby hydrothermal vent if present.

4.3 Dissolved Ga in the North Pacific Ocean

Past studies in the eastern North Pacific and North Atlantic oceans have shown that general distributions of dissolved Ga in seawater comprises a sub-surface maximum, low concentration in intermediate waters and levels that increase with depth in deeper waters [3, 53, 54]. The sub-surface maximum may be caused by either horizontal advection and/or a vertical process involving exchange with sinking particles. These studies suggest complex controls including multiple sources, reversible exchange and scavenging processes all of which contribute to the distribution of dissolved Ga in the ocean. The primary sources of Ga to the open ocean may be atmospheric inputs of crustal dust to the surface waters and diffusion out of the sediments and/or a sediment-surface remineralization to the deep water. Asian continental dust source may be a major atmospheric source of Ga to the North Pacific.

Depth profiles of dissolved Ga measured for this study from Stations 1,5 and 10, Stations 15 and 16 and Station P26 are presented in Figures 4.24, 4.25 and 4.26, respectively. Dissolved Ga concentrations are found to range from 3 to 30 pmol/kg in the North Pacific Ocean. The values are low in the surface (4 to 14 pmol/kg), and the profiles often show a sub-surface maximum between 300 and 500 m, (ranging between 10 and 18 pmol/kg where present), a definite mid-depth minimum between 500 to 1000 m (3 to 9 pmol/kg) and increasing concentrations with depth (13 to 30 pmol/kg). Generally, these results are in agreement with previously published dissolved Ga data in the North Pacific Ocean [3].

The work presented in the following sections indicates two sources of Ga to the oceans. Surface distributions indicate aeolian input from the Asian continent, which is known to be a major dust source to the surface waters of the

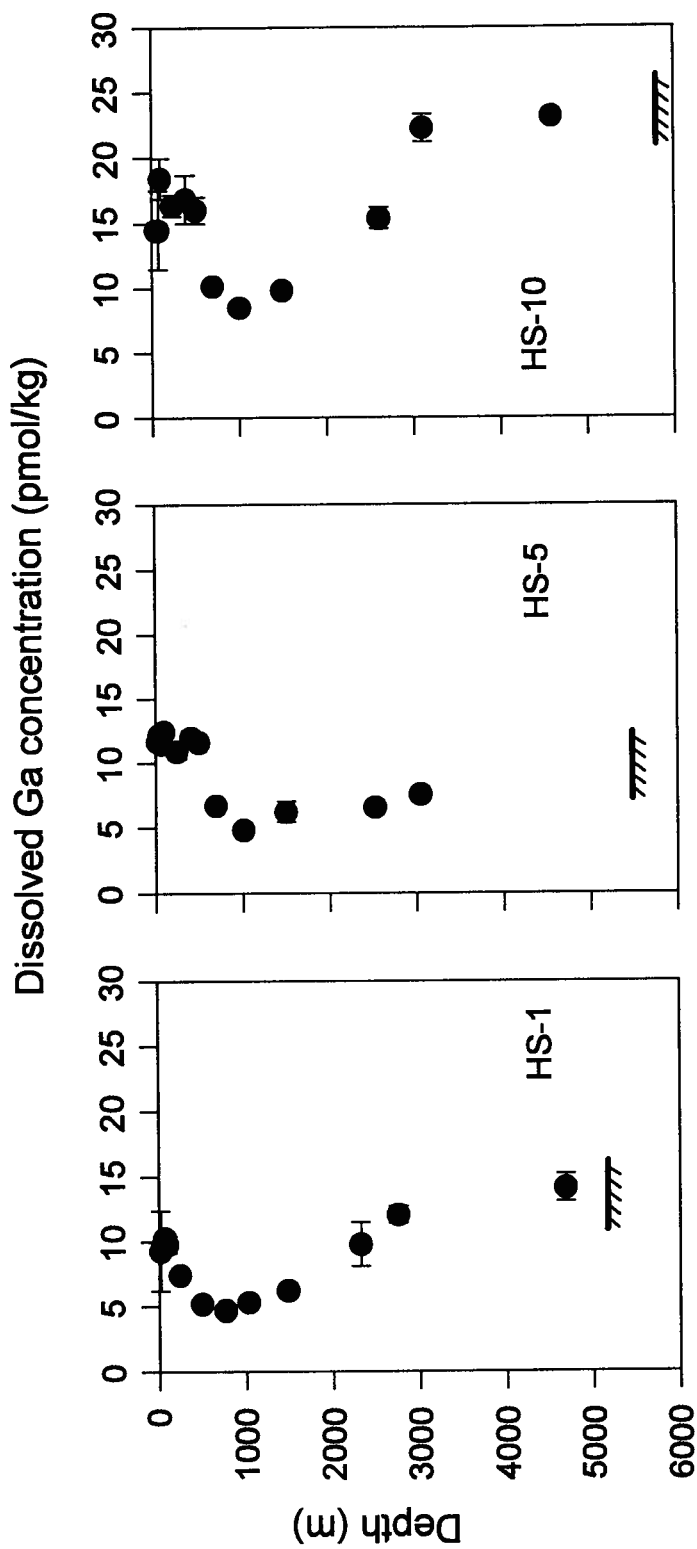


Figure 4.24 Dissolved Ga in the western North Pacific. Each point is the average of two analyses. The error bars indicate the range.

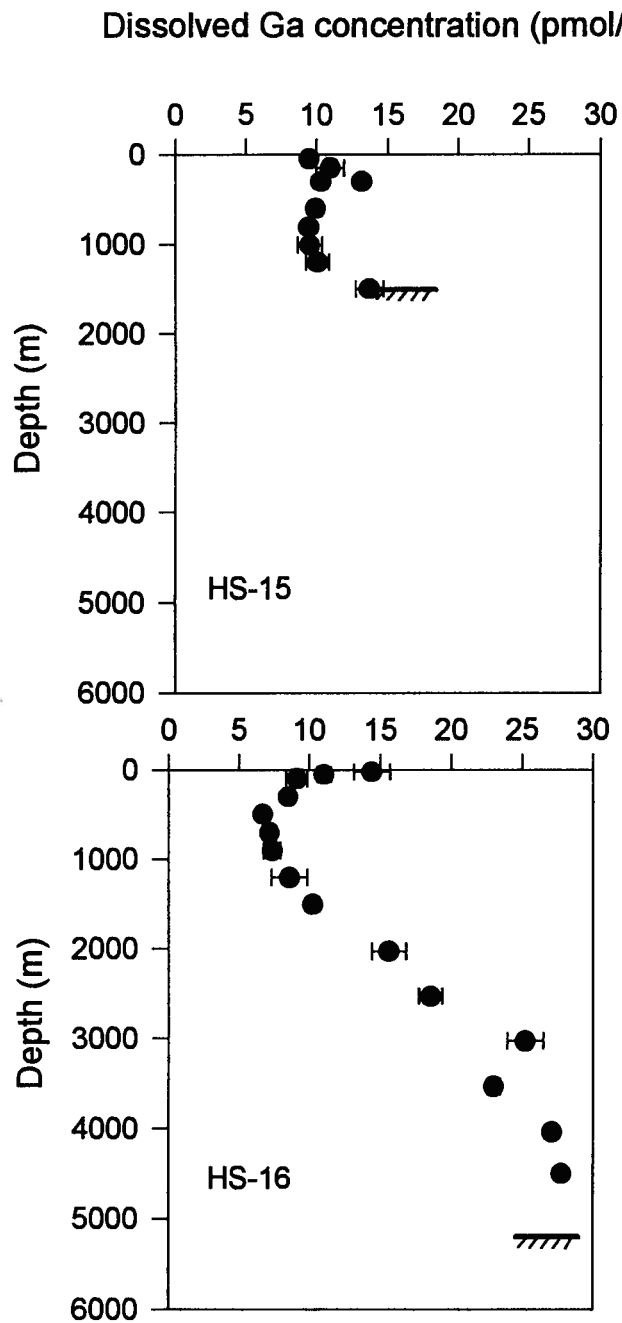


Figure 4.25 Dissolved Ga in the central North Pacific. Each point is the average of two analyses. The error bars indicate the range.

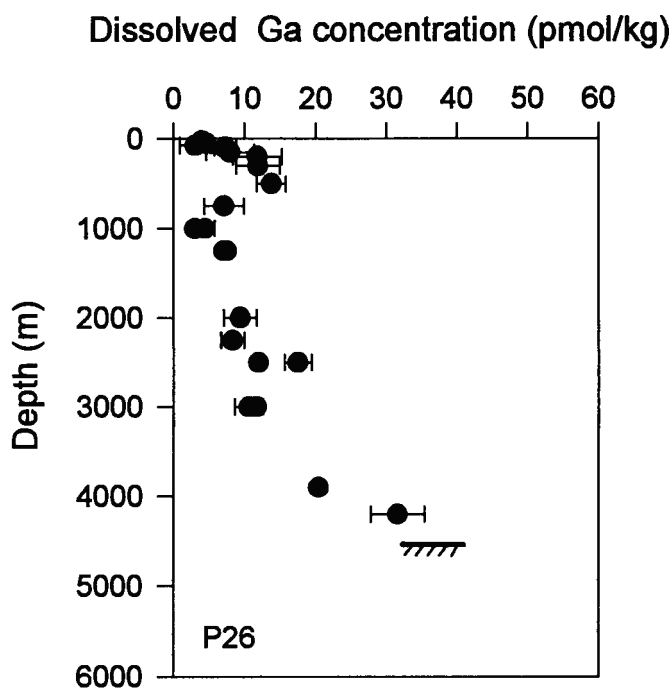


Figure 4.26 Dissolved Ga in the sub-Arctic station in the eastern North Pacific. Each point is the average of two analyses. Error bars indicate range. N.B. Note change in scale on the abscissa.

North Pacific. Deep waters indicate bottom water sources such as diffusion from sediments and/or surface-sediment remineralization. A sub surface maximum is not always observed in these profiles, but when present may be attributed to vertical exchange processes and/or isopycnal mixing. However, isopycnal mixing cannot explain the high Ga results observed at Station 10, relative to the other stations. Removal by scavenging is indicated throughout the water column.

4.3.1 Ga Distribution in Surface Waters

The Ga concentration in surface waters increases from the western Pacific into the central gyre and then decreases again at high latitude. The

surface concentration in the Oyashio Current (Station 1) is 9 - 10 pmol/kg; in the Kuroshio Current (Station 5), ~ 12 pmol/kg; in the central gyre (Station 10), ~ 14 pmol/kg; in Equatorial Current (Stations 15 and 16) ~ 10 and 14 pmol/kg respectively; and in the sub-Arctic North Pacific (Station P26), ~ 4 pmol/kg.

The Ga distribution in the surface waters resembles the distribution of ^{210}Pb , which has an aeolian source. Concentrations of ^{210}Pb were found to be highest in the central gyre surface waters [114]. While there are no Al data from the western North Pacific, this metal also has an aeolian source, and like Ga and ^{210}Pb exhibits high concentrations in the central gyre that decrease to the east, away from the Asian continent [8, 114]. This is contrary to what is observed in the dissolved anthropogenic Pb distribution at these stations (section 4.2.3), which shows increasing levels of Pb closer to Asia, consistent with the east-west and north-south gradient in the North Pacific of the dust input from the Asian continent.

Figure 4.27 shows the global fluxes of mineral aerosol to the ocean [6]. Together with Figure 4.1, these data indicate that the dust input at Station 10 is less than that at Stations 1 and 5. Therefore, it appears that the higher dust input to Stations 1 and 5 may be countered by the increased productivity and particle scavenging in the eutrophic coastal Oyashio and Kuroshio Current waters. This would lead to the low dissolved Ga values in the surface waters observed at Stations 1 and 5 relative to the levels in the central gyre.

The concentrations determined in surface waters from Station 15, atop Karin Ridge in the North Equatorial Current, is similar to those observed in the Oyashio and Kuroshio Current (Stations 1 and 5). Station 16, near Karin Ridge but also in the Equatorial Current, exhibits a higher Ga concentration in surface waters, similar to that found in the central gyre (Station 10). The difference between Stations 15 and 16 may be due to patchiness in the upper ocean.

Results obtained for Zn, Cd, Ni, Pb and Mn also show higher concentrations in surface waters at Station 16. The lowest Ga values are in the high latitude eastern North Pacific surface waters (P26), due to a combination of lower dust input in this area (Figure 4.27) and an increase in particle interactions with dissolved Ga due to the known high productivity at this station [113].

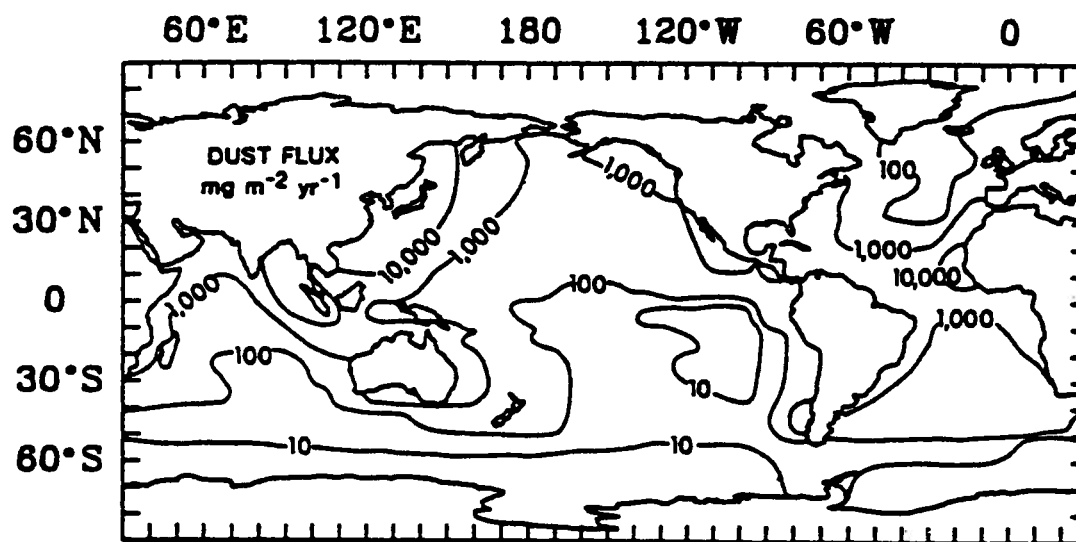


Figure 4.27 Global fluxes of mineral aerosol to the oceans in $\text{mg m}^{-2} \text{yr}^{-1}$ [6].

4.3.2 Ga Distribution in Intermediate Waters

No dissolved Ga sub-surface maxima are found at Stations 1 and 5. Instead, at Station 1, dissolved Ga steadily decreases from 9 - 10 pmol/kg at the surface to ~ 5 pmol/kg between 750 to 1000 m and at Station 5, the surface maximum extends down to 500 m and then decreases to a minimum of ~ 5 pmol/kg at 1000m. These profiles differ from vertical distributions in the eastern North Pacific and North Atlantic Oceans where sub-surface maxima are observed at depths between 300 and 500 m [3,54]. In the central gyre (Station

10), dissolved Ga shows a sub-surface maximum of ~18 pmol/kg between 100 and 500 m, which then decreases to a mid-depth minimum of 9 pmol/kg at 1000 m. This is similar to vertical profiles previously determined in the eastern part of the central gyre, but Station 10 exhibits a broader sub-surface maximum [3].

At Stations 15 and 16, the Ga concentration decreases to a mid-depth minimum (~9 pmol/kg between 700 and 1000 m and ~7 pmol/kg between 500 and 700 m at Stations 15 and 16, respectively). The Ga distribution at Station 16 is similar to that at Stations 1 and 5, but with higher concentrations at the mid-depth minima. The Ga concentrations in intermediate waters at Stations 15 and 16 are lower than at Station 10, suggesting that the former may be intermediate between the high productivity regime at Stations 1 and 5 and the low productivity at Station 10. In addition, the dust input to Stations 15 and 16 is expected to be lower since these sites are more distal from the Asian continent (Figures 4.1 and 4.27).

In the high latitude eastern North Pacific (P26), dissolved Ga increases to a sub-surface maximum of 13 pmol/kg between 300 and 500 m, and then decreases to a minimum of 3 pmol/kg at 1000 m, presumably due to a combination of less dust input into these waters (Figure 4.27) and an increase in particle interactions with dissolved Ga due to the extent of biological productivity at this station. These results generally agree with the data obtained from this station by Orians and Bruland [3], except that the sub-surface maximum is more pronounced in this study. The higher concentration in bottom water observed in this work is due to the greater sampling depth (4200 m vs. 3900 m).

The mid-depth minima observed in all the dissolved Ga profiles (Figures 4.24, 4.25 and 4.26) and the sub-surface maxima observed in the central gyre and the eastern North Pacific could be advective features or the result of reversible exchange processes with sinking particles. Dissolved Ga could be

associated with solid particles which undergo shallow regeneration, and the released Ga could then be adsorbed onto particle surfaces resulting in a mid-depth minimum. This has been argued for Al which has a mid-depth minimum [8] but not a mid-depth maximum. The sub-surface maxima observed at Stations 10 and P26, could be due to a combination of increased regeneration at this depth and reduced Ga reactivity allowing dissolved Ga to reach appreciable levels before being re-scavenged.

Advective origins of mid-depth water features have been suggested for trace elements including Mn [51] and Pb [45]. Bismuth and $^{239, 240}\text{Pu}$ have sub-surface maxima which show no correlation with density and salinity features, implying more complex controls. Advective transport of water with high levels of dissolved Ga from the ocean boundaries cannot produce the high the sub-surface dissolved Ga maximum observed in the central gyre since dissolved Ga concentrations are lower in coastal waters. Therefore vertical exchange processes seem more probable.

To visualize the possible horizontal and vertical processes in the upper 1500 m of water in the North Pacific, a contour plot was generated (SURFER, Golden Software, Golden CO), compiled from the data presented here and previous results [3] (Figure 4.28). This plot indicates that the Ga concentrations in surface waters increase from the Asian coast (Stations 1 and 5) to a maximum in the western edge of the central gyre (Stations 10) and that the Ga sub-surface maximum does not occur in the western Pacific. Surface water Ga levels also decrease in equatorial waters and increase in the eastern part of the central gyre (VERTEX IV), which shows the presence of the sub-surface maximum. Eastward of the central gyre, surface concentrations of Ga decrease and the sub-surface maximum becomes less pronounced (VERTEX VA and VC). The 12

pmol/kg contour line in this figure does shallow considerably at Station 16, indicating a north-south effect since it is the most southerly station shown.

The Ga distribution shown in Figure 4.28 suggests that the increasing Ga concentrations and broadening surface maxima between Stations 1 and 5 and the eventual formation of a sub-surface maximum of greater concentration at Station 10 is likely due to the extent of reversible exchange with sinking particles at each station and not to horizontal advection from elsewhere. Station P26 is not included in the plot since it is at least 20° north of the other stations. Note that the low dissolved Ga concentrations observed in the high latitude eastern North Pacific indicate that lateral advection from this area is not the source of the sub-surface maximum in the central gyre.

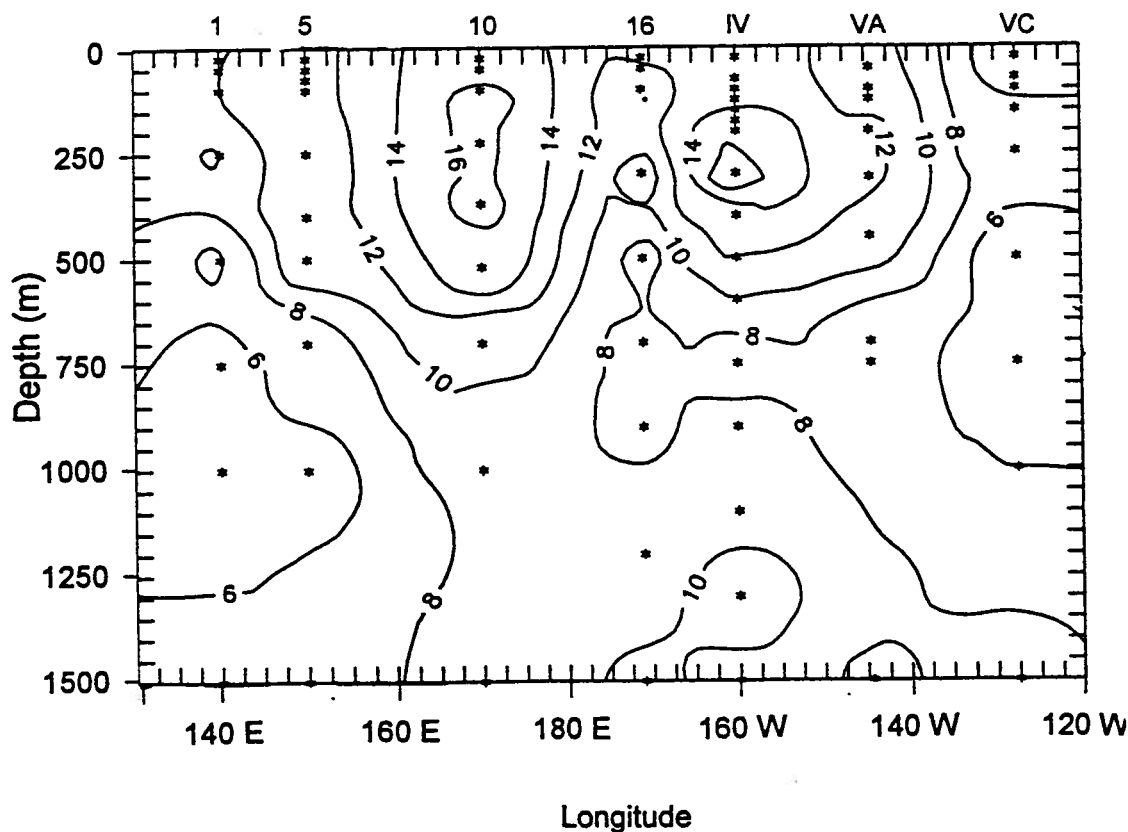


Figure 4.28 Contours generated by combining data from this study with those from previous work [3]. Values are in pmol/kg. Please refer to Figure 4.1 for the latitudes of these stations.

4.3.3 Dissolved Ga Distribution in Deep Waters

The vertical profiles of Ga below 1000 m at all stations show increasing concentrations with depth. Elements which such distributions have geochemistries dominated by: *in situ* dissolution and oxidation of organic matter which releases trace constituents in the deep waters and at the sediment interface (e.g. Si and Zn); a flux from the sediments and subsequent mixing with upper waters by eddy diffusion and gradual upwelling (e.g. Ra); or a flux from the sediments which is advected upwards and subsequently removed by particle scavenging (e.g. Cu, Al).

The behaviour of an element which shows increasing concentrations with depth in the deep waters can be determined by plotting the concentration of that element against salinity, S , (Figure 4.29), provided that a plot the two conservative tracers, S and potential temperature, θ , (the surface temperature of a small volume of water at depth adiabatically raised to the surface), yields a linear relationship. A non-linear S - θ diagram may indicate the influence of horizontal advection, which would affect the element-salinity plot. Element-salinity plots which show convex relationships indicate net release of an element, linear relationships indicate conservative mixing, and concave relationships indicate net removal of an element which has a bottom water source. These relationships are shown in Figure 4.29.

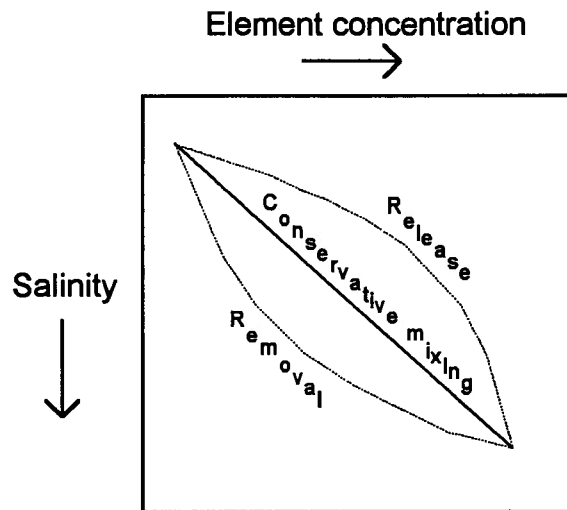


Figure 4.29 Element versus salinity plots in deep waters showing net release, conservative mixing and removal by particle scavenging.

4.3.4 Vertical-Advection Diffusion Model

A simple vertical advection-diffusion model may be used to estimate the deep water scavenging times for scavenged elements which have a bottom source. The model may be expressed as [29,117]:

$$0 = K \left(\frac{\partial^2 [C]}{\partial z^2} \right) - W \left(\frac{\partial [C]}{\partial z} \right) + J \quad (\text{Eq. 4.1})$$

where K is the vertical eddy diffusivity, W is the vertical advection velocity (positive downwards), $[C]$ is the concentration of the element of interest, z is the depth in kilometres and J is the term that accounts for scavenging removal. The solution to this equation can be arranged as:

$$[C] = \alpha + \left(\frac{J}{W} \right) z + \beta S \quad (\text{Eq. 4.2})$$

where α and β are constants and S is the salinity. Multiple linear regression of $[C]$, S and z from equation 4.2 can be used to determine J/W , α and β . The value of J , the scavenging term, can be determined assuming an upwelling rate (W) of 3.5 m/yr (estimated from radioisotope distributions [117]).

The scavenging residence times are calculated using the following equation:

$$\tau_{1/2} = \frac{\ln 2}{\left(\frac{W \left(\frac{J}{W} \right)}{[C]_{\text{ave}}} \right)} \quad (\text{Eq. 4.3})$$

4.3.4.1 Application of this model to Ga

The model was used to determine the scavenging residence times of Ga in the deep waters at Stations 10, 16 and P26. These three stations are found to have linear S - θ diagrams and the required convex $[Ga]$ - S relationships (Figures 4.30, 4.31, 4.32). The advection diffusion model was not applied to Station 5 since seawater samples below 3000 m were not collected (hence, no bottom water data). Station 15 has a linear S - θ diagram and the required convex $[Ga]$ - S relationship, but the depth of the site was only 1550 m (Figure 4.33). Station 1 was found to have a non-linear S - θ diagram (Figure 4.34) and therefore the Ga data from this site was not modeled.

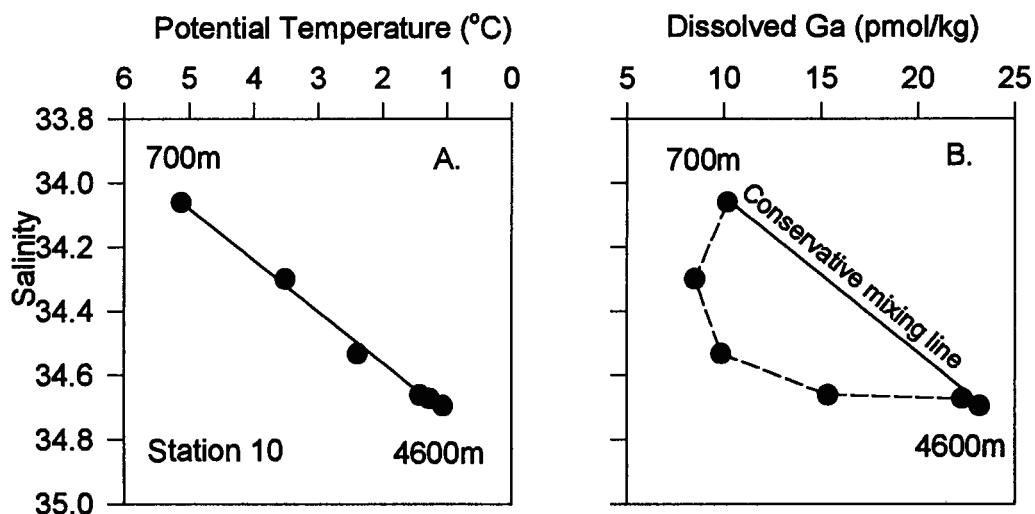


Figure 4.30 The A) Potential temperature-salinity and B) dissolved Ga-salinity relationships below 700 m at Station 10 in the western North Pacific Ocean.

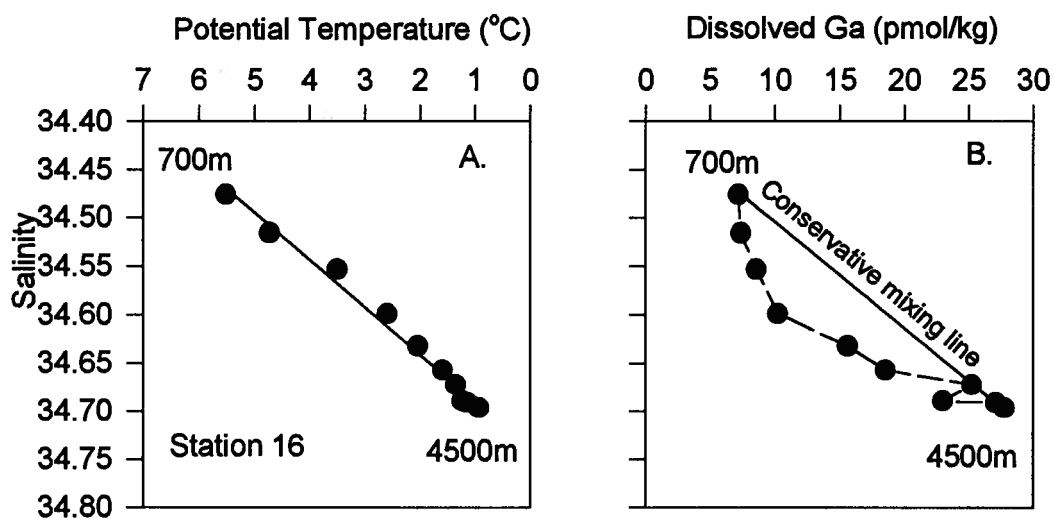


Figure 4.31 The A) Potential temperature-salinity and B) dissolved Ga-salinity relationships below 700 m at Station 16 in the central North Pacific Ocean.

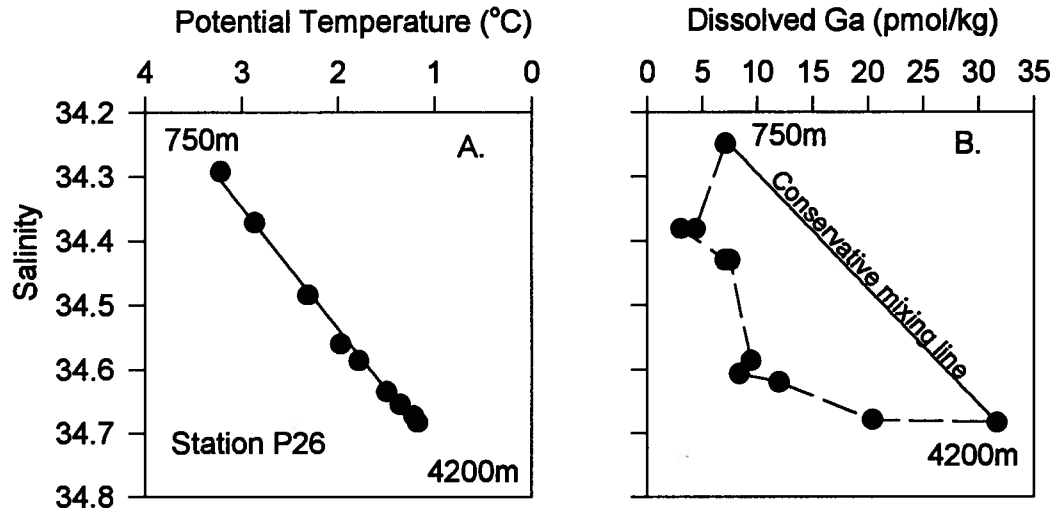


Figure 4.32 The A) Potential temperature-salinity and B) dissolved Ga-salinity relationships below 750 m at Station P 26 in the eastern North Pacific Ocean.

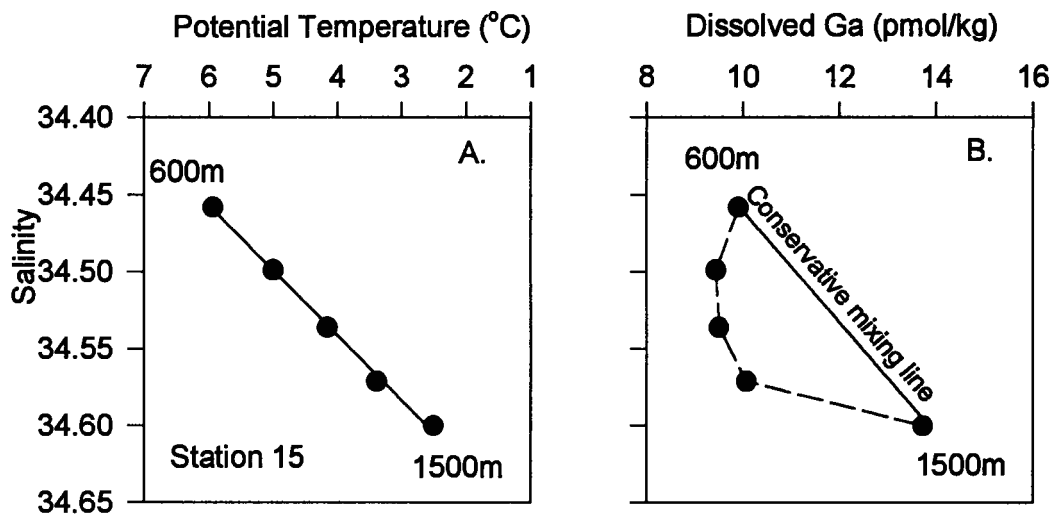


Figure 4.33 The A) Potential temperature-salinity and B) dissolved Ga-salinity relationships below 600 m at Station 15 in the central North Pacific Ocean.

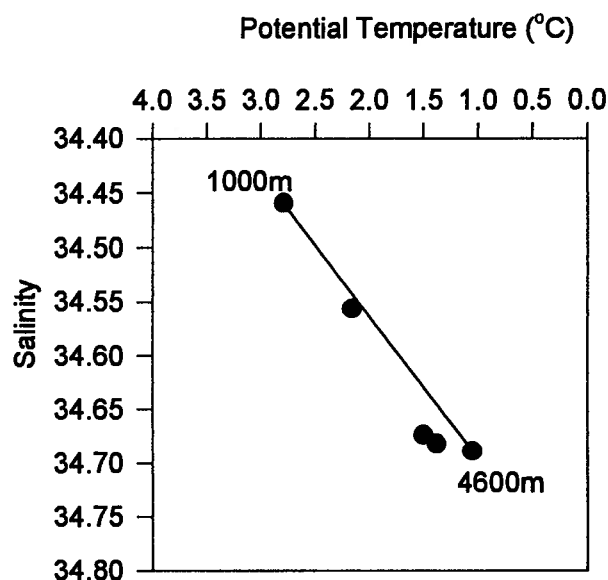


Figure 4.34 Potential temperature - salinity relationship below 1000m at Station 1 in the western North Pacific Ocean.

Parameter	Stn. 10	Stn. 16	Stn. P26
α (pmol/kg)	119	361	1300
β (pmol/kg)	-3.33	10.4	-38.0
J/W (pmol kg ⁻¹ yr ⁻¹ km ⁻¹)	4.61	5.58	10.7
W (km/yr)	-0.0035	-0.0035	-0.0035
$[Ga]_{avg}$ (pmol/kg)	16	15	11
scavenging $\tau_{1/2}$ (yr)	700	530	200

Table 4.1 Results obtained from the vertical-advection diffusion model for dissolved Ga in the deep waters of the North Pacific.

The results obtained and the parameters used are shown in Table 4.1. It should be noted that there is an increase of only 20-30 years in residence times if the shallowest deep water depth of 1000 m is used instead of 700 m. The

scavenging residence times for Ga ranged from 700 years in the central gyre (HS 10) to 200 years at the edge of the sub-Arctic gyre (P26). Longer residence times in the central gyre as compared to Station P 26 have been previously observed for Ga and Al, with residence times for Ga determined to be 750 years in the central gyre and 100 years in the sub-Arctic North Pacific Current [3]. The results presented here are very similar. The difference between Stations 10 and P26 is attributed to lower biological production in the surface waters in the central gyre, resulting in fewer particles sinking to the sediments. The residence time of Ga determined in the North Equatorial Current (Station 16) is found to be 530 years, which is slightly less than that of Station 10.

A flux from the sediments is required to maintain concentrations in bottom waters since removal by scavenging is occurring. The Ga flux from the sediments at these stations can be estimated using the method of Munk [118]:

$$\text{Flux}_B = -W [C]_B + K \left(\frac{dC}{dz} \right)_B \quad (\text{Eq. 4.4})$$

where W is the vertical advective velocity, K is the vertical eddy diffusion coefficient, $[C]$ is the concentration of the element of interest, z is the depth. The subscript B refers to the change of concentration with depth at the seafloor. Using an estimate of $3.2 \times 10^7 \text{ cm}^2 \text{ yr}^{-1}$ for K [119] and integrating from the seafloor to the penultimate bottom-water point available to calculate (dC/dz) , the fluxes needed to support the bottom and deep water distribution of Ga at Stations 10, 16 and P26 are 8.3, 9.7 and 23 $\text{pmol cm}^{-2} \text{ yr}^{-1}$, respectively. The calculated fluxes at Stations 10 and 16 are similar, while that at Station P26 is much higher since a higher flux out of the sediments is needed to sustain the concentration of Ga in the bottom-waters in this region of high scavenging. At present, the source of the bottom water supply of Ga cannot be distinguished between a flux from sub-surface pore waters and sediment-surface

rem mineralization, both of which have been suggested to account for the distribution of Al [8]. In the North Atlantic, advection has also been argued for Al, but not in the North Pacific and hence advection is not considered to be a bottom water source of Ga [120, 121].

4.3.5 Comparison with Al

To understand the behaviour of Ga further, it is useful to compare it to Al, another hydrolysis-dominated element that sits just above Ga in the periodic table. Al is the most abundant metal in the earth's crust and has been shown to have a high atmospheric input to the surface oceans and to be very reactive. Aluminum data exist for Stations 15 and 16 (Figure 4.25) [112] and a detailed comparison of Ga and Al at Station P26 already exists [3]. Dissolved Al in the North Pacific is rapidly removed from the surface waters with a mid-depth minimum at 1000 m [3, 8]. Slightly higher Al concentrations in the deep waters suggest the possibility of a bottom source. Profiles of dissolved Al at Stations 15 and 16 are shown in Figure 4.35.

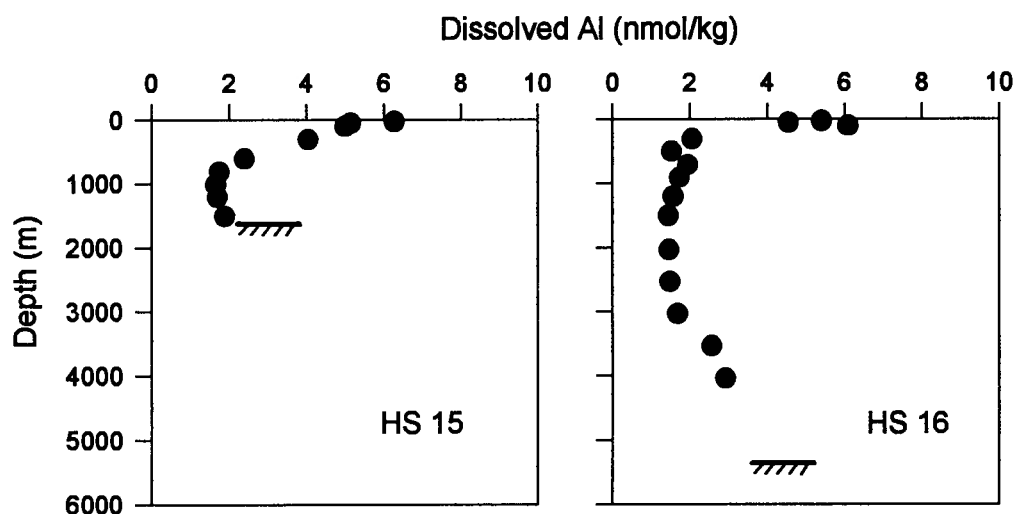


Figure 4.35 Depth profiles of dissolved Al at Stations 15 and 16 [112].

Comparing the crustal abundance ratio of Ga/Al to that of surface seawater (<500 m) and deep seawater (>1500 m at Stations 10 and 16; >1000 m at Station 15) should reveal any fractionation between Ga and Al in the oceans. From previous studies, it has been found that Ga/Al ratios are enriched 50 to 100 times in surface waters with respect to those in average crust [3, 54]. Explanations offered for the additional Ga present in surface waters include preferential scavenging of Al in surface water, an additional but unknown Ga source, a greater abundance of Ga in the atmosphere source relative to the crust and/or enhanced dissolution of Ga from dust inputs. Since no Al data are available from Station 10, Al values from another station, VERTEX IV, approximately 30° east of Station 10 were used in calculating Ga/Al ratios since dissolved Al levels have been found to be relatively uniform in the central Pacific gyre [8]. A detailed comparison of Ga with Al was previously made at Station 10 using Al data from VERTEX IV [122]. Therefore, the Ga/Al ratios at Station 10, determined by combining dissolved Ga data obtained here with dissolved Al data from Station VERTEX IV, are included here for comparison only. A plot of Ga/Al ratios at Stations 15 and 16 are shown in Figure 4.36.

The ratio data show that the enrichment factor of Ga with respect to Al in the surface waters is higher than that in the average crust and increases further with depth (Table 4.2). Thus, the geochemistries of Ga and Al must be different in seawater. Sources of Al and Ga to the surface waters are believed to be similar since dissolved Ga and Al concentrations have been correlated over a range of environments [54] and Al has a known aeolian source to the North Pacific [123]. The most likely explanation for the high dissolved Ga/Al ratios is that they result from a combination of enhanced scavenging of Al throughout the water column and preferential dissolution of solid phase Ga. At Stations 15 and

16 the surface enrichment factors are similar if slightly lower than the 50 to 100 fold range reported previously [3, 21].

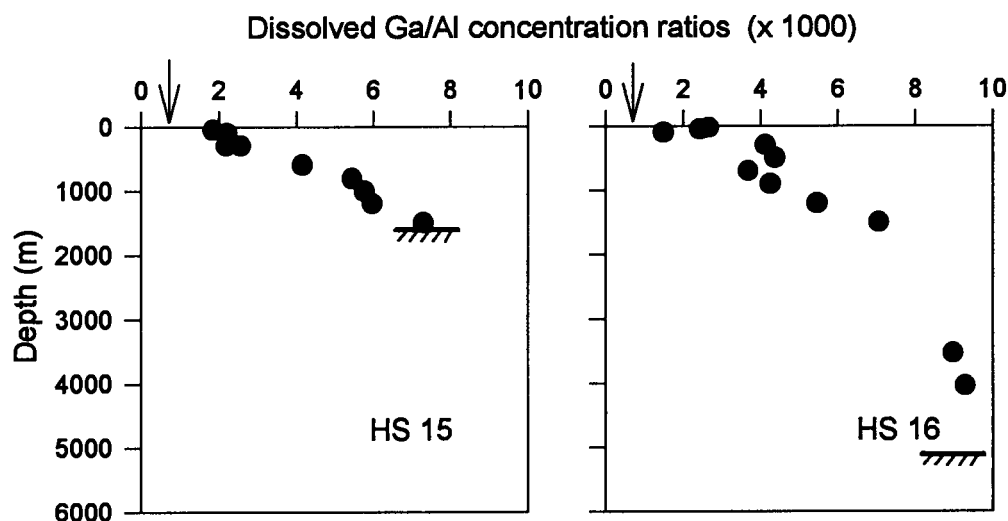


Figure 4.36 Depth profiles of dissolved Ga/Al ratios at Stations 15 and 16. Al data from reference [112]. The arrows indicate the crustal Ga/Al ratios.

Station	Expected Ratio (mmol/mol)	Surface Enrichment	Deep water Enrichment
HS 10	0.0705	120	340
HS 15	0.0705	31	95
HS 16	0.0705	38	163

Table 4.2 Enrichment factors of Ga with respect to Al from Stations 10, 15 and 16. [Al] at Stations 15 and 16 from reference [112]. [Al] used to compare Station 10 are from Station VERTEX IV also in the central gyre [21]

The extent of dissolution of Al from aerosols in surface waters is between 5 and 10 % due to the refractory nature of the alumino-silicate component [124]. Gallium has a larger ionic radius than Al (0.062 nm and 0.050 nm, respectively)

[125] and may be more associated with the readily leachable fractions of marine aerosols. This is the case for Cd, Zn and Pb [126] and Mn [127] which all undergo greater than 30% dissolution from marine aerosols in seawater. At present, the exact source of Ga/Al enrichment is not known, though it appears that the supply of Ga is greater than the supply of Al to the surface waters.

Preferential scavenging of Al over Ga in deep waters might be due to enhanced scavenging of neutral species over anionic species onto anionic particle surfaces. The majority of Ga in seawater exists as $\text{Ga}(\text{OH})_4^-$ while Al exists mainly as the neutral $\text{Al}(\text{OH})_3$ [53, 54, 128]. Indeed, the scavenging residence time for Al at Station 16 is calculated to be 430 years which is less than that estimated for Ga at this station (see Table 4.1). Previous work also have shown that the scavenging residence time for Al is shorter than that for Ga at P26 and at VERTEX IV [3]. This supports the notion that Al is more reactive than Ga in seawater.

4.3.6 Conclusions

Dissolved Ga concentrations in the upper waters have been found to be the highest in the central gyre, an area with low dust input from the Asian continent and with low productivity resulting in fewer sinking particles. A mid-depth maximum was also observed at this site. Stations 1 and 5, which are areas with high dust inputs and high productivity, had Ga values which were lower with no mid-depth maxima. This indicates that the high levels of Ga in the central gyre and the presence of the sub-surface maximum in this region is not due to advection of water from the western North Pacific, but instead reflects the importance of productivity and scavenging in dissolved Ga distributions. Gallium distributions in the North Equatorial Current were similar to those in the coastal stations and is an area with lower dust inputs and higher productivity than in the

central gyre. The lowest near-surface Ga levels were found in the sub-Arctic North Pacific Current (Station P26) which is an area with high productivity and the lowest dust input of all sites, reflecting the added effect of lowered aeolian input into this region.

In deep waters, the calculated scavenging residence times at Stations 10, 16 and P26 are 700, 530 and 200 years, respectively, indicating increased particle scavenging at P26.

Ratios of Ga/Al at Stations 15 and 16 indicate enrichment of Ga with respect to Al in surface and deep waters. The extent of enrichment was similar to that found at other Stations [3, 21]. Previous work in the North Pacific found surface Al values which were low in the sub-Arctic North Current (P26) [3] and values ten times higher at sites bordering and in the North Equatorial Current [21]. Aluminum data at Stations 15 and 16 show similar high surface values found in the North Equatorial Current. Scavenging residence times of Al at Station 16 show reactivity higher than that of Ga. Therefore, the high Ga/Al ratios in seawater with respect to average crust are apparently due primarily to enhanced scavenging of Al. In addition, it is possible that the supply of dissolved Ga to surface waters is greater than that expected by the crustal Ga/Al ratio.

4.4 Dissolved Nb in Seawater

Very little is known about the behaviour of Nb in seawater. The only previously published results were analyses of two surface samples taken from the English Channel made to aid a study of the accumulation of Nb by ascidians [55]. Unfiltered surface samples in that work were found to contain Nb concentrations between 0.01 to 0.1 $\mu\text{g/l}$ (0.1 to 1 nmol/kg). Niobium is predicted to exist in its +V oxidation state and to be fully hydrolyzed in natural waters. The predicted speciation at pH of 8.2 is 88% as $\text{Nb}(\text{OH})_6^-$ and 12% as $\text{Nb}(\text{OH})_5$ [128]. In this section, the first profiles of dissolved Nb in seawater are presented and possible mechanisms which control dissolved Nb in the North Pacific are discussed.

4.4.1 Depth Profiles

The dissolved Nb profiles were determined at six sites in the North Pacific (Stations 1, 5, 10, 15, 16 and P 26) and are shown in Figures 4.37, 4.38 and 4.39. The profiles show similar distributions: near-surface concentrations ranging from 10 to 80 pmol/kg; slight sub-surface maxima in the upper 500 m with concentrations between 40 and 100 pmol/kg; and mid-depth minima below 500 m (between 10 and 40 pmol/kg). Between 1000 and 1500 m, larger maxima between 40 and 200 pmol/kg are observed. Concentrations decrease at greater depths to levels between 10 and 100 pmol/kg. The trio of Nb profiles at Stations 1, 5 and 10 (Figure 4.37), show an overall decrease of dissolved Nb with distance from the Asian coast, with Nb concentrations at Stations 16 and P26 being similar to Stations 1 and 5.

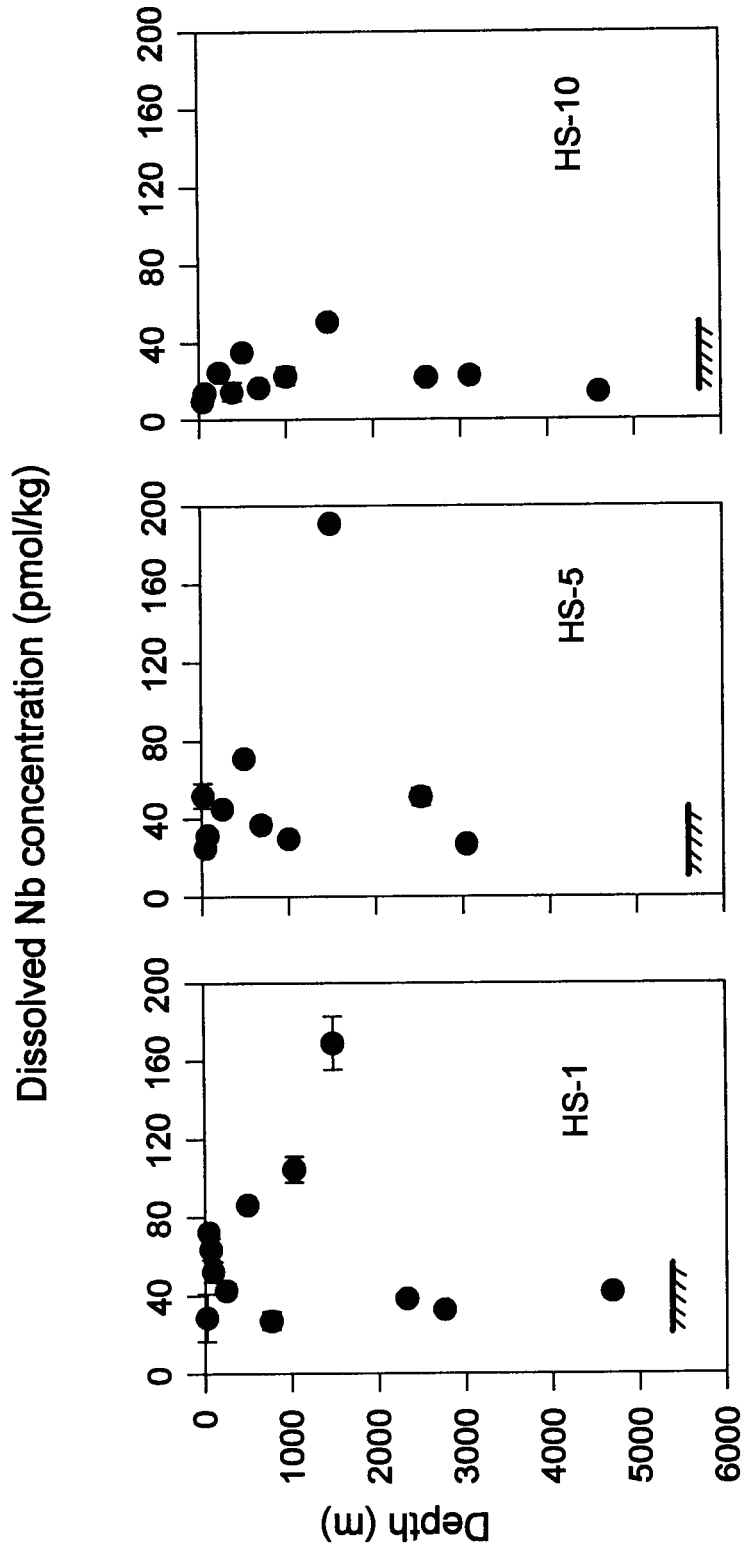


Figure 4.37 Dissolved Nb profiles from the Western North Pacific. Each point is the average of two analyses. The error bars indicate the range.

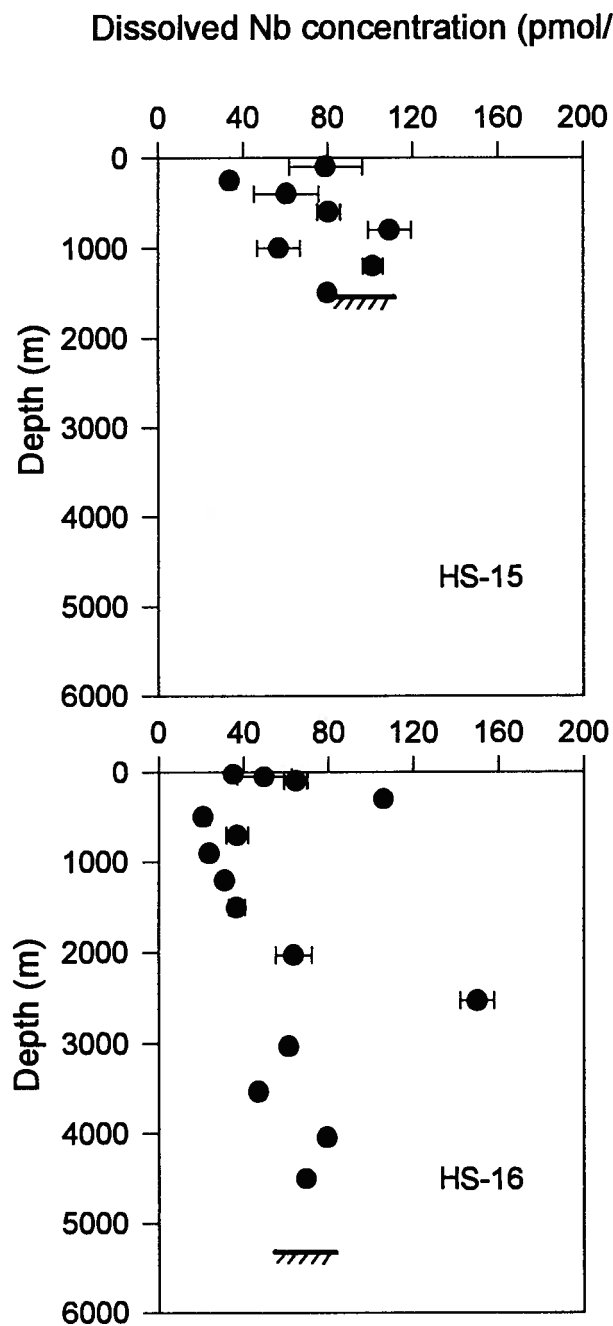


Figure 4.38 Dissolved Nb in the central North Pacific. Each point is the average of two analyses. The error bars indicate the range.

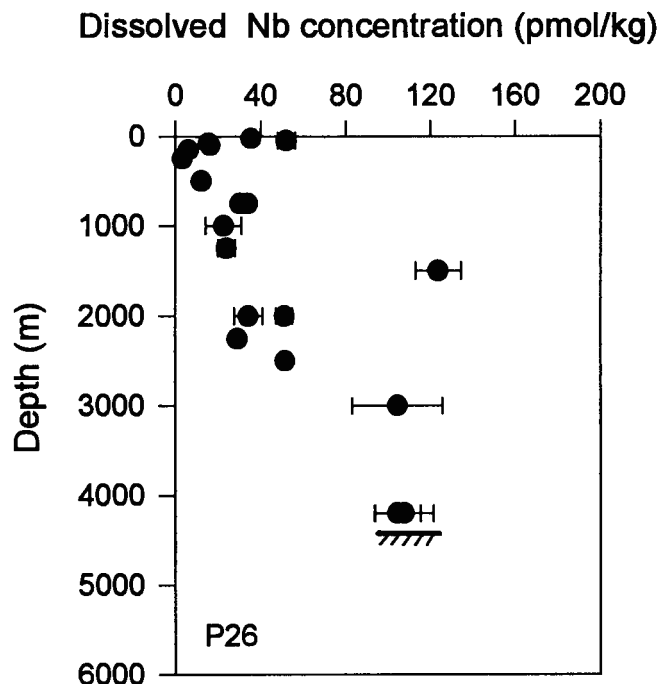


Figure 4.39 Dissolved Nb in the sub-Arctic North Pacific (P26). Each point is the average of two analyses. Error bars indicate range.

Although the depth resolution of the samples collected at these stations is not sufficient to see smooth transitions in mid waters and the data show some scatter, the fact that the sub-surface and mid-depth maxima occur in every profile suggests that these features are real. Hypotheses to account for them will be explored in the following sections.

4.4.1.1 Dissolved Nb in the Surface Waters

The surface concentrations of dissolved Nb at Stations 1, 5 and 10 show decreasing levels with distance from the coast. At Stations 16 and P26, the concentrations are similar to those at Stations 1 and 5. The sources of Nb to the oceans are unknown, though the decreasing surface concentrations with distance from the Asian coast observed at Stations 1, 5 and 10 are similar to the Pb and Mn distributions described earlier (sections 4.2.3 and 4.2.4), which

reflect atmospheric sources and in the case of Mn, riverine sources to surface waters [5, 22, 127]. Therefore, there does appear to be a source of Nb to the surface waters of the oceans, though its extent is unknown.

At Stations 1, 5 and P26, dissolved Nb concentrations decrease in the sub-surface waters to 100 m and then increase with depth resulting in sub-surface maxima at 500 m for Stations 1 and 5 and 750 m at Station P26. Stations 10 and 16 show low values in the surface waters, with Nb increasing with depth to sub-surface maxima at 500 m at Station 10 and 300 m at Station 16 (the surface values at Station 15 were lost). At all stations dissolved Nb immediately decreases below these maxima to concentrations equivalent to or less than the surface dissolved Nb concentrations. This suggests that Nb, like other hydrolyzed elements such as Al, Ga, Bi and Th, may be scavenged in seawater [3, 8, 115, 129]. The sub-surface maxima and minima observed at these stations may be the result of advective features and/or due to reversible exchange processes involving sinking particles. The declining Nb content with distance from the Asian coast observed at Stations 1, 5 and 10 may suggest a lateral advective source. Niobium may be incorporated into solid phases which undergo shallow regeneration such as biological soft tissue and then may be rescavenged onto particles present throughout the water column. This has been postulated for Ga [3, 53] and Co [130]. In 1958, Carlisle had shown that Nb is organically bound in ascidians [131], thus it is possible that Nb could be found in soft tissue of plankton.

4.4.1.2 Dissolved Nb in the Intermediate and Deep Waters

In intermediate waters (below 1000 m), the mid-depth minima increase to large sharp mid-depth maxima at all stations, which occurs at 1500 m at Stations 1, 5, 10 and P26, and at 2500 m at Station 16. Below these depths, dissolved

Nb rapidly decreases to levels similar to or slightly higher than the mid-depth minima and surface concentrations. At Station P26, dissolved Nb shows a gradual increase with depth. The narrow zone of the mid-depth maximum suggests that Nb is rapidly scavenged throughout the water column as are other particle reactive elements. The source of this mid-depth maximum is unknown, though it may be a result of lateral advection of waters with high concentrations of Nb, possibly from the continent boundaries, reversible exchange with sinking particles or cycling between a reactive and less reactive form of Nb.

4.4.2 Comparison with Dissolved O₂ and Manganese

A comparison between Nb and dissolved O₂ distributions indicates an apparent relationship: in four out of five profiles (Figure 4.40), the Nb maxima occur at low O₂ levels. However, neither of the two Nb maxima in each profile occur exactly at the O₂ minimum. Instead, stations in the western North Pacific (HS1, 5 and 10) show a small sub-surface maximum which coincides with the top of the O₂ minimum and a higher mid depth maximum which coincides with the bottom of the O₂ depleted zone. At Station HS 16, the sub-surface Nb maximum occurs at the top of the O₂ boundary, but the mid-depth maximum which occurs at the bottom of the O₂ minimum is much lower in depth than at the other deep stations (2500 m compared to 1500 m for the rest).

Since Nb is not predicted to undergo redox chemistry in seawater, its distribution in seawater may be influenced by an element that does undergo redox chemistry in seawater. Manganese is known to be redox sensitive and be associated with the oxygen minimum in seawater, resulting in a large mid-depth maximum attributed to a combination of lateral advection and cycling between particulate Mn(III,IV) and dissolved Mn(II) forms in the O₂ minimum zones [15, 22, 47-51].

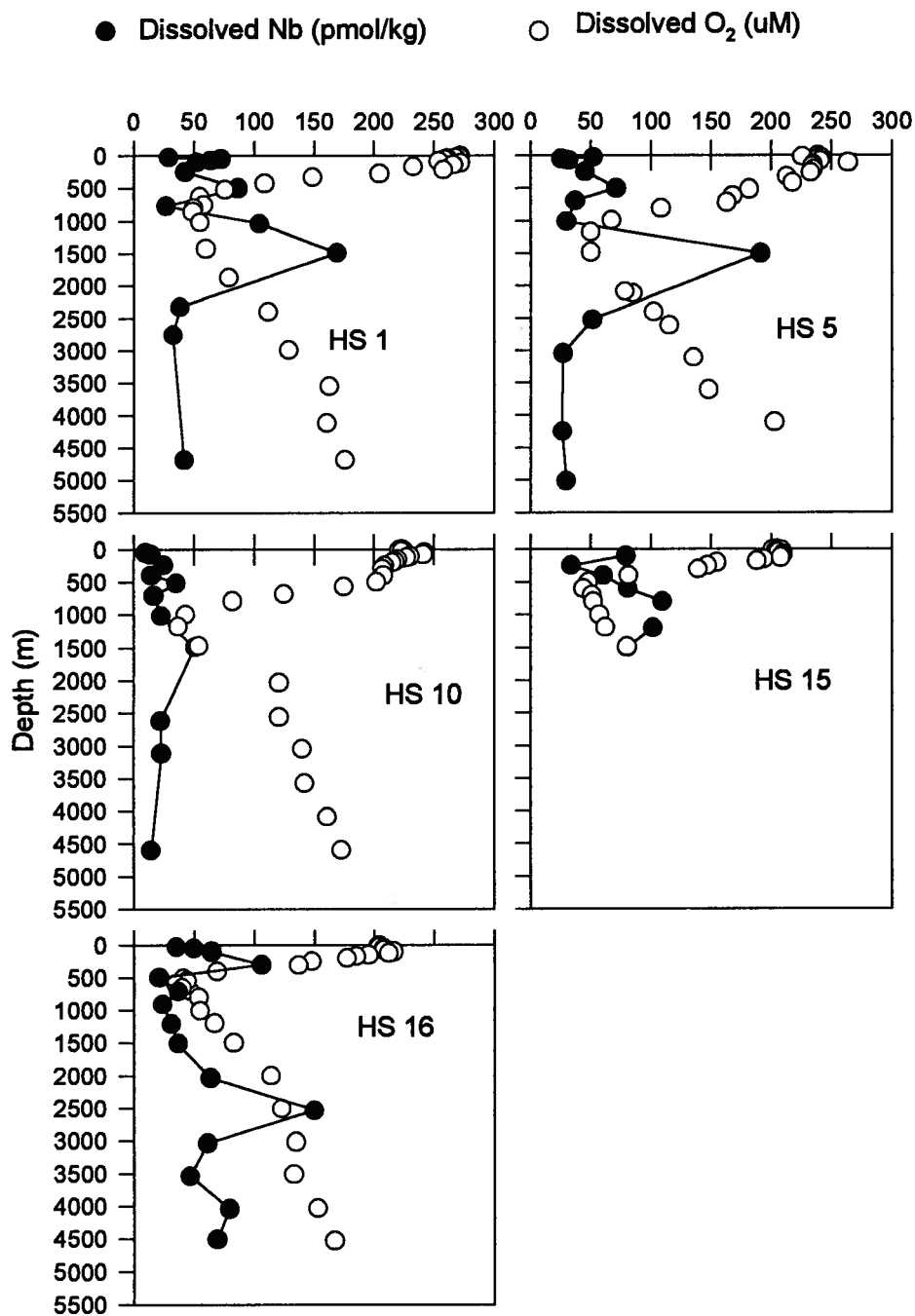


Figure 4.40 Dissolved Nb and O₂ in the North Pacific with respect to depth.
 For Nb: Each point is the average of two analyses.
 For O₂: Data obtained from IOS; uncertainties within the symbols.

Plots of superimposed Mn and Nb profiles, shown in Figure 4.41, illustrate differences in their distributions since the maximum dissolved Mn concentration occurs at the O₂ minimum. No particulate Mn data are available for these stations, but other studies have found that particulate Mn is high in surface waters, decreases in the O₂ minimum zone and then increases again with depth and increasing O₂ concentrations [51]. The Mn signal in the O₂ minimum zone has been attributed to a combination of reversible dissolution/precipitation between particulate Mn (III, IV) oxyhydroxides and dissolved Mn (II) and horizontal advection of water with high dissolved Mn concentrations from continental boundaries.

If one examines only the Nb levels at the surface, in the O₂ minimum and at depth (ignoring the O₂ minimum boundaries), it appears that the distribution of Nb may be controlled by scavenging onto sinking particles. At the upper O₂ minimum boundary, the constant cycling between dissolved and particulate Mn may contribute to the small sub-surface maximum observed in the dissolved Nb concentrations. Cobalt, which has a Mn type distribution, has been found to have a broader and shallower mid-depth maximum in the central North Pacific. This is attributed to complex controls including cycling between reduction and oxidation of Mn(III,IV) oxyhydroxides at the upper boundary of the O₂ minimum and nutrient cycling since Co is biologically important [112, 132]. The sub-surface maxima observed in the dissolved Nb distributions may be controlled by a combination of nutrient and Mn cycling.

At the lower end of the O₂ minimum boundary, once the dissolved Mn is oxidatively scavenged, it is not cycled back into the O₂ minimum zone. The more pronounced dissolved Nb mid-depth maximum may be influenced by the dissolution of Mn oxides in the upper end of the O₂ minimum zone, which results

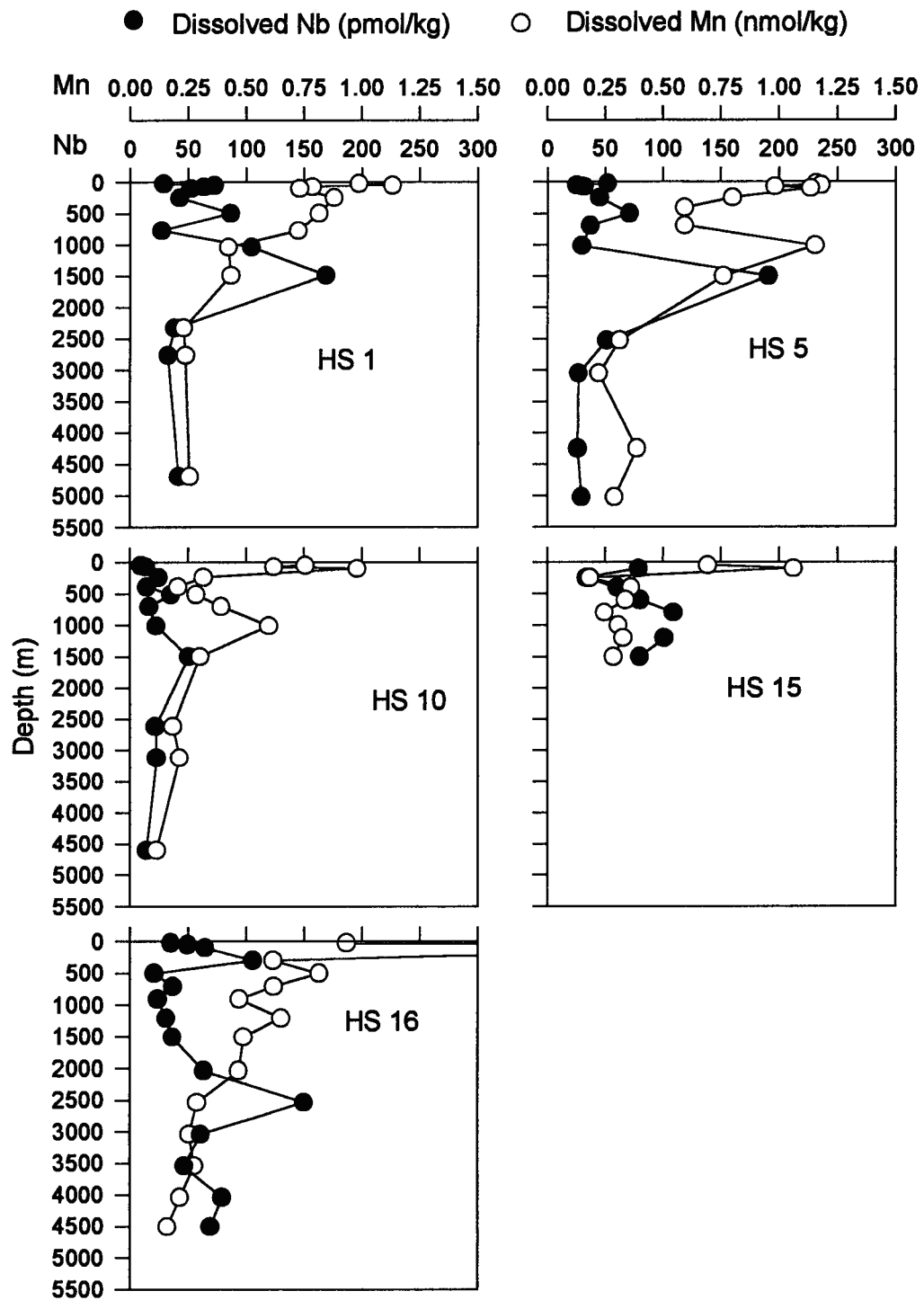


Figure 4.41 Dissolved Nb and Mn against depth in the North Pacific. Points are the averages of two analyses.

in a dissolved Mn mid-depth maximum. However the differences between the Nb and Mn maxima indicate that additional processes must be involved.

The offset between the dissolved Mn and Nb maxima suggests that the controls of dissolved Nb are much more complex, since if Mn cycling was a significant control, the dissolved Nb mid-depth maximum should occur at the same depth as that for Mn. The only published data of Nb in ferromanganese nodules (from a lake in the Malawi Rift, Central Africa) shows a 2.5 fold enrichment of Nb relative to crustal abundance, and a ratio of Nb/Al 16 times higher than the average crustal ratio shows, indicating an association between Nb and oxide phases [133]. Another control of the Mn mid-depth maximum is lateral advection from reducing shelf sediments [51]; thus lateral advection may be a possible control for dissolved Nb.

A further complication may be the effect of changing pH on dissolved Nb in seawater. The pH of seawater follows the O₂ distribution and the hydrolysis of Nb(OH)₅ to Nb(OH)₆⁻ occurs at pH ~7.5 in natural waters, resulting in ~12% of dissolved Nb existing in the Nb(OH)₅ form at pH 8.2 [128,134]. The average seawater pH is ~8, though this can decrease to < 7.6 at the O₂ minimum [135]. At pH 7.6, ~ 35% of dissolved Nb would be in the Nb(OH)₅ form, which may be more reactive in seawater. As O₂ and pH increase, the equilibrium between Nb(OH)₅ and Nb(OH)₆⁻ would shift back again to Nb(OH)₆⁻. Element reactivity as a function of its hydroxide form has been previously suggested to explain the enrichment of dissolved Ga with respect to dissolved Al in seawater since Ga exists predominantly in the less reactive Ga(OH)₄⁻ form while Al exists predominantly as Al(OH)₃ [3, 54]. It is possible that Nb scavenging is enhanced in the pH minimum which could partially explain the minimum observed between 500 and 1500 m.

4.4.3 North Pacific Intermediate Waters

The entrainment of low salinity North Pacific Intermediate water may influence the observed Nb distributions. Plots of potential temperature (θ) versus S are shown in Figure 4.42. The North Pacific Intermediate waters are shallowest at Station P26 (150 m), deeper at Stations 1, 15 and 16 (300 m), and deepest at Stations 5 and 10 (700 m). It appears that this water mass is not influencing the maxima observed at these stations. The smaller sub-surface maxima occur at 500 m (Stations 1, 5 and 10), 300 and 750 m (Stations 16 and P26, respectively). Neither does it appear that the North Pacific Intermediate waters influence the much larger mid-depth maxima occurring at these stations. This does not eliminate the possibility that horizontal advection of high concentrations of Nb waters are a control on the distribution of Nb.

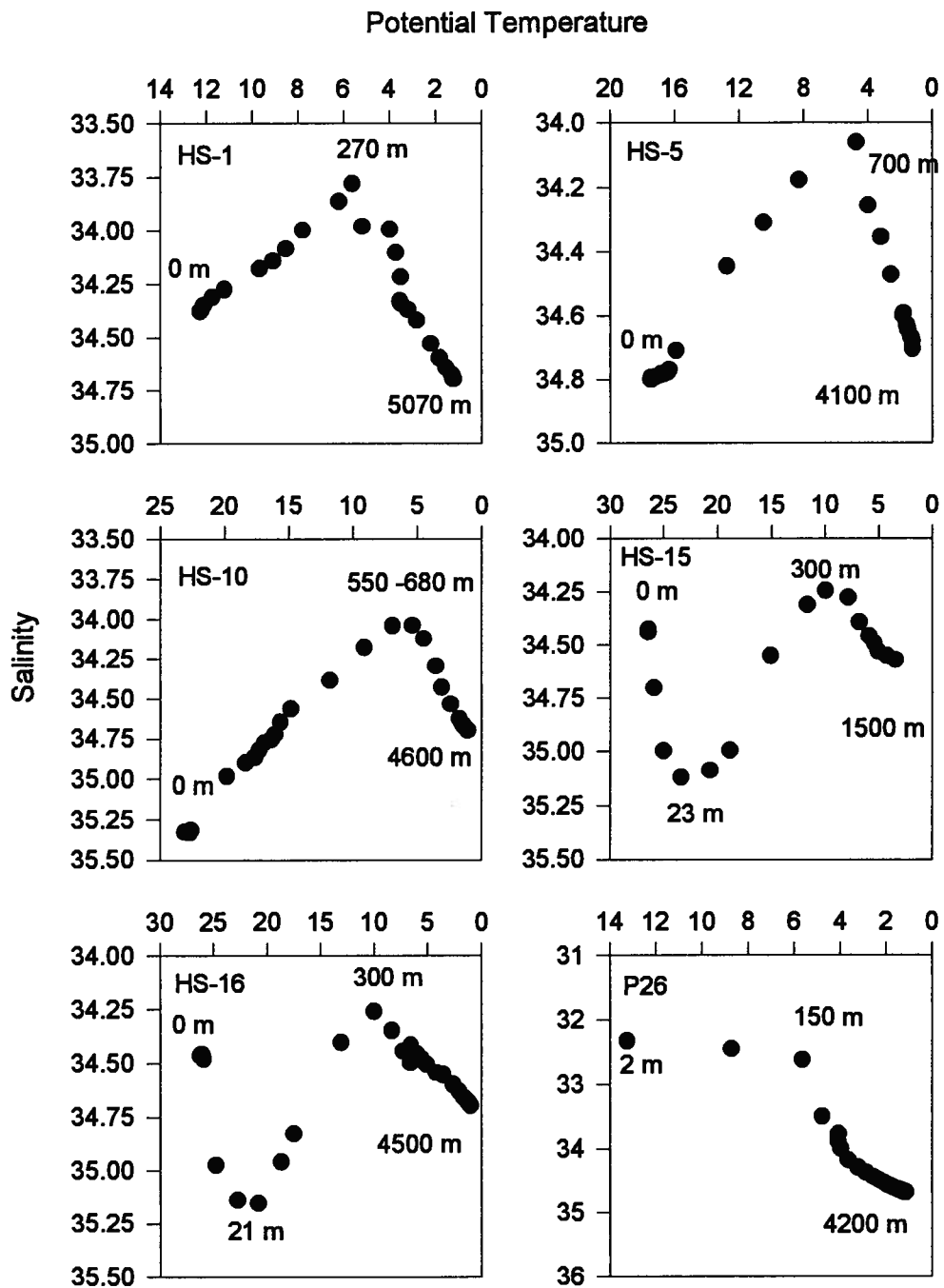


Figure 4.42 Plots of potential temperature versus salinity to determine where the North Pacific Intermediate waters are present at all stations.

4.4.4 Comparison with V

As an aid to understanding the distribution of a particular metal in seawater, it is sometimes beneficial to compare its distribution to the known distribution of another element in the same column of the periodic table. Similarities or differences between elements in the same column of the periodic table may help in determining which oceanic processes may or may not be a control in the biogeochemical behaviour of a particular metal in seawater. Vanadium is located directly above Nb in the periodic table and its behaviour in seawater is very different from that for Nb.

In seawater, V is predicted to exist in the (V) oxidation state as the metavanadate anion, H_2VO_4^- [128]. A typical depth profile shows a slight surface depletion (10 % of average concentration) and then relatively uniform concentration with depth. It is generally considered to be unreactive, though the surface depletion may be explained by a biochemical uptake associated with phosphate. Early measurements indicated no fractionation of V between the Pacific and Atlantic basins [136], though more recent studies indicate an increase of 5 to 15 nmol/kg between the Atlantic Ocean deep waters and the deep waters of the Pacific Ocean [137]. A typical profile of V is shown in Figure 4.43.

Vanadium also exhibits redox chemistry, and can exist in the (IV) oxidation state under acidic and/or reducing conditions in natural waters. It is also enriched in organic rich sediments in anoxic or sub-oxic basins [138]. There is no known nor predicted redox chemistry for Nb in natural waters.

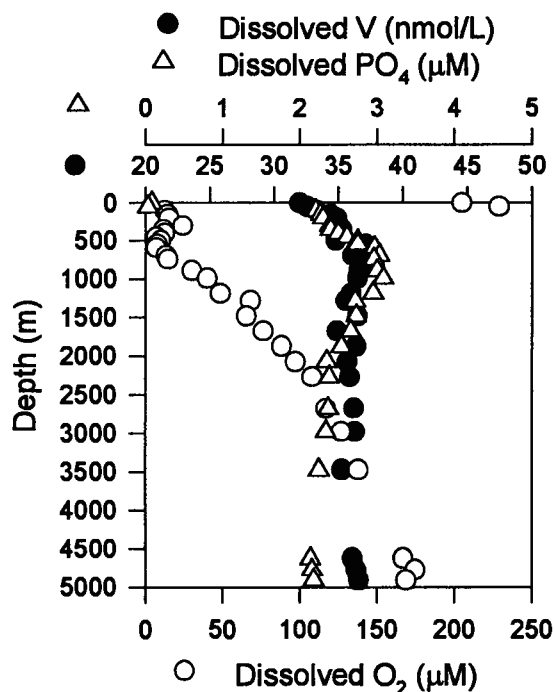


Figure 4.43 Profiles of dissolved V, PO_4 and O_2 in the North Pacific Ocean [136].

The V profile in the North Pacific shows that V has a nutrient-type distribution, correlated with phosphate, except at the surface. There is no indication of scavenging, nor any association with Mn cycling in the depleted O_2 zone. This is in direct contrast with the Nb distributions observed in the North Pacific, which show scavenging and a large mid-depth source coincident to the lower O_2 minimum boundary in the western Pacific Ocean. Clearly, Nb is not an analogue for V in seawater, indicating that the sources and reactivities of these elements are different.

4.4.5 Comparisons with Zr and Mo

Niobium is bracketed in the periodic table by Zr and Mo. These elements have extremely different distributions in seawater. Zirconium is predicted to exist mainly as the hydrolyzed $\text{Zr}(\text{OH})_4$ and $\text{Zr}(\text{OH})_5^-$ and has been found to

have a distribution very similar to those shown by the rare earth elements (REEs): a surface minimum with a gradual increase in concentration with depth [90, 139]. Molybdenum behaves conservatively and is present in seawater as MoO_4^{-2} [140]. Molybdenum can also undergo redox reactions under reducing conditions in seawater [138]. Typical profiles of Zr and Mo in the North Pacific are shown in Figure 4.44.

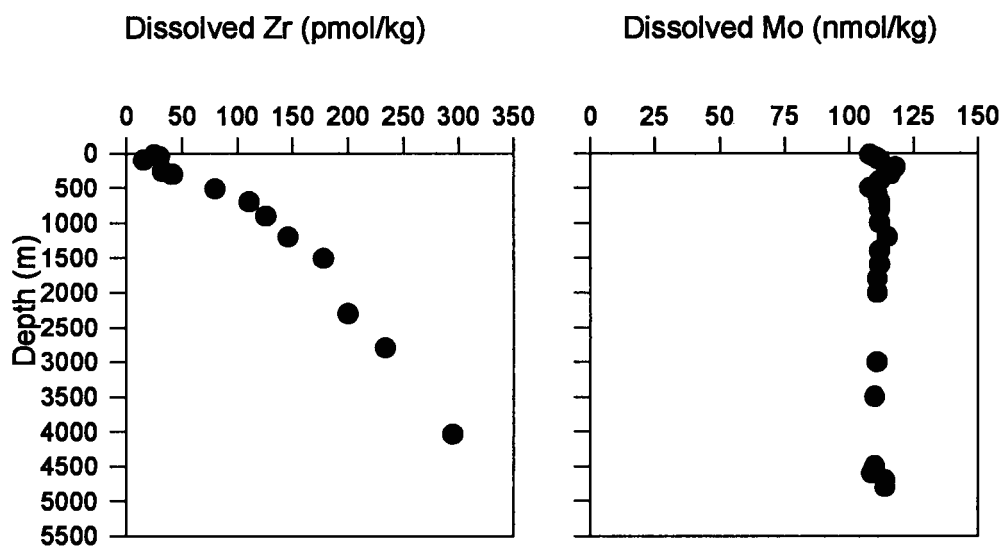


Figure 4.44 Dissolved Zr and Mo in the North Pacific Ocean [90, 140].

Both these elements have very different distributions in seawater compared to dissolved Nb. Niobium does not show a large increase with depth as does Zr (except at Station P26) and does not resemble the REEs, even though both Zr and Nb are expected to exist fully hydrolyzed in seawater. The distribution of dissolved Zr in the North Pacific is a result of removal by particle scavenging throughout the water column and an input from the sediments [139]. Niobium does not show evidence of a strong bottom source at all locations, though both elements do show scavenging throughout the water column. This shows that different processes must be controlling these two elements.

Molybdenum exists as an oxyanion in seawater and has a conservative distribution, thus the processes controlling its distribution are different from those controlling Nb.

4.4.6 Conclusions

These full-depth North Pacific profiles of dissolved Nb are the first reported for this element. The element generally shows a sub-surface concentration maximum at the top of the O₂ minimum and a much larger mid-depth maximum at the bottom boundary of the O₂ minimum. Concentrations of Nb decrease from the Asian coast (Station 1) to the central gyre (Station 10), though the sub-surface and mid-depth maxima occur at the same depths for all three stations. The concentrations of Nb in the North Equatorial Current (Stations 15 and 16) are similar to those observed near Asia, except that at Station 16, the sub-surface maximum is much larger than at the other stations and the mid-depth maximum is deeper. In the sub-Arctic North Pacific Current (P26), the Nb profile is similar except for elevated concentrations in the deep waters. Decreasing concentrations with distance from the continents indicate the possibility of horizontal advection of deep waters with high concentrations of Nb originating from both sides of the Pacific Ocean. The distribution of Nb may also be affected by Mn and nutrient cycling and pH changes in the O₂ minimum zone, although the relative influences of these phenomena cannot be ascertained at present.

To understand the distribution of Nb in the North Pacific better, and how this distribution is affected by the O₂ minimum zone, Mn cycling, pH changes and horizontal advection, more profiles need to be analyzed in other parts of the ocean, with emphasis on high resolution sampling through the O₂ minimum, preferentially in the eastern tropical Pacific.

CHAPTER 5. CONCLUSIONS

An on-line method using FI-ICP-MS to preconcentrate and analyze Zn, Cd, Ni, Cu, Pb, Mn, Ga and Nb was developed. The accuracy of this method was determined by analyzing Mn, Ni, Cu, Zn, Cd and Pb in a NASS-3 open ocean seawater standard. The results obtained with this method agreed with the certified values. The accuracy of this method for the elements Ga and Nb could not be determined since there are no seawater standards with certified values for these two elements. The precision of the on-line method was evaluated by examining the RSDs determined for 10 replicate analyses on the NASS-3 seawater standard. The RSDs were between 5 and 12 % for all elements, except for Cu which had an RSD of 25 %.

A prototype sampler with multi-sampling capabilities was developed to preconcentrate trace metals from seawater remotely. The sampler was submerged for a period of one week in-house, and operated successfully. Repeated testing over time indicated that though the sampler functioned, the deterioration of various components and structural degradation with use in a corrosive medium such as seawater, obviated the deployment of this instrument for the collection of uncontaminated trace metal samples. Significant redesigning of the sampler is needed; because the chemical aspects have been satisfactorily explored as described elsewhere in this thesis, future development should be directed by an engineer rather than a chemist.

This FI-ICP-MS method was used to determine six depth profiles of Mn, Ni, Cu, Zn, Cd, Pb, Ga and Nb from samples obtained in the western, central and north-eastern North Pacific Ocean. The results obtained for Zn, Cd, Ni, Cu, Pb and Mn using this novel technique agree well with profiles previously determined using the same samples but by other methods, as well as with profiles measured in the general area.

The distributions of Mn showed high surface values ranging from 0.8 - 1 nmol/kg, sub-surface minima of 0.15 and 0.7 nmol/kg at 100 to 500 m, mid-depth maxima of 0.3 to 1.2 nmol/kg at depths between 500 and 1500 m, and decreasing concentrations with depth. The profiles for Zn, Cd and Ni showed the expected nutrient distributions with low surface water concentrations increasing with depth to broad maxima coherent with the nutrient maxima and decreasing slightly below this depth. Surface values for Zn, Cd and Ni were 0.4 - 2.5 nmol/kg, 0.01 - 0.25 nmol/kg and 1.5 - 3.5 nmol/kg, respectively, and increased to mid-depth maxima of 7 - 9 nmol/kg between 1000 and 1500 m, 0.9 - 1 nmol/kg between 500 and 1500 m, and 9 - 11 nmol/kg between 800 and 2500 m, respectively. The Cu distributions showed low surface values of 0.7 - 1 nmol/kg and increased linearly with depth to values of 3.5 - 4.5 in deep waters. The profiles of Pb showed high surface values of 10 - 60 pmol/kg, sub-surface maxima of 25 - 40 pmol/kg between 200 and 500 m at all stations excluding Stations 1 and 5, and decreased with depth to values of 10 - 15 pmol/kg in deep waters at all stations.

The first set of dissolved Ga data from the western North Pacific have been presented here, and together with published data from the sub-Arctic North Pacific Current and from the central gyre, result in a better understanding of the controls of dissolved Ga in the North Pacific. The Ga profiles had low surface concentrations of 4 - 14 pmol/kg, mid-depth minima of 3 - 9 pmol/kg and increasing concentrations with depth to 13 - 30 pmol/kg in deep waters. In the central gyre and the sub-Arctic North Pacific sub-surface maxima of 10 - 18 pmol/kg between 300 and 500 m were observed, a feature not seen in the western North Pacific. Dissolved Ga was found to be highest in the central gyre, an area with low dust input from the Asian continent and with low productivity resulting in fewer sinking particles. In the Kuroshio and Oyashio

Current, areas with high dust input and high productivity, Ga values were lower. This indicates that the high levels of Ga in the central gyre and the presence of the sub-surface maximum in this region is not advected from the western North Pacific, where sub-surface maxima were not observed. The lowest Ga concentrations in surface waters were found in the sub-Arctic North Pacific Current, an area with low dust input and high productivity. This indicates that particle scavenging may provide the dominant control of the dissolved Ga content in seawater, although dust inputs also play a role. In the deep waters, scavenging residence times were estimated for stations 10, 16 and P26 to be 700, 530 and 200 years, respectively,

The first full depth profiles of Nb in the oceans are reported in this dissertation. The Nb distributions in the North Pacific show low surface concentrations (10 - 80 pmol/kg), slight sub-surface maxima in the upper 500 m of the water column (40 - 100 pmol/kg), mid-depth minima similar to surface concentrations between 500 and 1000 m, large mid-depth maxima of 50 to 200 pmol/kg between 1000 and 2500 m, and lower deep waters concentrations (10 - 100 pmol/kg). Both maxima were found to occur at the O₂ minimum zone boundary, with the larger maxima just beneath the oxygen minimum. The Nb distributions decreased with distance from the Asian continent, and increased in the North Equatorial Current, indicating horizontal advection of high Nb waters from both the western and eastern Pacific boundaries. The distribution of Nb may also be affected by nutrient cycling in upper waters, Mn cycling in the O₂ minimum zone and decreased pH in the O₂ minimum zone, though the extent cannot be ascertained at present.

CHAPTER 6. FUTURE WORK

Many areas of this research could be extended further. The suite of metals currently being measured by the on-line FI-ICP-MS method could be expanded and the precision of the Cu determination improved. The on-line method should be further automated, by incorporating a second switching valve into the manifold to switch between the 1% nitric acid rinse solution and the eluent streams entering the ICP-MS. A major improvement to the on-line manifold would be to trigger the PlasmaQuad's data acquisition program automatically upon the elution of the preconcentrated sample off the column. This would improve the precision between analyses and eliminate human error. The sampling rate of this system could be increased, either by using a pump with a faster flow rate, or by minimizing the system blanks further to decrease the volume of seawater needed.

The manifold should be used to determine other profiles of Mn, Ni, Cu, Zn, Cd and Pb in different parts of the ocean. Further profiles of Ga in the western North Pacific, including a north-south transect, should be analyzed to study further the influences of productivity and eolian input in its distributions. To obtain a better understanding of the behaviour of Nb in seawater, more profiles with high resolution sampling in the oxygen minimum zone in different areas need to be collected and analyzed. These areas should include the eastern equatorial Pacific Ocean which has a pronounced oxygen minimum. These results could be compared with those obtained for Mn, to determine to what extent Mn cycling contributes to the Nb distributions.

Finally, the work on the prototype sampler can be further extended by utilizing the positives and negatives discovered during the design, building and testing of the prototype to the redesigning and development of a second generation sampler.

BIBLIOGRAPHY

1. K.W. Bruland, "Chapter 45: Trace Elements in Sea-water", in: *Chemical Oceanography*. J. Riley and P. Chester, eds. Academic press, London, pp 157-220 (1983).
2. The Guide to Techniques and Applications of Atomic Spectroscopy, Perkin-Elmer Corporation, Norfolk CT (1988).
3. K.J. Orians and K.W. Bruland, "The marine geochemistry of dissolved Ga: a comparison with dissolved Al", *Geochim. Cosmochim. Acta*, **52**, 2955-2962 (1988).
4. J.S. Hanor and L.H. Chan, "Non-conservative behavior of barium during mixing of Mississippi River and Gulf of Mexico waters", *Earth Planet. Sci. Lett.*, **37**, 242 (1977).
5. E.R. Sholkovitz, "Flocculation of dissolved organic and inorganic matter during the mixing of river water and seawater", *Geochim. Cosmochim. Acta*, **40**, 831-845 (1976).
6. R.A. Duce, P.S. Liss, J.T. Merrill, E.L. Atlas, P. Buat-Menard, B.B. Hicks, J.M. Miller, J.M. Prospero, R. Arimoto, T.M. Church, W. Ellis, J.N. Galloway, L. Hansen, T.D. Jickells, A.H. Knap, K.H. Reinhardt, J. K. Schneider, A. Soudine, J.J. Tokos, S. Tsunogai, R. Wollast and M. Zhou, "The atmospheric input of trace species to world ocean". *Global Biogeochemical Cycles*, **5**, No. 3. 193-259 (1991).
7. V. Hodge, S.R. Johnson and E.D. Goldberg, "Influence of atmospherically transported aerosols on surface ocean water composition", *Geochem. J.*, **12**, 7-20 (1978).
8. K.J. Orians and K.W. Bruland, "Dissolved Al in the central North Pacific", *Nature*, **316**, 427-429 (1985).
9. B.K. Schaule and C.C. Patterson, "Lead concentration in the northeast Pacific: evidence for global anthropogenic perturbations", *Earth Planet. Sci. Lett.*, **54**, 97-116 (1981).

10. J.M. Edmond, C. Measures, R.E. McDuff, L.H. Chan, R. Collier, B. Grant, L.I. Gordon and J.B. Corliss, "Ridge crest hydrothermal activity and the balances of the major and minor elements in the ocean: The Galapagos data", *Earth Planet. Sci. Lett.*, **46**, 1-18 (1979).
11. J.M. Edmond, C. Measures, B. Magnum, B. Grant, R.F. Sclater, R. Collier and A. Hudson, "On the formation of metal-rich deposits at the ridge crests", *Earth Planet. Sci. Lett.*, **46**, 19-30 (1979).
12. G.A. Jackson and J.J. Morgon, "Trace metal-chelator interactions and phytoplankton growth in the seawater media: Theoretical analysis and comparison with reported observations", *Limnol. Oceanogr.*, **23**, 268-282 (1978).
13. I.N. McCave, "Vertical flux of particles in the ocean", *Deep-Sea Res.*, **298**, 491-502 (1975).
14. P.G. Brewer, Y. Nozaki, D.W. Spencer and A.P. Fleer, "Sediment trap experiments in the deep North Atlantic: Isotopic and elemental fluxes", *J. Mar. Res.*, **38**, 703-728 (1980).
15. J.H. Martin and G.A. Knauer, "Mn cycling in northeast Pacific waters", *Earth Planet. Sci. Lett.*, **51**, 266-274 (1980).
16. T.W. Barth, *Theoretical Petrology*, John Wiley, New York (1952).
17. K.W. Bruland, R.P. Franks, G.A. Knauer and J.H. Martin, "Sampling and analytical methods for the determination of copper, cadmium, zinc and nickel at the nanogram per liter level in seawater", *Anal. Chim. Acta*, **105**, 233-245 (1979).
18. K.W. Bruland, "Oceanographic distributions of Cd, Zn, Ni and Cu in the North Pacific.", *Earth Planet. Sci. Lett.*, **47**, 176-198 (1980).
19. L. Danielsson, B. Magnusson and S. Westerlund, "Cd, Cu, Fe, Ni and Zn in the North-east Atlantic Ocean", *Mar. Chem.*, **17**, 23-41 (1985).
20. K. Kremling and D. Hydes, "Summer distribution of dissolved Al, Cd, Co, Cu, Mn and Ni in surface waters around the British Isles", *Continental Shelf Res.*, **8**, 89-106 (1988).

21. K.J. Orians and K.W. Bruland, "The biogeochemistry of Al in the Pacific Ocean", *Earth Planet. Sci. Lett.*, **37**, 397-410 (1986).
22. W.M. Landing and K.W. Bruland, "The contrasting biogeochemistry of Fe and Mn in the Pacific Ocean", *Geochim. Cosmochim. Acta*, **51**, 29-43 (1987).
23. S.A.S. Wilhelmy and A.R. Flegal, "Trace element distributions in coastal waters along the US-Mexican boundary: Relative contributions of natural processes vs. anthropogenic inputs", *Mar. Chem.*, **33**, 371-392 (1991).
24. H.M. Kingston, I.L. Barnes, T.J. Brady and T.C. Rains, "Separation of eight transition elements from alkali and alkaline earth elements in estuarine and seawater with chelating resin and their determination of GFAAS", *Anal. Chem.*, **50**, 2064-2070 (1978).
25. S.S. Berman, J.W. McLaren and S.N. Willie, "Simultaneous determination of five trace metals in seawater by ICP-AES", *Anal. Chem.*, **52**, 488-492 (1980).
26. W.M. Landing, C. Haraldsson and N. Paxéus, "Vinyl polymer agglomerate based transition metal cation chelating ion-exchange resin containing the 8-hydroxyquinoline function group", *Anal. Chem.*, **58**, 3031-3035 (1986).
27. R.E. Sturgeon, S.S. Berman, S.N. Willie and J.A.H. Desaulniers, "Preconcentration of trace elements from seawater with silica-immobilized 8-hydroxyquinoline", *Anal. Chem.*, **53**, 2337-2340 (1981).
28. S.N. Willie, R.E. Sturgeon and S.S. Berman, "Comparison of 8-quinolinol-bonded polymer supports for the preconcentration of trace metals from sea water", *Anal. Chim. Acta*, **149**, 59-66 (1983).
29. E.A. Boyle, F.R. Sclater and J.M. Edmond, "The distribution of dissolved copper in the Pacific", *Earth Planet. Sci. Lett.*, **37**, 38-54 (1977).
30. C.R. German and H. Elderfield, "Rare earth elements in the NW Indian Ocean", *Geochim. Cosmochim. Acta*, **54**, 1929-1940 (1990).
31. K.W. Bruland, K.H. Coale and L. Mart, "Analysis of seawater for dissolved Cd, Cu and Pb: An intercomparison of voltammetric and atomic absorption methods", *Mar. Chem.*, **17**, 285-300 (1985).

32. J.R. Donat and K.W. Bruland, "A comparison of two voltammetric techniques for determining Zn speciation in northeast Pacific Ocean waters", *Mar. Chem.*, **28**, 301-323 (1990).
33. J.R. Donat and C.M.G. van den Berg, "A new cathodic stripping voltammetric method for determining organic Cu complexation in seawater", *Mar. Chem.*, **38**, 69-90 (1992).
34. K.S. Johnson, K.H. Coale and H.W. Jannasch, "Analytical Chemistry in Oceanography", *Anal. Chem.*, **64**, 1065A-1075A (1992).
35. K.W. Bruland, G.A. Knauer and J.H. Martin, "Zinc in the Northeast Pacific waters", *Nature*, **271**, 741-743 (1978).
36. K.W. Bruland, G.A. Knauer and J.H. Martin, "Cadmium in the Northeast Pacific waters", *Limnol. Oceanogr.*, **23**, 618-625 (1978).
37. P.A. Yeats and J. Campbell, "Ni, Cu, Cd and Zn in the north west Atlantic Ocean", *Mar. Chem.*, **12**, 43-58 (1983).
38. S. Westerlund and P. Ohman, "Cd, Cu, Co, Ni, Pb and Zn in the water column of the Weddell sea, Antarctica", *Geochim. Cosmochim. Acta*, **55**, 2127-2146 (1991).
39. G.A. Knauer and J.H. Martin, "Phosphorus-Cd cycling in North East Pacific waters", *J. Mar. Res.*, **39**, 65-76 (1980).
40. N.M. Price and F.M.M. Morel, "Cd and Co substitution for Zn in a marine diatom", *Nature*, **344**, 12, 658-660 (1990).
41. E.A. Boyle, F. Sclater and J.M. Edmond, "On the marine geochemistry of Cd", *Nature*, **263**, 42-44 (1976).
42. F.R. Sclater, E. Boyle and J.M. Edmond, "On the marine geochemistry of Ni", *Earth Planet. Sci. Lett.*, **31**, 119-128 (1976).
43. E.A. Boyle and J.M. Edmond, "Determination of Cu, Ni and Cd in sea water by APDC chelate coprecipitation and flameless atomic absorption spectrometry", *Anal. Chim. Acta*, **91**, 189-197 (1977).
44. E.A. Boyle and J.M. Edmond, "Copper in surface waters south of New Zealand", *Nature*, **253**, 107-109 (1975).

45. E.A. Boyle, S.D. Chapmick and G.T. Shen, "Temporal variability of lead in the western North Atlantic", *J. Geophys. Res.*, **91C7**, 8573-8593 (1986).
46. A.R. Flegal and C.C. Patterson, "Vertical concentration profiles of lead in the central pacific at 15°N and 20°S", *Earth Planet. Sci. Lett.*, **64**, 19-32 (1983).
47. W.M. Landing and K.W. Bruland, "Manganese in the North Pacific", *Earth Planet. Sci. Lett.*, **49**, 45-56 (1980).
48. P.A. Yeats and J.M. Bowers, "Manganese in the western North Atlantic Ocean", *Mar. Chem.*, **17** No. 2, 255-263 (1985).
49. J.H. Martin and G.A. Knauer, "Manganese cycling in Northeast Pacific Equatorial waters", *J. Mar. Res.*, **40**, 1213-1225 (1982).
50. M.L. Bender, G.P. Klinkhammer and D.W. Spencer, "Manganese in seawater and the marine manganese balance", *Deep Sea Res.*, **24**, 799-812 (1977).
51. J.H. Martin and G.A. Knauer, "VERTEX: manganese transport through oxygen minima", *Earth Planet. Sci. Lett.*, **67**, 35-47 (1984).
52. F. Culkin and J.P. Riley, "Germanium and gallium in sea-water", *Nature*, **181**, 179-180 (1958).
53. K.J. Orians and K.W. Bruland, "Dissolved gallium in the open ocean", *Nature*, **332**, 717-719 (1988).
54. A.M. Shiller, "Enrichment of dissolved Ga relative to dissolved Al in natural waters", *Geochim. Cosmochim. Acta*, **52**, 1879-1882 (1988).
55. D.B. Carlisle and L.G. Hummerstone, "Niobium in seawater", *Nature*, **181**, 1002-1003 (1958).
56. S.A. Abbasi, "Niobium in the environment and a new method for its trace determination using molecular or atomic absorption spectrometry", *Inter. J. Environ. Anal. Chem.*, **33**, 43-57 (1988).
57. Y. Suzuki, M. Nakahara and T. Ueda, "Accumulation and Excretion of ⁹⁵Zr and ⁹⁵Nb by Common goby", *Bulletin of the Japanese society of Scientific Fisheries*, **45**(10), 1293-1298 (1979).

58. J. Ruzicka and E.H. Hansen, in *Flow Injection Analysis*, 2nd. ed., John Wiley and Sons, New York (1988).
59. J. Ruzicka and J.W.B. Stewart, "Flow Injection Analysis Part II: Ultrafast Determination of Phosphorous in Plant Material by Continuous Flow Spectrophotometry", *Anal. Chim. Acta*, **79**, 79-91 (1975).
60. J. Ruzicka and E.H. Hansen, "Flow Injection Analysis Part I: A New Concept of Fast Continuous Flow Analysis", *Anal. Chim. Acta*, **78**, 145-157 (1975).
61. G. Nagy, Z.S. Feher and E. Pungor, "Application of silicone rubber-based graphite electrodes for continuous flow measurements", *Anal. Chim. Acta*, **52**, 47-55 (1970).
62. K.K. Stewart, G.R. Beecher and P.E. Hare, "Automated high speed analyses of discrete samples-the use of nonsegmented, continuous flow systems", *Fed. Proc.*, **33**, 1439 (1974).
63. R. Tijssen, "Axial dispersion and flow phenomena in helically coiled tubular reactors for flow analysis and chromatography", *Anal. Chim. Acta*, **114**, 71-89 (1980).
64. H. Engelhardt and R. Klinkner, "Phosphate determination by flow injection analysis with geometrically deformed open tubes[in German]", *Fresenius Z. Anal. Chem.*, **317**, 277 (1984).
65. J.F.K. Huber, K.M. Jonker and H. Poppe, "Optimal design of tubular and packed-bed homogeneous flow chemical reactors for column liquid chromatography", *Anal. Chem.*, **52**, 2-9 (1980).
66. J.M. Reijn, W.E. van der Linden and H. Poppe, "Dispersion in open tubes and tubes packed with large glass beads. The single bead string reactor", *Anal. Chim. Acta.*, **123**, 229-237 (1981).
67. J. Ruzicka and E.H. Hansen, "Flow injection analysis. Principles, applications and trends", *Anal. Chim. Acta*, **114**, 19-44 (1980).
68. S. Olsen, L.C.R. Pessenda, J. Ruzicka and E.H. Hansen, "Combination of flow injection analysis with flame atomic absorption spectrophotometry. Determination of trace amounts of heavy metals in polluted seawater", *Analyst*, **108**, 905 (1983).

69. F. Malamas, M. Bengtsson and G. Johansson, "On-line trace metal enrichment and matrix isolation in atomic absorption spectrometry by a column containing immobilized 8-Quinolinol in a flow injection system", *Anal. Chim. Acta*, **160**, 1-10 (1984).
70. Z. Fang, S. Xu and S. Zhang, "The determination of trace amounts of heavy metals in waters by a flow-injection system including ion-exchange preconcentration and flame atomic absorption spectrometric detection", *Anal. Chim. Acta*, **164**, 41 (1984).
71. Z. Fang, J. Ruzicka and E.H. Hansen, "An efficient flow-injection system with on-line ion-exchange preconcentration for the determination of trace amounts of heavy metals by atomic absorption spectrometry", *Anal. Chim. Acta*, **164**, 23-39 (1984).
72. S.D. Hartenstein, J. Ruzicka and G.D. Christian, "Sensitivity enhancements for flow injection analysis-ICP-AES using an on-line preconcentrating ion-exchange column", *Anal. Chem.*, **57**, 21-25 (1985).
73. C.M. Sakamoto-Arnold and K.S. Johnson, "Determination of picomolar levels of cobalt in seawater by flow injection analysis with chemiluminescence detection", *Anal. Chem.*, **59**, 1789-1794 (1987).
74. V.A. Elrod, K.S. Johnson and K.H. Coale, "Determination of subnanomolar levels of Fe(II) and total dissolved Fe in seawater by flow injection analysis with chemiluminescence detection", *Anal. Chem.*, **63**, 893-898 (1991).
75. T.P. Chapin, K.S. Johnson and K.H. Coale, "Rapid determination of manganese in sea water by flow-injection analysis with chemiluminescence detection", *Anal. Chim. Acta*, **249**, 469-478 (1991).
76. J.A. Resing and M.J. Mottl, "Determination of Mn in seawater using flow injection analysis with on-line preconcentration and spectrophotometric detection", *Anal. Chem.*, **64**, 2682-2686 (1992).
77. D. Beauchemin and S.S. Berman, "Determination of trace metals in reference water standards by ICP-MS with on-line preconcentration", *Anal. Chem.*, **61** 1857-1862 (1989).

78. J.W. McLaren, K. Akatsuka, M.A. Azeredo, J.W.H. Lam and S.S. Berman, "An on-line method for the analysis of seawater for trace elements by inductively coupled plasma mass spectrometry", *J. Anal. At. Spectrom.*, **8**, 279-286 (1993).
79. A.L. Gray, "Mass spectrometry with an ICP as an ion source: the influence on ultratrace analysis of background and matrix response", *Spectrochim. Acta*, **41B**, 151-167 (1986).
80. R.S. Houk, V.A. Fassel, G.D. Flesch, H.J. Svec, A.L. Gray and C.E. Taylor, "Inductively coupled argon plasma as an ion source for mass spectrometric determination of trace elements", *Anal. Chem.*, **52**, 2283-2289 (1980).
81. B.K Esser, A. Volpe, J.M. Kenneally and D.K. Smith, "Preconcentration of REE in natural waters using silica-immobilized 8-HQ and a supported organophosphorus extractant", *Anal. Chem.*, **66**, 1736-1742 (1994).
82. S.H. Tan and H. Horlick, "Background spectral feature in ICP-MS". *Appl. Spectrosc.*, **40** (4), 445-460 (1986).
83. J.R. Dean, L. Ebdon, J.M. Crews and R.C. Massey, "Characteristics of flow injection inductively coupled plasma mass spectrometry for trace metal analysis", *J. Anal. At. Spectrom.*, **3**, 349-354 (1988).
84. D. Beauchemin, K.W.M. Siu and S.S. Berman, "Determination of organomercury in biological reference materials by inductively coupled plasma mass spectrometry using flow injection analysis", *Anal. Chem.*, **60**, 2587-2590 (1988).
85. D.S. Bushee, "Speciation of mercury using liquid chromatography with detection by inductively coupled plasma mass spectrometry", *Analyst*, **113**, 1167-1170 (1988).
86. R.S. Houk and J.J. Thompson, "Trace metal isotopic analysis of microliter solution volumes by inductively coupled plasma mass spectrometry", *Biomed. Mass Spectrom.*, **10**, 107-112 (1983).
87. B.A. McKelvey and K.J. Orians, "Dissolved Zr in the North Pacific Ocean", *Geochim. Cosmochim. Acta*, **57**, 3801-3805 (1993).

88. K.K. Falkner and J.M. Edmond, "Determination of Au at femtomolar levels in natural waters by flow injection inductively coupled plasma quadrupole mass spectrometry", *Anal. Chem.*, **62**, 1477-1481 (1990).
89. J.W. McLaren, A.P. Mykytiuk, S.N. Willie and S.S. Berman, "Determination of trace metals in seawater by ICP-MS with preconcentration on silica-immobilized 8-hydroxyquinoline", *Anal. Chem.*, **57**, 2907-2911 (1985).
90. R.K. Mugo and K.J. Orians, "Seagoing method for the determination of Cr(III) and total Cr in seawater by electron-capture detection gas chromatography", *Anal. Chim. Acta*, **271**, 1-9 (1993).
91. Canadian DFO vessels, incremental costs for 1994/95, NSERC form 605-10 (1993).
92. C.J. Measures and J.M. Edmond, *Anal. Chem.*, "Determination of Be in natural waters in real time using electron capture detection gas chromatography", *Anal. Chem.*, **58**, 2065-2069 (1986).
93. C.J. Measures and J.M. Edmond, "Shipboard determination of Al in seawater at the nanomolar level by electron capture detection gas chromatography", *Anal. Chem.*, **91**, 544-547 (1989).
94. J.R. Donat and K.W. Bruland, Ch 12 in: Trace Metals in Natural Waters, E. Steinne and B.Salbu Eds., CRC Press, Boca Raton, FI, (1994).
95. D.W.R. Wallace and C.D. Wirick, "Large air-sea gas fluxes associated with breaking waves", *Nature*, **356**, 694-696 (1992).
96. C. Goyet, D.R. Walt and P.G. Brewer, " Development of a fiber optic sensor for measurement of pCO₂ in sea water: design criteria and sea trials", *Deep-Sea Res.*, **39**, 1015-1026 (1992).
97. C.E. Reimers, "An *in situ* microprofiling instrument for measuring interfacial pore water gradients: methods and oxygen profiles from the North Pacific Ocean", *Deep-Sea Res.*, **34**, 2019-2055 (1987).
98. K.S. Johnson, C.L. Beehler and C.M. Sakamoto-Arnold, "A submersible flow analysis system", *Anal. Chim. Acta*, **179**, 245-257 (1986).

99. K.S. Johnson, C.M Sakamoto-Arnold and C.L. Beehler, Continuous determination of nitrate concentrations *in situ*", *Deep-Sea Res.*, **36**, 1407-1413 (1990).
100. K.H. Coale, C.S. Chin, G.J. Massoth, K.S. Johnson and E.T. Baker, "*In situ* chemical mapping of dissolved iron and manganese in hydrothermal plumes", *Nature*, **352**, 325-327 (1991).
101. W. Davison and H. Zhang, "*In situ* speciation measurements of trace components in natural waters using thin-film gels", *Nature*, **367**, 546-548 (1994).
102. INFILTREX II user manual, published and distributed by Axys Environmental Ltd. (formerly Seastar Instruments), Sidney, BC (1990).
103. J.A. Tielrooij, H. Compaan, H. Hofstraat and W.H. Mulder, "Time-integrated methods for autonomous, *in situ* sampling of dissolved trace materials in open ocean, coastal and inland waters", *Wat. Sci. Tech.*, **24**, 283-284 (1991).
104. H. Nicolidakis and K.J. Orians, NSERC-CRC proposal: "Development of an Improved In Situ Apparatus for Selective Trace Metal Preconcentration and Determination in Natural Waters: A Request for matching funds from NSERC", (1991).
105. A.J. Paulson, "Effects of flow rate and pretreatment on the extraction of trace metals from estuarine and coastal seawater by Chelex-100", *Anal. Chem.*, **58**, 183-187 (1986).
106. M.A. Marshall and H.A. Mottola, "Synthesis of silica-immobilized 8-quinolinol with (aminophenyl)trimethoxysilane", *Anal. Chem.*, **55**, 2089-2340 (1983).
107. ZT8801 and ZT88CT01 single board V40 computers operating manuals, Ziatech Corporation, San Luis Obispo, CA (1991).
108. STD DOS system manual revision 3.2, Ziatech Corporation, San Luis Obispo, CA (1991).
109. T.E. Miller Jr. and H. Small, "Thermal pulse time-of-flight liquid flow meter", *Anal. Chem.*, **54**, 907-910 (1982).

110. P.W. Shiundu, "Automated methods development in flow injection analysis", Ph.D. dissertation, University of British Columbia (1991).
111. M.A. Vaughn and G. Horlick, "Oxide, hydroxide, doubly charged analyte species in ICP-MS", *Appl. Spectrosc.*, **40** (4), 434-445 (1986)
112. L. Yang, "Dissolved Trace Metals in the Western North Pacific", M.Sc. dissertation, University of British Columbia (1993).
113. J.H. Martin, R.M. Gordon, S. Fitzwater and W.W. Broenkow, "VERTEX: Phytoplankton/iron studies in the Gulf of Alaska", *Deep Sea Res.*, **36**, 649-680 (1989).
114. Y. Nozaki, J. Thomson and K.K. Turekian, "The distribution of ^{210}Pb and ^{210}Po in the surface waters of the Pacific Ocean", *Earth Planet. Sci. Lett.*, **32**, 304-312 (1976).
115. D.S. Lee, J.M. Edmond and K.W. Bruland, "Bi in the Atlantic and North Pacific: a natural analogue to Pu and Pb?", *Earth Planet. Sci. Lett.*, **76**, 254-262 (1985/86).
116. V.T. Bowen, V.E. Noshkin, H.D. Livingston and H.L. Volchok, "Fallout radionuclides in the Pacific Ocean: vertical and horizontal distributions, largely from GEOSECS stations", *Earth Planet. Sci. Lett.*, **49**, 411-434 (1980).
117. H. Craig, "A scavenging model for trace elements in the deep sea", *Earth Planet. Sci. Lett.*, **23**, 149-159 (1974).
118. W.H. Munk, "Abyssal recipes", *Deep Sea Res.*, **13**, 707-730 (1966).
119. A. Gargett, "Vertical eddy diffusivity in the ocean interior", *J. Mar. Res.*, **42**, 359-393 (1984).
120. C.I. Measures, J.M. Edmond and T.J. Jickells, "Al in the northwest Atlantic", *Geochim. Cosmochim. Acta*, **50**, 1423-1429 (1986).
121. S.B. Moran and R.M. Moore, "The potential source of dissolved Al from resuspended sediments to the North Atlantic Deep Water", *Geochim. Cosmochim. Acta*, **55**, 2745-2751 (1991).

122. S. Chan, "ETV-ICP-MS and Ti, Ga and In in the ocean", M.Sc. dissertation, University of British Columbia (1993).
123. M. Uematsu, R.A. Duce, J.M. Prospero, Chen, J. T. Merrill and R.L. McDonald, "Transport of mineral aerosol from Asia over the North Pacific", *J. Geophys. Res.*, **88**(C9), 5343-5352 (1983).
124. H.B. Maring and R.A. Duce, "The impact of atmospheric aerosols on trace metal chemistry in open ocean surface seawater, 1. Al", *Earth Planet. Sci. Lett.*, **84**, 381-392 (1987).
125. F.A. Cotton and G. Wilkinson, "Advanced Inorganic chemistry 4th edition", pp. 12-16, J. Wiley and Sons, New York, 1980.
126. R. Chester, K.J.T. Murphy, J. Towner and A. Thomas, "The partitioning of elements in crust-dominated marine aerosols", *Chem. Geol.*, **54**, 1-15 (1986).
127. P.J. Statham and R. Chester, "Dissolution of Mn from marine atmospheric particulates into seawater and rainwater", *Geochim. Cosmochim. Acta*, **52**, 2433-2437 (1988).
128. D.R. Turner, M. Whitfield and A.G. Dickson, "The equilibrium speciation of dissolved components in freshwater and seawater at 25 C and 1 atm pressure", *Geochim. Cosmochim. Acta*, **45**, 855-881 (1981).
129. C. Huh and T.M. Beasley, "Profiles of dissolved and particulate Th isotopes in the water column of coastal Southern California", *Earth Planet. Sci. Lett.*, **85**, 1-10 (1987).
130. T.D. Jickells and J.D. Burton, "Co, Cu, Mn and Ni in the Sargasso Sea", *Mar. Chem.*, **23**, 131-144 (1988).
131. D.B. Carlisle, "Niobium in ascidians", *Nature*, **181**, 993 (1958).
132. G.A. Knauer, J.H. Martin and R.M. Gordon, "Co in the north-east Pacific waters", *Nature*, **297**, 49-51 (1982).
133. T.M. Williams and R.B. Owen, "Geochemistry and origins of lacustrine ferromanganese nodules from the Malawi Rift, Central Africa", *Geochim. Cosmochim. Acta*, **56**, 2703-2712 (1992).

134. C.F. Baes, Jr. and R.E. Mesmer, "The hydrolysis of Cations", John Wiley and Sons, New York (1976).
135. R. Chester, "Marine Geochemistry", Unwin Hyman, London (1990).
136. R.W. Collier, "Particulate and dissolved vanadium in the North Pacific Ocean", *Nature*, **309**, 441-444 (1984).
137. C. Jeandel, M. Caisso and J.F. Minster, "Vanadium behaviour in the global ocean and in the Mediterranean sea", *Mar. Chem.*, **21**, 51-74 (1987).
138. S.R. Emerson and S.S. Husted, "Ocean anoxia and the concentrations of molybdenum and vanadium in seawater", *Mar. Chem.*, **34**, 177-196 (1991).
139. B.A. McKelvey, "Dissolved Zr and Hf in Seawater", Ph.D. dissertation, University of British Columbia (1994).
140. R. Collier, "Molybdenum in the Northeast Pacific Ocean", *Limnol. Oceanogr.*, **30**, 1351-1354 (1985).

APPENDIX A. INFILTREX II *IN SITU* SAMPLER

A.1 The INFILTREX II sampler

Axys Environmental Ltd. (Sidney, BC), manufactures an *in situ* water sampler, the INFILTREX II [102]. This unit is lowered from a ship or a buoy and suspended at a known depth for sampling. As the sample is collected and concentrated in its own environment, the chance of contamination during sample collection is minimized.

A.1.1 Physical Appearance

A schematic of the INFILTREX II sampler is shown in Figure A.1. The spine of the sampler is approximately 75 cm long with hydrowire brackets attached at the top and bottom of one side. In addition, the pressure housing, a single extraction column and a filter sandwich are attached to the spine. The pressure housing is 55 cm in length, and its inner diameter is approximate 10 cm. This housing contains the electronics, the gear pump, the flow meter and a battery pack consisting of two 6 V lantern size batteries.

The extraction column has an inner diameter of 2.5 cm and a length of 37 cm. The resin supplied with the INFILTREX II system is an 8-hydroxyquinoline functional group on a polystyrene divinylbenzene backbone (8-HQ-XE-305). To prevent contamination, all the tubing and column parts are made of Teflon[®]. To remove particulate matter, the seawater is passed through a 0.45 µm pre-filter. The polycarbonate filter, which has a diameter of 142 mm, is contained within a filter sandwich. The filter sandwich is made of two pieces of a plastic fitted with a Teflon[®] coated silicone o-ring.

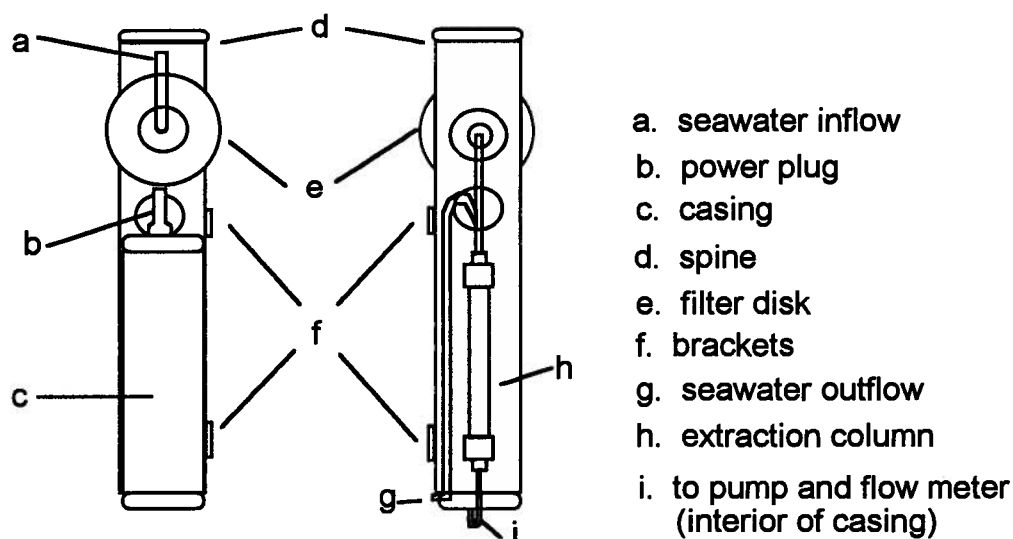


Figure A.1 Front and back view of the INFILTREX II

A.1.2 Operation

Operation of the INFILTREX II sampler is controlled using a single board microcomputer. Software, supplied with the sampler, permits timed operation of the unit and the storage of key information such as battery voltage. Variables such as the pump speed and the total volume of seawater to be pumped may be set prior to deployment with the aid of a RS-232 serial interface between the sampler computer board and a personal computer. An in-built clock allows for the sampler to be programmed days in advance of its actual operation.

When the sampler is operating, the seawater is drawn into the filter sandwich. After filtering, the seawater passes through the extraction column where dissolved metals chelate to the active sites on the resin. The filtrate is then drawn into the pressure housing through stainless steel tubing. Here, the flow rate is measured prior to the filtrate being drawn through the pump and back into the environment.

A.1.3 Limitations of the INFILTREX II sampler

Although the INFILTREX II sampler has been used for several years to sample trace metals in the seawater, a number of limitations exist:

Flow rate: The sampler was originally designed for extracting trace organics from seawater, and due to pump limitation, only operates between 50 and 500 L/min. The flow rates available using the INFILTREX II sampler were not considered suitable for the extraction of trace metals from seawater.

Column Design: The single column configuration of the INFILTREX II sampler allows for only one sample per deployment. The used column must be replaced with a fresh column before the sampler can be redeployed. The sampler must be deployed many times to gather replicate samples, a complete depth profile or to undertake temporal variability studies. This is time consuming and can become costly since many columns must be at hand if multiple sampling is performed.

In the INFILTREX II sampler, a large column is employed in order to withstand the force of the high flow rates used and to increase the contact time between the resin and the seawater. The column has a volume of *ca.* 725 ml and a large volume of resin is required. Even when using a large volume of resin, there would be no guarantee that a complete extraction of the trace metals from the seawater would be achieved when such high flow rates are used. To completely elute the metals from the column, the elution volume should be at least three times that of the resin. Therefore a high volume of seawater is needed since the eluent volume required will reduce the concentration factor. In addition, using a large volume of resin results in high column blanks, *i.e.*, the background level of metals from the resin. Cost becomes a major consideration as the resin, the special columns and the eluent become expensive.

A.1.4 Attempted Modification of the INFILTREX II Sampler

To make the INFILTREX II sampler more versatile and more attractive to potential users for trace metals, several modifications were proposed. The addition of more columns would allow multiple samples to be taken per deployment. As discussed above, slower flow rates were required for trace metal extraction. Lowering the flow rates would permit the use of smaller extraction columns, requiring less resin and eluent, which in turn would decrease the column blanks and lower the cost.

As a result of initial discussions with the scientists at Axy's Environmental Ltd., it was concluded that the main limiting factor preventing the use of the INFILTREX II sampler at slow flow rates was the operating range of its flow meter. The original intent was to replace the existing flow meter and subsequently lower the pump speed [106]. The INFILTREX II's pump speed is adjusted by varying the voltage supplied to the pump motor. Higher voltages result in faster pump speeds and a quicker drain of the power supply. The Axy's scientists suggested that it would be a simple operation to divide the voltage to the pump motor in order to obtain the slower flow rates.

A number of minor changes to the sampler were also required to enable the multiple column design to function. For example, minor electronics for controlling the valves for the multiple column design would have to be added. In addition, the column manifold was to be adapted for flow injection type fittings.

After the INFILTREX II sampler had been delivered, it was soon realized that the pump speed could not be slowed, nor could the necessary electronics be incorporated. The only course of action was to design and construct a new sampler incorporating the required modifications.

APPENDIX B. SOFTWARE ROUTINES

LISTING OF PROGRAM "HIGHLO.BAS"

```

OUT &HFA01, &HFF      ' set port 1 bits LO (false HI)
OUT &HFA02, &HFF      ' set port 2 bits LO  "
OUT &HFA03, &HFF      ' set port 3 bits LO  "
OUT &HFA04, &HFF      ' set port 4 bits LO  "
OUT &HFA05, &HFF      ' set port 5 bits LO  "
END

```

LISTING OF PROGRAM "SAMPLER.BAS"

```

DECLARE SUB BUFFER (col%(), i%, buf%)
DECLARE SUB FLOW (TMD%, CT2ADD%, Count&(), j%)
DECLARE SUB BUFFER (col%(), i%, buf%)

pts% = 50
DIM Count&(1 TO pts%)
DIM col%(5)
ctbase% = &H40      ' looks like base is TULA
TMD% = ctbase% + 3
CT2ADD% = ctbase% + 2  ' (TCT2, LB-HB, mode 0, binary)

col%(1) = &HFE      ' sets pin 28(i/o24, bit0) high for valve 1 on 6-way valve
col%(2) = &HFD      ' sets pin 29(i/o25, bit1) high for valve 2 on 6-way valve
col%(3) = &HF7      ' sets pin 30(i/o26, bit2) high for valve 3 on 6-way valve
col%(4) = &HEF      ' sets pin 31(i/o27, bit3) high for valve 4 on 6-way valve
col%(5) = &HDF      ' sets pin 32(i/o28, bit4) high for valve 5 on 6-way valve
' col%(6) = &HDF      ' sets pin 33(i/o29, bit5) high for valve 6 on 6-way valve
pump% = &HFE      ' sets pin 37(i/o32,bit0) high and turns on pump
pumpoff% = &HFF    ' used to set pin 37 low and turn off pump
buf% = &H80

OUT &HFFF0, &H10    ' clock and prescale select

```

```

OUT TMD%, &HB0          ' general mode register init
OUT &HFA01, 0          ' set port 1 bits LO

't = TIMER: DO: t1 = TIMER: LOOP WHILE t1 < (t + 900) 'total time sampler on

OUT &HFA04, pumpon% ' turn on pump
FOR i% = 1 TO 5
'   file$ = "R:test.dat"
file$ = "R:test" + LTRIM$(STR$(i%)) + ".DAT"
OPEN file$ FOR OUTPUT AS 1
OUT &HFA03, col%(i%) ' turn on each column in its turn
startt = TIMER: totalt = startt + 100 ' total time per column
CALL BUFFER(col%(), i%, buf%)
DO
  t = TIMER: DO: t1 = TIMER: LOOP WHILE t1 < (t + 30)
  CALL FLOW(TMD%, CT2ADD%, Count&(), j%) ' measure the flow rate
  PRINT #1, Count&(j%)
  CALL BUFFER(col%(), i%, buf%)
  chk = TIMER
LOOP UNTIL (chk > totalt)
CLOSE #1
NEXT i%                ' if yes, start with new column

OUT &HFA04, pumpoff%   ' once all columns done, turn off pump
OUT &HFA03, &HFF       ' turn off valves
OUT &HFA01, &HFF
END

```

SUB BUFFER (col%(), i%, buf%)

```

nice% = col%(i%) - buf%      ' inject first buffer
OUT &HFA03, nice%
onesecond = TIMER
anothercheck:
  yikes = TIMER
  IF yikes < (onesecond + 1) GOTO anothercheck
  OUT &HFA03, col%(i%)
END SUB

```

SUB FLOW (TMD%, CT2ADD%, Count&(), j%)

```

' zero counter 2
OUT CT2ADD%, &HFF: OUT CT2ADD%, &HFF
OUT &HFA01, &HFF      ' set port 1 bits HI

t = TIMER: DO: t1 = TIMER: LOOP WHILE t1 < (t + 1.32)
  OUT &HFA01, 0      ' set port 1 bits LO
  ' wait for the pulse to reach the thermistor
  t = TIMER: DO: t1 = TIMER: LOOP WHILE t1 < (t + 13)
  ' read the contents of counter 2
  OUT TMD%, &H80    'counter latch
  OUT TMD%, &H80    'latch counter 2
  countLo% = INP(CT2ADD%)      ' get the LO byte
  countHi% = INP(CT2ADD%)      ' get the HI byte
  countHi% = &HFF - countHi%
  countLo% = &HFF - countLo%
  Count&(j%) = countHi% * 256& + countLo%
END SUB

```

APPENDIX C. CIRCUIT SCHEMATICS

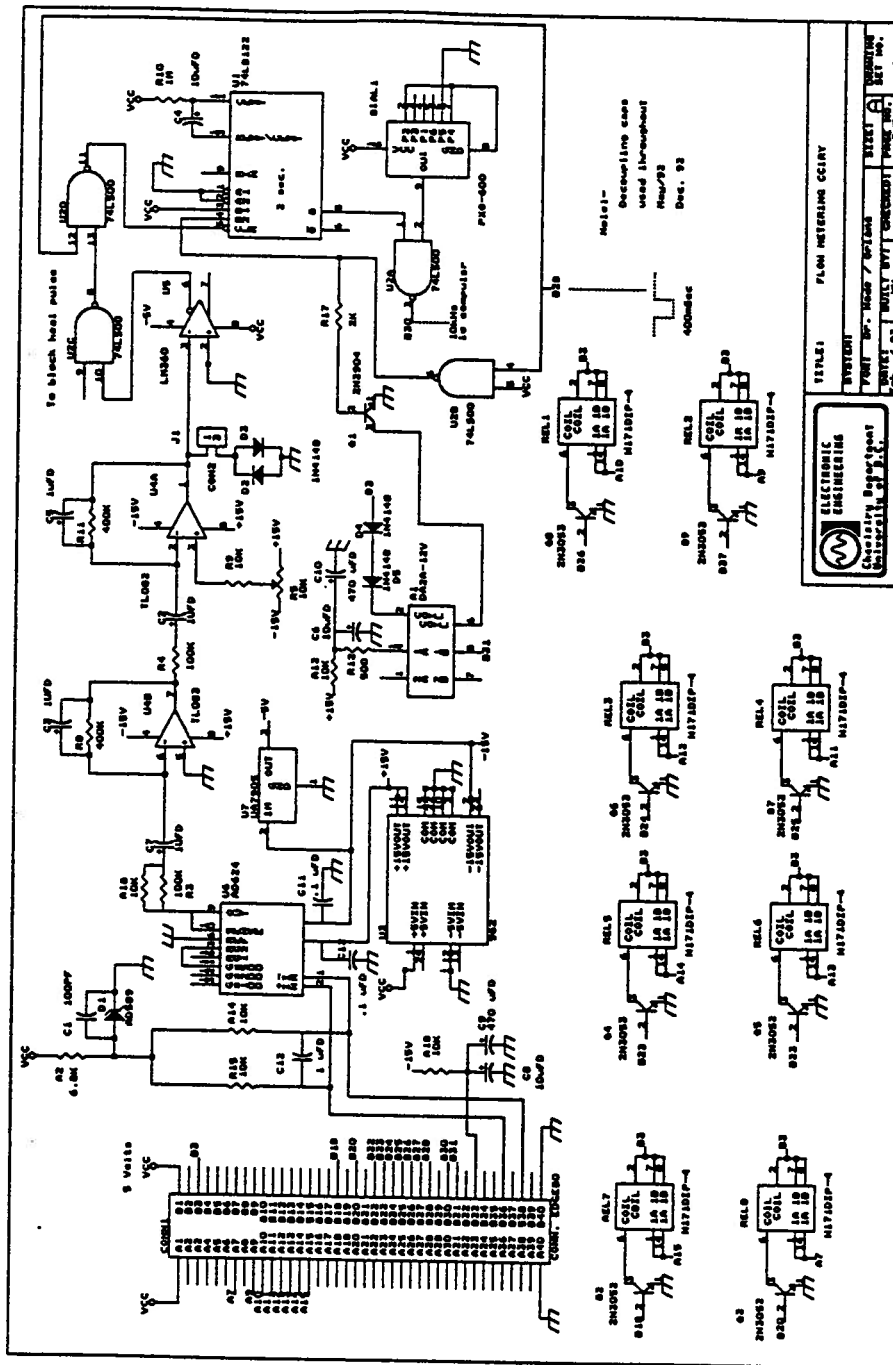


Figure C.1. Flow meter and valve and pump control circuits on circuitry board.

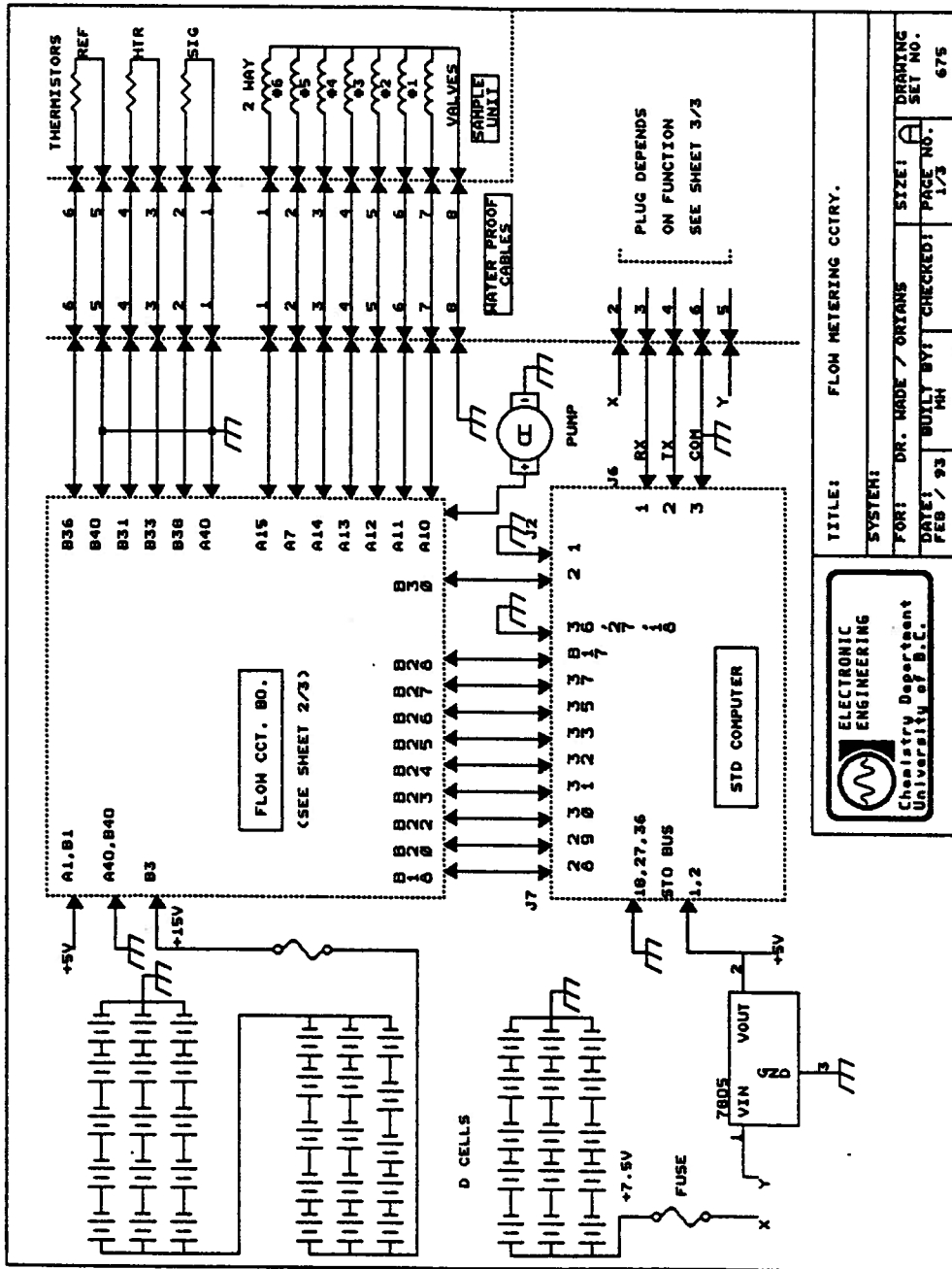


Figure C.2. Schematic of connections between computer board, circuitry board and physical components mounted on the exterior of the prototype sampler.

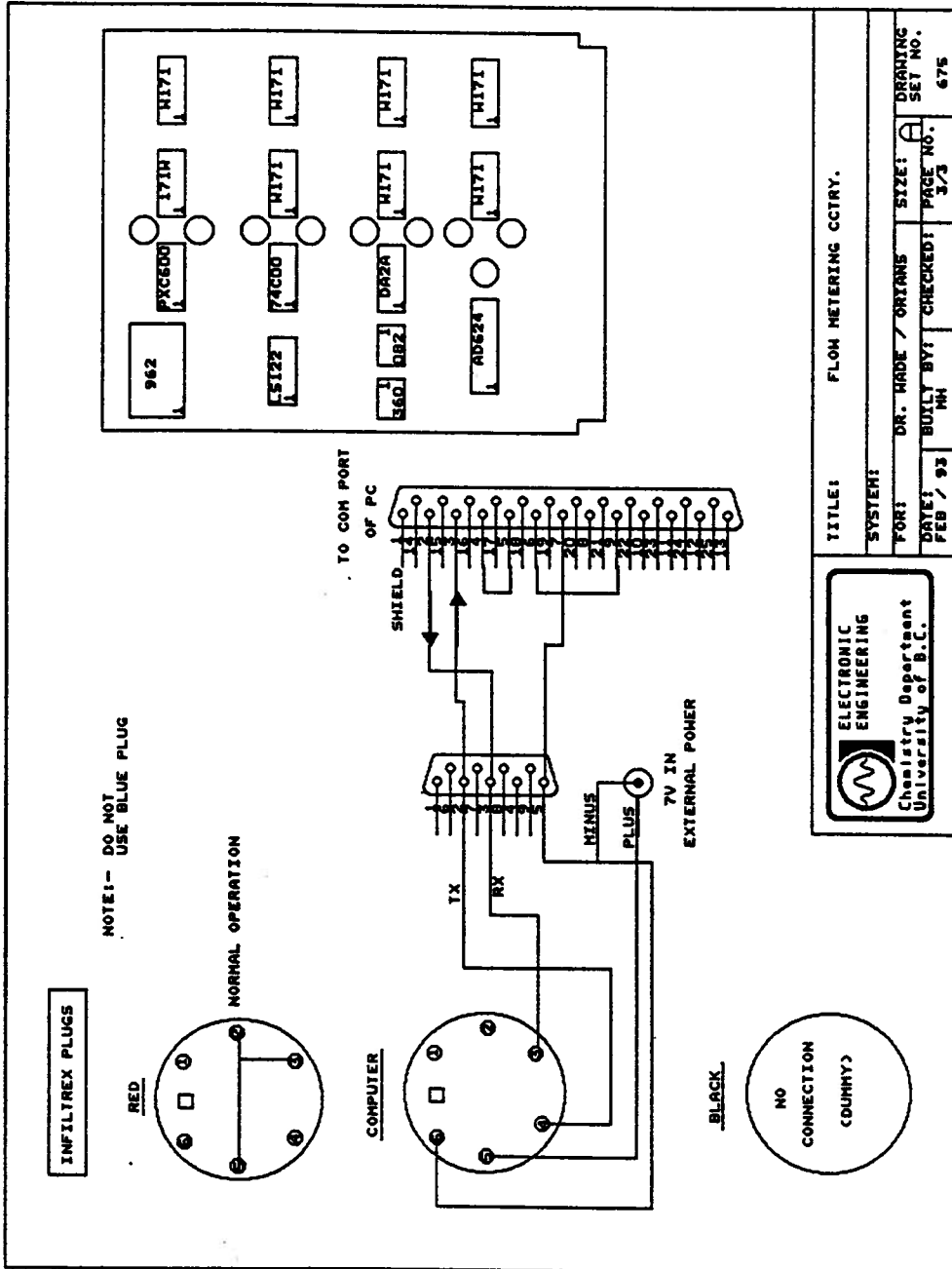


Figure C.3. Schematic representation of the normal operation and computer connecting plugs of the prototype sampler.

APPENDIX D. SINGLE ION MONITOR SCANS

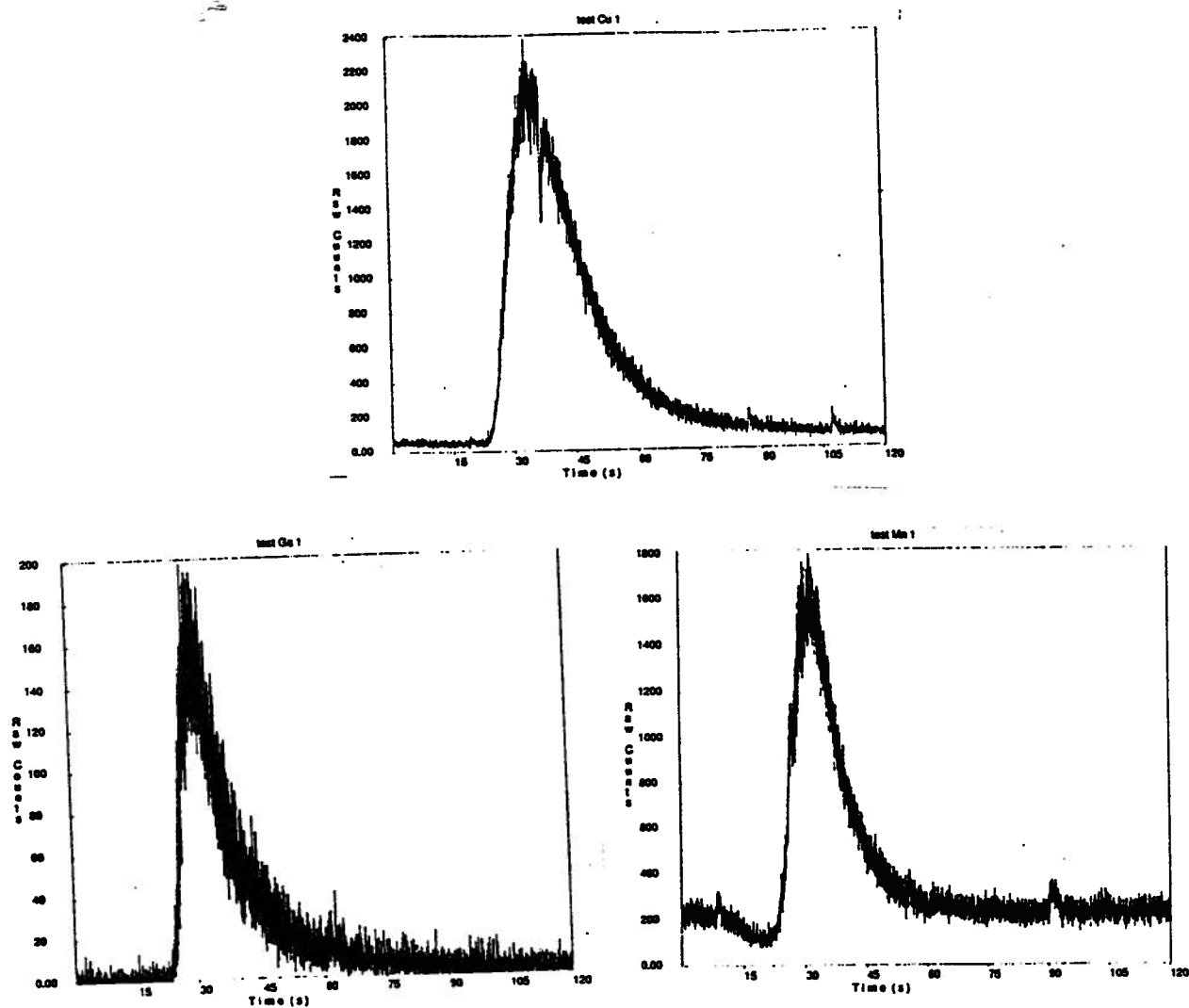


Figure D.1. SIM scans of Cu, Ga and Mn.

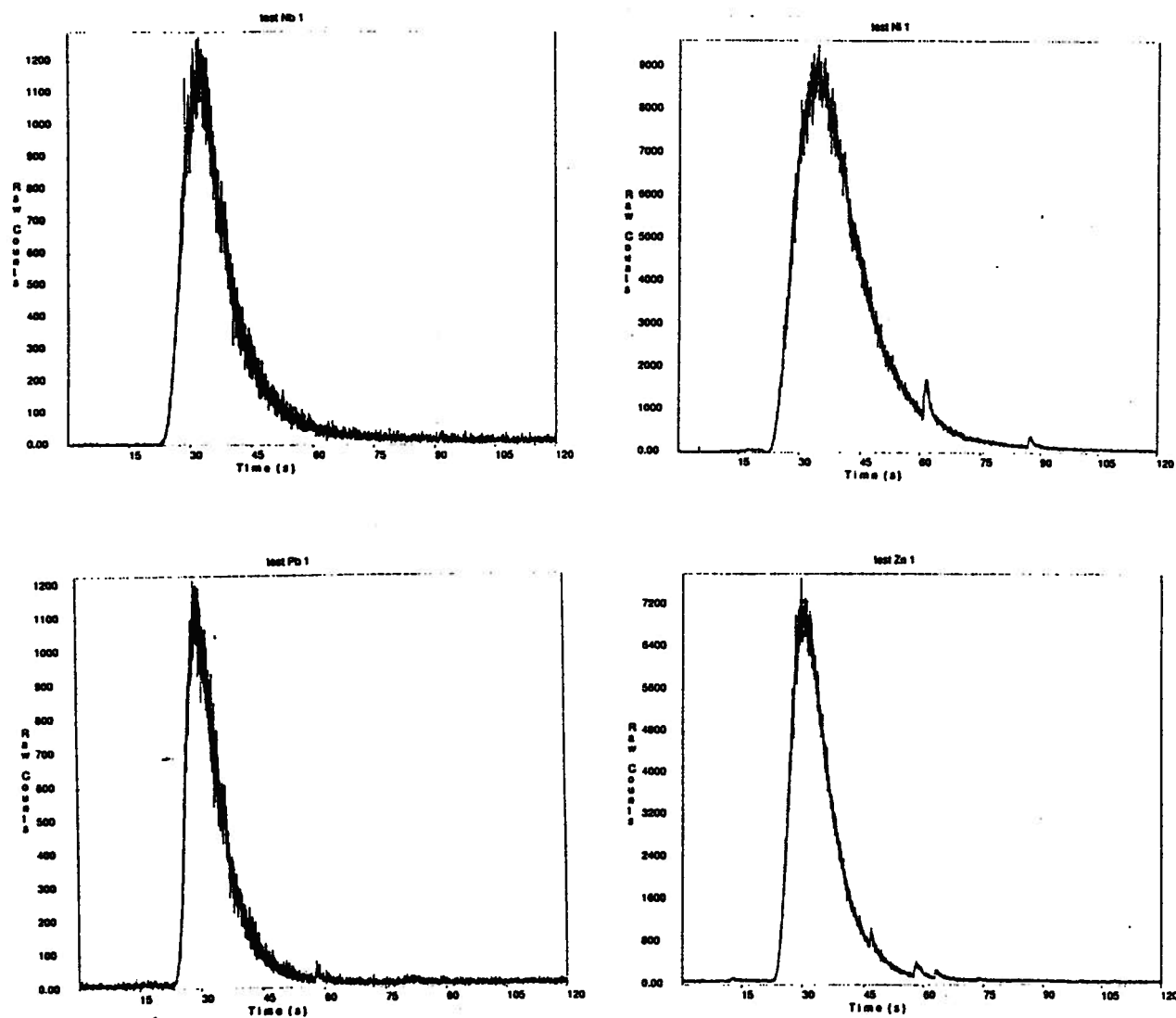


Figure D.2 SIM scans of Nb, Ni, Pb and Zn.

APPENDIX E. OCEANOGRAPHICAL DATA

Station	Location	Sea Floor Depth (m)
HS 1	38 14.3N 145 50.9E	5200
HS 5	34 57.8N 155 02.3E	5630
HS 10	27 46.5N 174 59.4E	5820
HS 15	16 27.6N 168.29.8W	1550
HS 16	17 14.0N 168 07.0W	5210
P 26	55.00N 145.00W	4500

Table E.1. Locations and depths of the stations studied.

Station	Depth (m)	Zn (nmol/kg)	Cd (nmol/kg)	Ni (nmo/kg)	Cu (nmol/kg)
HS 1	25	2.678 ± 0.2311	0.202 ± 0.024	3.603 ± 0.578	0.920 ± 0.122
	50	1.969 ± 0.603	0.335 ± 0.035	2.418 ± 0.244	0.823 ± 0.093
	75	1.567 ± 0.078	0.277 ± 0.019	3.182 ± 0.066	0.632 ± 0.034
	100	1.895 ± 0.057	0.260 ± 0.007	4.762 ± 0.020	1.196 ± 0.005
	250	3.471 ± 0.112	0.911 ± 0.001	5.487 ± 0.043	1.046 ± 0.001
	499	6.299 ± 0.213	0.863 ± 0.047	7.893 ± 0.091	1.285 ± 0.039
	770	6.984 ± 0.251	1.013 ± 0.053	7.585 ± 0.192	0.867 ± 0.048
	1036	8.594 ± 0.208	1.056 ± 0.061	9.535 ± 0.364	1.327 ± 0.081
	1489	8.830 ± 0.147	1.126 ± 0.032	9.849 ± 0.365	2.096 ± 0.091
	2326	8.149 ± 0.653	0.950 ± 0.072	10.828 ± 0.426	3.174 ± 0.104
	2759	8.443 ± 0.604	0.868 ± 0.051	10.837 ± 0.497	4.070 ± 0.182
4689	8.418 ± 0.359	0.817 ± 0.032	10.308 ± 0.226	4.497 ± 0.097	
HS 5	25	0.570 ± 0.001	0.071 ± 0.015	3.050 ± 0.309	1.039 ± 0.019
	50	0.430 ± 0.031	0.026 ± 0.001	2.635 ± 0.100	0.917 ± 0.057
	75	0.309 ± 0.011	0.024 ± 0.001	2.327 ± 0.098	0.764 ± 0.012
	100	0.543 ± 0.029	0.039 ± 0.003	2.571 ± 0.011	1.079 ± 0.046
	250	0.258 ± 0.009	0.038 ± 0.001	1.763 ± 0.080	0.637 ± 0.016
	410	1.276 ± 0.038	0.235 ± 0.001	4.364 ± 0.223	1.333 ± 0.021
	500	1.460 ± 0.065	0.207 ± 0.005	3.794 ± 0.400	1.883 ± 0.080
	692	3.566 ± 0.023	0.579 ± 0.011	6.931 ± 0.396	2.397 ± 0.108
	1013	5.751 ± 0.085	0.752 ± 0.001	8.567 ± 0.393	3.177 ± 0.110
	1502	6.954 ± 0.386	0.886 ± 0.039	9.845 ± 0.359	3.439 ± 0.079
	2526	5.772 ± 0.029	0.730 ± 0.004	7.651 ± 0.203	1.750 ± 0.013
	3051	7.110 ± 0.309	0.782 ± 0.042	8.852 ± 0.362	3.373 ± 0.094
HS 10	50	0.511 ± 0.162	0.012 ± 0.005	2.715 ± 0.296	0.690 ± 0.030
	75	0.421 ± 0.019	0.013 ± 0.004	1.918 ± 0.154	0.704 ± 0.067
	100	0.768 ± 0.041	0.032 ± 0.001	2.934 ± 0.087	0.840 ± 0.043
	238	0.355 ± 0.002	0.060 ± 0.003	1.755 ± 0.014	0.699 ± 0.003
	388	1.029 ± 0.024	0.191 ± 0.006	4.996 ± 0.248	1.155 ± 0.032
	511	5.728 ± 0.163	0.355 ± 0.009	5.639 ± 0.016	1.284 ± 0.010
	700	5.284 ± 0.330	0.654 ± 0.032	9.016 ± 0.435	2.222 ± 0.107
	1009	7.142 ± 0.300	0.879 ± 0.041	11.662 ± 0.318	2.568 ± 0.127
	1492	7.78 ± 0.053	0.907 ± 0.011	13.068 ± 0.318	2.435 ± 0.019
	2615	8.104 ± 0.133	0.780 ± 0.008	9.869 ± 0.263	2.194 ± 0.027
	3116	7.473 ± 0.182	0.766 ± 0.014	12.873 ± 0.687	2.863 ± 0.153
4599	6.992 ± 0.191	0.646 ± 0.031	11.484 ± 0.138	7.922 ± 0.155	

Table E.2 Dissolved Zn, Cd, Ni and Cu in the western North Pacific. Each value is the average of two measurements and the error represents the range.

Station	Depth (m)	Pb (pmol/kg)	Mn (nmol/kg)	Ga (pmol/kg)	Nb (pmol/kg)
HS 1	25	57.5 ± 5.7	0.988 ± 0.145	9.3 ± 3.1	28.8 ± 12.1
	50	45.2 ± 7.2	1.129 ± 0.193	9.7 ± 0.6	72.6 ± 1.4
	75	36.2 ± 2.7	0.778 ± 0.036	10.3 ± 0.5	63.8 ± 5.4
	100	43.1 ± 0.4	0.733 ± 0.001	9.8 ± 0.6	52.4 ± 5.2
	250	49.2 ± 0.5	0.882 ± 0.014	7.5 ± 0.1	42.8 ± 3.4
	499	31.4 ± 2.3	0.816 ± 0.027	5.2 ± 0.4	86.7 ± 0.3
	770	26.3 ± 1.7	0.726 ± 0.019	4.7 ± 0.1	27.1 ± 4.5
	1036	31.1 ± 2.1	0.423 ± 0.042	5.4 ± 0.2	104.6 ± 6.5
	1489	23.4 ± 0.6	0.435 ± 0.014	6.3 ± 0.3	169.3 ± 13.5
	2326	23.5 ± 0.6	0.230 ± 0.024	9.8 ± 1.7	38.4 ± 1.6
	2759	24.3 ± 2.2	0.240 ± 0.019	12.1 ± 0.6	32.6 ± 0.7
4689	21.3 ± 0.8	0.257 ± 0.019	14.1 ± 1.1	42.0 ± 1.8	
HS 5	25	27.1 ± 2.6	1.160 ± 0.112	11.7 ± 0.2	52.1 ± 6.3
	50	23.4 ± 0.8	1.180 ± 0.046	12.3 ± 0.3	25.4 ± 1.5
	75	22.8 ± 1.5	0.983 ± 0.002	11.5 ± 0.3	31.7 ± 0.9
	100	22.3 ± 1.2	1.135 ± 0.054	12.5 ± 0.3	
	250	12.4 ± 0.1	0.801 ± 0.002	10.9 ± 0.6	45.4 ± 0.2
	410	5.9 ± 0.4	0.594 ± 0.047	12.0 ± 0.5	
	500	19.0 ± 0.1		11.6 ± 0.0	71.1 ± 3.1
	692	18.1 ± 0.4	0.594 ± 0.028	6.7 ± 0.2	37.2 ± 3.2
	1013	15.7 ± 0.5	1.154 ± 0.021	4.8 ± 0.5	29.9 ± 2.6
	1502	13.4 ± 1.0	0.762 ± 0.058	6.2 ± 0.8	191.1 ± 2.7
	2526	8.2 ± 0.1	0.314 ± 0.024	6.6 ± 0.2	51.3 ± 4.4
	3051	7.4 ± 0.1	0.223 ± 0.018	7.5 ± 0.2	27.1 ± 1.4
HS 10	50	40.7 ± 4.4	0.757 ± 0.069	14.5 ± 0.6	9.8 ± 2.6
	75	37.2 ± 3.1	0.621 ± 0.048	14.5 ± 3.0	14.1 ± 1.6
	100	39.7 ± 1.5	0.981 ± 0.076	18.4 ± 1.5	
	238	26.0 ± 0.5	0.317 ± 0.004	16.4 ± 0.8	24.7 ± 0.1
	388	46.4 ± 1.8	0.207 ± 0.006	16.8 ± 1.8	14.7 ± 4.8
	511	43.9 ± 2.1	0.286 ± 0.014	16.0 ± 1.0	35.3 ± 0.3
	700	40.1 ± 1.8	0.393 ± 0.036	10.2 ± 0.3	16.7 ± 2.8
	1009	38.7 ± 0.1	0.600 ± 0.023	8.5 ± 0.2	22.7 ± 4.73
	1492	21.7 ± 1.6	0.302 ± 0.029	9.9 ± 0.3	50.7 ± 1.7
	2615	19.0 ± 0.4	0.185 ± 0.008	15.4 ± 0.8	22.0 ± 1.4
	3116	13.2 ± 0.4	0.213 ± 0.014	22.3 ± 1.1	22.9 ± 1.0
4599	17.1 ± 0.9	0.115 ± 0.008	23.2 ± 0.2	14.4 ± 0.1	

Table E.3. Dissolved Pb, Mn, Ga and Nb in the western North Pacific. Each value is the average of two measurements with the error being the range.

Station	Depth (m)	Zn (nmol/kg)	Cd (nmol/kg)	Ni (nmol/kg)	Cu (nmol/kg)
HS 15	50	0.277 ± 0.170	0.007 ± 0.002	0.965 ± 0.164	0.613 ± 0.163
	100	0.467 ± 0.188	0.013 ± 0.003	1.957 ± 0.132	0.529 ± 0.047
	300	1.745 ± 0.055	0.321 ± 0.017	5.513 ± 0.158	1.579 ± 0.074
	300	2.830 ± 0.002	0.186 ± 0.005	3.791 ± 0.358	0.909 ± 0.018
	600	3.711 ± 0.126	0.518 ± 0.017	6.175 ± 0.134	1.070 ± 0.062
	800	6.534 ± 0.259	0.680 ± 0.029	8.818 ± 0.040	1.144 ± 0.015
	1000	6.483 ± 0.050	0.681 ± 0.013	9.622 ± 0.229	2.062 ± 0.010
	1200	7.123 ± 0.088	0.719 ± 0.036	9.173 ± 0.071	1.982 ± 0.026
	1500	8.861 ± 0.152	0.725 ± 0.034	10.657 ± 0.004	1.656 ± 0.039
HS 16	25	0.900 ± 0.172	0.016 ± 0.000	1.429 ± 0.051	0.684 ± 0.097
	50	0.683 ± 0.194	0.016 ± 0.003	2.255 ± 0.116	0.466 ± 0.033
	100	1.031 ± 0.102	0.012 ± 0.000	2.309 ± 0.088	0.487 ± 0.058
	300	1.230 ± 0.011	0.280 ± 0.003	3.774 ± 0.082	0.470 ± 0.021
	500	3.636 ± 0.037	0.652 ± 0.013	7.073 ± 0.206	1.276 ± 0.013
	706	5.651 ± 0.050	0.690 ± 0.003	8.511 ± 0.166	1.349 ± 0.012
	906	5.229 ± 0.204	0.707 ± 0.039	7.611 ± 0.143	0.658 ± 0.035
	1204	5.759 ± 0.216	0.679 ± 0.013	6.401 ± 0.127	0.917 ± 0.030
	1504	8.111 ± 0.104	0.697 ± 0.019	9.716 ± 0.160	1.126 ± 0.001
	2032	9.535 ± 0.387	0.697 ± 0.026	10.595 ± 0.351	2.848 ± 0.069
	2532	9.141 ± 0.195	0.663 ± 0.024	9.292 ± 0.118	1.235 ± 0.020
	3034	9.906 ± 1.093	0.635 ± 0.050	9.945 ± 0.833	2.524 ± 0.211
	3534	7.972 ± 0.672	0.622 ± 0.038	7.843 ± 0.454	3.354 ± 0.184
	4041	10.032 ± 0.541	0.609 ± 0.047	10.006 ± 0.236	3.299 ± 0.009
	4500	9.884 ± 0.012	0.628 ± 0.010	9.472 ± 0.004	4.543 ± 0.035

Table E.4. Dissolved Zn, Cd, Ni and Cu in the central North Pacific. Each value is the average of two measurements and the error represents the range.

Station	Depth (m)	Pb (pmol/kg)	Mn (nmol/kg)	Ga (pmol/kg)	Nb (pmol/kg)
HS 15	50	10.9 ± 2.2	0.6946 ± 0.086	9.5 ± 0.1	(368.2)
	100	10.1 ± 1.4	1.063 ± 0.039	11.0 ± 1.0	79.2 ± 17.3
	300	21.3 ± 1.2	0.184 ± 0	13.2 ± 0.1	33.8 ± 1.8
	300	34.2 ± 3.1	0.363 ± 0.013	10.3 ± 0.4	60.6 ± 15.4
	600	19.6 ± 0.6	0.339 ± 0.013	9.9 ± 0.4	80.6 ± 5.5
	800	14.1 ± 1.0	0.248 ± 0.012	9.5 ± 0.2	109.3 ± 10.2
	1000	10.5 ± 1.2	0.308 ± 0.011	9.5 ± 0.9	57.0 ± 10.2
	1200	8.1 ± 1.1	0.329 ± 0.008	10.1 ± 0.8	101.4 ± 4.8
	1500	7.7 ± 0.2	0.287 ± 0.012	13.7 ± 1.0	80.0 ± 0.9
HS 16	25	16.7 ± 0.6	0.934 ± 0.007	14.4 ± 1.3	35.3 ± 0
	50	25.5 ± 2.1	2.377 ± 0.315	11.1 ± 0.5	49.8 ± 12.8
	100	38.3 ± 0.3	2.755 ± 0.161	9.1 ± 0.7	64.7 ± 5.4
	300	38.3 ± 0.4	0.617 ± 0.007	8.5 ± 0.2	106.0 ± 1.1
	500	31.9 ± 0.6	0.816 ± 0.035	6.7 ± 0.4	21.0 ± 2.9
	706	28.7 ± 1.0	0.619 ± 0.024	7.2 ± 0.3	37.0 ± 5.2
	906	19.0 ± 1.3	0.472 ± 0.016	7.4 ± 0.6	23.9 ± 1.9
	1204	14.3 ± 0.3	0.652 ± 0.001	8.6 ± 1.3	31.1 ± 2.2
	1504	13.3 ± 0.2	0.490 ± 0.009	10.3 ± 0.4	36.8 ± 3.8
	2032	16.3 ± 1.1	0.468 ± 0.003	15.6 ± 1.2	63.7 ± 8.5
	2532	12.3 ± 0.8	0.289 ± 0	18.6 ± 0.8	150.1 ± 7.9
	3034	15.3 ± 0.7	0.256 ± 0.040	25.3 ± 1.3	61.2 ± 0.1
	3534	11.5 ± 0.7	0.277 ± 0.037	23.0 ± 0.4	46.9 ± 2.3
	4041	11.8 ± 0.5	0.216 ± 0.027	27.1 ± 0.1	79.4 ± 0.4
4500	15.6 ± 0.1	0.160 ± 0.005	27.8 ± 0	69.4 ± 1.2	

Table E.5. Dissolved Pb, Mn, Ga and Nb in the central North Pacific. Each value is the average of two measurements with the error being the range. Values in brackets believed to be contaminated.

Station	Depth (m)	Zn (nmol/kg)	Cd (nmol/kg)	Ni (nmol/kg)	Cu (nmol/kg)
P 26	25	0.388 ± 0.012	0.143 ± 0.015	2.806 ± 0	0.897 ± 0.102
	50	0.293 ± 0.001	0.204 ± 0.009	2.471 ± 0.048	0.827 ± 0.007
	75	0.463 ± 0.047	0.340 ± 0.005	NA	1.045 ± 0.005
	100	0.338 ± 0.004	0.413 ± 0.013	2.376 ± 0.031	0.996 ± 0.003
	100	0.416 ± 0.019	0.748 ± 0.078	NA	1.224 ± 0
	150	NA	0.951 ± 0.057	NA	NA
	200	NA	0.922 ± 0.057	2.827 ± 0	0.728 ± 0
	250	1.531 ± 0	NA	2.554 ± 0.189	0.788 ± 0.030
	300	NA	0.847 ± 0.067	NA	1.549 ± 0.142
	500	2.600 ± 0.034	0.849 ± 0.058	2.289 ± 0.027	1.362 ± 0.126
	500	2.536 ± 0.116	NA	1.870 ± 0.291	1.196 ± 0.019
	750	4.553 ± 2.572	0.833 ± 0.034	4.543 ± 0.444	1.599 ± 0.010
	750	6.130 ± 0.127	NA	NA	NA
	1000	6.905 ± 0.150	0.928 ± 0	5.445 ± 1.317	2.002 ± 0.009
	1000	5.156 ± 0.303	NA	NA	NA
	1250	5.496 ± 0	0.702 ± 0.048	7.857 ± 0	NA
	1500	7.242 ± 0.614	NA	NA	1.926 ± 0.167
	2000	8.219 ± 1.181	0.716 ± 0.008	9.438 ± 0.430	1.425 ± 0.005
	2250	8.818 ± 0.346	0.758 ± 0.019	9.531 ± 0.290	3.703 ± 0.091
	2500	10.253 ± 0.815	0.855 ± 0.072	9.199 ± 0.737	2.041 ± 0.060
	2500	NA	0.752 ± 0.027	9.403 ± 0.050	2.380 ± 0.138
	3000	9.394 ± 0.468	0.747 ± 0.048	9.530 ± 0.207	2.773 ± 0.388
	3000	NA	0.606 ± 0	9.523 ± 0.415	3.929 ± 0.145
3900	8.940 ± 0	0.842 ± 0.029	9.633 ± 0	3.042 ± 0	
4200	NA	NA	9.147 ± 0.123	6.663 ± 0.522	

Table E.6. Dissolved Zn, Cd, Ni and Cu in the eastern North Pacific. Each value is the average of two measurements and the error represents the range.
NA = not analyzed.

Station	Depth (m)	Pb (pmol/kg)	Mn (nmol/kg)	Ga (pmol/kg)	Nb (pmol/kg)
P 26	25	23.5 ± 2.1	0.548 ± 0.064	4.0 ± 0.8	35.4 ± 0.7
	50	41.3 ± 4.5	0.539 ± 0.025	4.8 ± 0.2	51.9 ± 4.1
	75	31.3 ± 4.3	0.423 ± 0.007	3.1 ± 2.2	15.6 ± 1.5
	100	38.2 ± 2.3	0.490 ± 0.021	7.3 ± 1.5	16.4 ± 0.3
	100	NA	0.301 ± 0.013	NA	NA
	150	18.0 ± 2.0	NA	8.0 ± 3.4	6.3 ± 0
	200	NA	NA	11.8 ± 3.5	NA
	250	22.3 ± 2.2	0.278 ± 0.035	NA	3.3 ± 1.2
	250	NA	0.496 ± 0.024	NA	NA
	300	21.3 ± 2.8	NA	11.9 ± 3.1	NA
	500	26.8 ± 1.5	0.816 ± 0.004	13.8 ± 2.1	12.3 ± 2.3
	750	28.5 ± 1.1	0.626 ± 0.019	7.1 ± 2.8	34.0 ± 2.2
	750	18.8 ± 2.0	NA	NA	30.4 ± 1.9
	1000	20.9 ± 6.6	0.511 ± 0.005	4.4 ± 1.4	22.7 ± 8.4
	1000	NA	NA	3.1 ± 0.5	NA
	1250	15.3 ± 0	NA	7.1 ± 0.4	23.9 ± 3.9
	1250	NA	NA	7.5 ± 0.2	NA
	1500	19.6 ± 1.4	0.430 ± 0.042	NA	123.8 ± 10.6
	2000	14.3 ± 0.5	0.380 ± 0.004	9.4 ± 2.3	34.2 ± 6.6
	2000	8.3 ± 2.3	NA	NA	51.2 ± 3.8
	2250	7.9 ± 0.2	NA	8.4 ± 1.6	29.2 ± 0
	2500	10.0 ± 1.3	0.346 ± 0.025	12.0 ± 0.6	51.5 ± 2.5
	2500	8.5 ± 1.3	NA	17.5 ± 1.9	NA
	3000	8.8 ± 0.8	0.339 ± 0.027	11.7 ± 0	104.5 ± 21.3
	3000	8.8 ± 0.1	NA	10.7 ± 2.0	NA
	3500	5.0 ± 0.1	0.363 ± 0.029	NA	NA
3900	5.3 ± 0	NA	20.4 ± 0	NA	
4200	5.2 ± 5.9	0.479 ± 0.023	31.7 ± 3.8	107.7 ± 13.8	
4200	NA	NA	NA	104.6 ± 11.0	

Table E.7. Dissolved Pb, Mn, Ga and Nb in the eastern North Pacific. Each value is the average of two measurements with the error being the range. NA = not analyzed.